Aus der Klinik für Psychiatrie & Psychotherapie, Abteilung für
Neuropsychiatrie und Labor für Molekulare Psychiatrie
der Medizinischen Fakultät Charité – Universitätsmedizin Berlin

DISSERTATION

Heterogenität der myeloiden Zellen bei Multipler Sklerose
mittels Einzelzell-Massenzytometrie

Heterogeneity of myeloid cells in multiple sclerosis as
evidenced by single-cell mass cytometry

zur Erlangung des akademischen Grades
Doctor of Philosophy (PhD)

vorgelegt der Medizinischen Fakultät
Charité – Universitätsmedizin Berlin

von

María Camila Fernández Zapata

Datum der Promotion: 25.11.2022

Preface

The data presented in this thesis was published as a joint-first author in the following international peer-reviewed journals:

- Böttcher, C.*, Fernández-Zapata, C.*, Schlickeiser, S.* *et al.* Multi-parameter immune profiling of peripheral blood mononuclear cells by multiplexed single-cell mass cytometry in patients with early multiple sclerosis. *Sci Rep* **9,** 19471 (2019).

- Böttcher, C.*, van der Poel, M.*, Fernández-Zapata, C.* *et al.* Single-cell mass cytometry reveals complex myeloid cell composition in active lesions of progressive multiple sclerosis. *Acta Neuropathol Commun* **8,** 136 (2020).

- Böttcher, C.*, Fernández-zapata, C.*, Snijders, G. J. L., Schlickeiser, S., Sneeboer, M. A. M., Kunkel, D., Witte, L. D. De & Priller, J. Single-cell mass cytometry of microglia in major depressive disorder reveals a non-inflammatory phenotype with increased homeostatic marker expression. *Transl. Psychiatry* 1–11 (2020).

(* These authors contributed equally to the work)

Contents

Figures

Abstract

Multiple sclerosis (MS) is a chronic inflammatory and demyelinating disease of the central nervous system. To date, there are no established biomarkers beyond magnetic resonance imaging that can predict either disease activity and severity in patients nor confirmed mechanisms for the first-line MS treatments. Likewise, there is no cure or effective treatment at late stages of the disease. Recent studies in mouse models of demyelination and neuroinflammation have pointed towards important roles of myeloid cells in the development of the disease. Despite this, the roles and impact of this cell population on human MS pathogenesis and disease progression remain obscure. Here we have used single-cell mass cytometry to study the phenotypes of myeloid cells from peripheral blood of early MS patients and from myeloid cells isolated from post-mortem brains of progressive MS (PMS) patients. We performed the characterization of PBMCs from drug naïve early MS patients as compared with healthy donors using two antibody panels comprising a total of 64 antibodies. Our results show increased abundance of several subsets of CD4$^+$ and CD8$^+$ T cells and only mild changes in the myeloid compartment. For the study on myeloid cells from late PMS we designed three antibody panels targeting a total of 74 markers which we used to compare between isolated myeloid cells from active lesions and normal-appearing white matter. In this case the results show high heterogeneity of myeloid phenotypes in the brains of PMS patients and an increase in expression of markers associated with phagocytic activity and activation in lesion-associated populations. Such inflammatory signature could not be detected in major depressive disorder, a common co-morbidity in patients with MS.

Zusammenfassung

Multiple Sklerose (MS) ist eine chronisch entzündliche und demyelinisierende Erkrankung des Zentralnervensystems. Bisher gibt es keine etablierten Biomarker außerhalb der Kernspintomographie, die entweder die Krankheitsaktivität und den Schweregrad bei Patienten vorhersagen können, noch bestätigte Mechanismen für die Erstlinien-MS-Therapie. Ebenso gibt es für die späten Stadien der Krankheit keine Heilung oder wirksame Behandlung. Jüngste Studien an Mausmodellen zur Demyelinisierung und Neuroinflammation haben gezeigt, dass myeloide Zellen eine wichtige Rolle bei der Entwicklung der Krankheit spielen. Trotzdem bleiben die Rolle und der Einfluss von Monozyten auf die Pathogenese und das Fortschreiten der MS beim Menschen unklar. Hier haben wir die Einzelzell-Massenzytometrie verwendet, um die Phänotypen von myeloischen Zellen aus peripherem Blut von frühen MS-Patienten und von myeloiden Zellen zu untersuchen, die aus post-mortem-Gehirnen von progressiven MS-Patienten (PMS) isoliert wurden. Wir führten die Charakterisierung von PBMCs von arzneimittel-naiven frühen MS-Patienten im Vergleich zu gesunden Spendern unter Verwendung von zwei Antikörper-Panels durch, die insgesamt 64 Antikörper umfassten. Unsere Ergebnisse zeigen eine erhöhte Häufigkeit mehrerer Untergruppen von CD4$^+$ und CD8$^+$ T Zellen und nur geringfügige Veränderungen im myeloischen Kompartiment. Für die Studie an myeloischen Zellen aus spätprogressiver MS haben wir drei Antikörper-Panels entworfen, die auf insgesamt 74 Marker abzielen, die wir zum Vergleich zwischen isolierten myeloiden Zellen aus aktiven Läsionen und normal erscheinender weißer Substanz verwendeten. In diesem Fall zeigen die Ergebnisse eine hohe Heterogenität der myeloischen Phänotypen im Gehirn von PMS-Patienten und eine Erhöhung der Expression von Markern, die mit der phagozytischen Aktivität und Aktivierung in läsionsassoziierten Populationen assoziiert sind. Eine solche entzündliche Signatur konnte bei schweren depressiven Störung, einer häufigen Komorbidität bei Patienten mit MS, nicht nachgewiesen werden.

List of abbreviations

MS	Multiple Sclerosis
CNS	Central Nervous System
EBV	Epstein-Barr Virus
RRMS	Relapsing Remitting Multiple Sclerosis
PPMS	Primary Progressive Multiple Sclerosis
CIS	Clinically Isolated Syndrome
SPMS	Secondary Progressive Multiple Sclerosis
MRI	Magnetic Resonance Imaging
PMS	Progressive Multiple Sclerosis
CSF	Cerebrospinal fluid
EAE	Experimental Autoimmune Encephalomyelitis
CyTOF	Cytometry by Time-of-Flight
huMG	Human Microglia
AD	Alzheimer's Disease
DAM	Disease-Associated Microglia
MDD	Major depressive disorder
IMC	Imaging Mass Cytometry
IHC	Immunohistochemistry
FFPE	Formalin-Fixed Paraffin Embedded
TOF	Time-of-Flight
PBMCs	Peripheral Blood Mononuclear Cells
TMA	Tissue Microarray
FCS	Flow Cytometry Standard
tSNE	t-Distributed Stochastic Neighbor Embedding
DN	Double Negative T Cells
NK	Natural Killer Cells
Exp I	*Experiment I*
Exp II	*Experiment II*
Exp III	*Experiment III*
GLMM	Generalized Linear Mixed Models
FDR	False Discovery Rate
BH	Benjamin-Hochberg
hoMG	Homeostatic microglia
NAWM	Normal-appearing white matter
SVZ	Subventricular zone
THA	Thalamus
GTS	Gyrus Temporalis Superior
GFM	Gyrus Frontalis Medialis
Th1	T helper 1
DCs	Dendritic Cells
UMAP	Uniform Manifold Approximation and Projection
T_{CM}	Central Memory T cells

1. Introduction

1.1 Multiple Sclerosis

Multiple sclerosis (MS) remains the most common cause of non-traumatic neurological disability in young adults, affecting over 2.3 million people worldwide. MS is associated with a high economic burden, given that around 50% of these patients will become disabled in the 25 years after disease onset[1]. The vast array of symptoms presented by patients suffering from MS hindered the description of the disease until 1868 when the French neurologist Jean Martin Charcot connected clinical observations, anatomo-pathology and physiology and established MS as a distinct disease of the central nervous system (CNS)[2]. MS is now widely accepted as a chronic inflammatory disease of the CNS in which there is an autoimmune attack on components of the myelin sheath, leading to focal areas of demyelination and eventually to neurodegeneration[1]. The exact cause of the disease is unknown but several studies have shown a certain genetic susceptibility, and the latest genome-wide association study has pointed to specific genetic associations, most of them linked to immune cell types including peripheral myeloid cells and microglia, the resident immune cells in the brain[3]. MS has also been linked to different environmental factors, which include a history of Epstein-Barr virus (EBV) infection, smoking, vitamin D deficiency or circadian disruption[1]. It is thus believed that complex gene-environment interactions lead to disease initiation[1].

The clinical presentation of the disease is very heterogeneous among patients and the symptoms will depend on the anatomical site of the lesions. MS can present as a temporary loss of vision, change in mood, pain, cognitive deficiency or muscular disturbance, to name a few disease manifestations. The clinical course of MS is also heterogeneous, and patients are categorized into either relapsing-remitting MS (RRMS) or primary progressive MS (PPMS) depending on the clinical course after disease onset. In RRMS, the most common form of the disease, the patients present a first clinical episode, known as clinically isolated syndrome (CIS) which will continue with a series of relapses of clinical disability followed by a complete or partial remission of the symptoms. In 80% of the cases, 10 to 20 years after the first episode, patients enter into the secondary progressive (SPMS) stage, in which clinical disability progresses with no recovery[4]. In the PPMS form of the disease, patients do not

present the relapsing-remitting phase and instead, disability progresses with no apparent relapse in the symptoms from the first clinical disturbance[4].

In early stages of the disease, neurological symptoms are induced by CNS inflammation, typically caused by an infiltration of peripheral immune cells (mainly monocytes and CD8^{+} T cells) to the CNS[4]. Areas of infiltration associated to demyelination can be visualized by magnetic resonance imaging (MRI), and are known as "focal plaques"[5]. In late stages of PMS, plaques associated with peripheral infiltration are rare and, instead, chronic demyelination leads to axonal loss ultimately resulting in neurological disability[6]. There is currently no treatment or effective cure in this late stage of the disease and most patients will eventually die due to either direct MS symptoms or secondary complications associated with the disease.

MS diagnosis is typically done following the suggested tests of the 2017 McDonald criteria[7] by proof of spatial or temporal dissemination of the demyelinating lesions. The criteria are a minimum of two immune attacks in the CNS proved by either clinical assessment, an MRI showing two sites of infiltration or the presence of cerebrospinal fluid (CSF) specific oligoclonal bands[7]. Despite this, the diagnosis is not always straightforward and following the first CIS, often the lack of clinical evidence of a second attack, inconclusive MRI scans or CSF oligoclonal bands prevent diagnosis, thus delaying commencement of disease-modifying treatments. In recent years, several studies have pointed to the importance of an early start in immunomodulatory treatments to delay relapses and reduce disease severity in the subsequent years. Therefore there is a need to better understand the pathological mechanisms driving the first stages of disease, to improve definitive diagnostic methods[8].

1.2 Monocytes in experimental autoimmune encephalomyelitis and MS

In the early stages of the disease, focal demyelinating plaques are characterized by infiltration of peripheral immune cells into the CNS parenchyma[4]. Histological analysis of the plaques in different stages of MS with a focus on lymphocytes has shown that lesions are dominated by the presence of CD8^{+} T and CD20^{+} B cells, especially in the early stages of disease[10].

However, low levels of T and B cells at the sites of myelin and axonal destruction indicates that they do not drive demyelination via cell-to-cell contacts[10]. Instead, myelin destruction and acute neurodegeneration are likely induced by soluble factors produced by CD8$^+$ T cells but mediated by microglia or other myeloid subsets[10].

Myeloid cells, especially monocytes, also enter the CNS parenchyma where they contribute to the perivascular infiltrates[10], as proved in post-mortem and biopsy brain samples[12], suggesting their important contribution to pathogenesis. Monocytes, as part of the innate immune system, patrol the body in search for inflammatory cues and are rapid responders to tissue insult. They constitute approximately 10% of the circulating leukocytes and can be classified into three main subsets depending on the expression of the surface markers CD14 and CD16: classical monocytes (CD14$^+$CD16$^-$) making up 80-90% of the monocyte pool while the remaining 10-20% are intermediate monocytes (CD14$^+$CD16$^+$) and non-classical monocytes (CD14$^-$CD16$^+$)[13]. Tissue-invading monocytes differentiate into monocyte-derived macrophages[11], distinct from CNS-resident macrophage pools that commonly originate from the yolk sac, as shown in mice[14]. Macrophages serve three main functions: phagocytosis, antigen presentation and cytokine release. During disease they contribute to active inflammation and tissue destruction, although they can also adopt phenotypes which promote lesion resolution and tissue repair[15].

Studies in experimental autoimmune encephalomyelitis (EAE), a mouse model for demyelination and neuroinflammation, have shown that monocytes are rapidly mobilized from the circulation to invade the CNS parenchyma upon immunization[11,16,17]. Selective gene targeting to deplete CCR2 expression on myeloid cells in EAE suggested that the CCR2$^+$CD11b$^+$Ly6C^{hi} monocyte subset (equivalent to classical CD14$^+$CD16$^-$ monocytes in human) is essential for the development of EAE[17]. They also showed that this monocyte subset is essential in modulating the effector phase of the disease by shaping the local innate immune response in the damaged CNS through the release of immune modulatory molecules including cytokines, oxygen radicals like nitric oxide and surface molecules required for antigen presentation[17]. Furthermore, there is evidence that impeding monocyte entry into the CNS prevents progression to severe disease and that the monocyte invasion is a transient event and does not provide prolonged contribution to the brain microglia pool[11]. When using single-cell mass cytometry (Cytometry by Time-of-Flight [CyTOF]) to phenotype monocyte

populations, four specific monocyte subsets were found at a significantly higher frequency in pre-symptomatic, onset and peak EAE. These populations were characterized by higher expression of CD80, CD86, CD38, CD39, MerTK, Axl, CD206 and TREM2[18]. Although the studies mentioned above provide evidence of monocyte involvement in different phases of EAE, the role of this cell population in the development of MS remains to be investigated.

1.3 Microglial diversity in health and MS

Microglia, the resident myeloid cells of the brain, are the first line of defense against pathogens, inflammation and neurodegeneration in the brain parenchyma[19]. Microglia were first described in 1919 by the Spanish neurologist Pío del Río Hortega who published a series of four papers describing their distribution and morphological phenotype[20]. In physiological conditions, microglia are small, ramified cells found diffusely spread throughout the CNS. They derive from myeloid progenitors originating in the yolk sac at embryonic day 7.25, from where they travel through blood vessels and invade the brain, as evidenced by studies in mice[21]. The microglial pool is maintained throughout adulthood by self-renewal and, in humans, microglia proliferate at a median rate of 28% per year, much slower than the turnover of other myeloid immune cells, which is a few days or weeks[22]. During development, microglia help in establishing the neuronal architecture in the CNS by phagocytosing apoptotic neurons, providing trophic support to neurons, oligodendrocytes and vasculature and mediating synaptic pruning[23,24]. In the adult homeostatic environment they survey the environment by continuously extending their processes and contacting neighboring cells, actively participate in clearance of debris from the CNS parenchyma and furthermore regulate synaptic plasticity and function through synaptic pruning[25].

It is important to note that microglia are not a homogeneous population but rather have different phenotypes depending on their anatomical location[26–28]. Human microglia (huMG) regional heterogeneity was recently investigated using CyTOF, showing that microglia from the subventricular zone and thalamus had similar phenotypes indicative of a more activated state and distinct from the other brain regions studied. Cerebellar microglia also showed a clear differentiating signature and as expected, frontal and temporal lobe microglia had a similar phenotype. Importantly, this study defined key markers for determining huMG

regional heterogeneity, namely CD11c, CD206, CD45, CD64, CD68, CX3CR1, HLA-DR and IRF8[28].

Microglia adopt different phenotypes during non-physiological conditions which vary depending on the type of insult, ranging from increased phagocytosis and secretion of pro-inflammatory molecules to promotion of remyelination and secretion of anti-inflammatory molecules[19]. Pío del Río Hortega had already described some of the changes that microglia undergo upon activation as they rapidly invade sites of lesion, including proliferation, retraction of processes and adoption of an amoeboid morphology[19,30]. Changes of phenotype during neurodegeneration have been studied mainly in mouse models of Alzheimer's disease (5xFAD mice and APP-PS1 overexpressing mice). By performing single-cell RNA sequencing on isolated microglia from mice with neurodegeneration two independent studies found a specific microglial signature associated with the pathology[31,32]. Neurodegeneration-associated microglia were characterized by downregulation of homeostatic genes, including purinergic receptors *P2ry12/P2ry13, Cx3cr1* and *Tmem119*, and upregulation of several genes mainly involved in lysosomal/phagocytic pathways, endocytosis and regulation of the immune response, including AD-associated risk factors such as *Apoe, Lpl, Tyrobp* and *Trem2*, [31]. Alterations in the microglia population have also been linked with psychiatric disorders. Recent genome-wide association studies have detected genetic associations between immune response pathways and adult psychiatric disorders such as major depressive disorder (MDD) and schizophrenia[33,34]. Furthermore, studies on HLA-DR microglia reactivity (as a marker of microglia activation) from MDD and schizophrenic patients showed increased microgliosis in suicide patients but not diagnosis-dependent microglial activation[35]. In contrast with these results, another study using positron emission topography to measure translocator protein (TSPO) total distribution volume (used as a measure of activated microglia), showed significant increase of TSPO density in all brain regions examined from MDD patients as compared with controls, providing evidence for microglial activation in MDD[36]. Detailed studies on microglial phenotypic signatures in MDD are still missing. Interestingly, depression is recognized as a common co-morbidity in patients with MS[37]. The clinical phenotype of MDD and MS-associated depression was found to be

similar[37]. However, the pathomechanism of both disorders remains to be investigated and whether this is driven and/or synergized by neuroinflammation as seen in MS is still unclear.

In EAE and the cuprizone model of demyelination, single-cell transcriptomic and proteomic analyses revealed microglial heterogeneity associated with CNS inflammation[18,27,38,39]. Single-cell RNA-seq on CD45^{+} isolated cells showed a specific EAE-associated microglial phenotype[39]. Mainly, downregulation of homeostatic genes and upregulation of *Ly86*, *Cxcl10*, *Ccl5* and *Cd74*[39]. Furthermore, results from single-cell RNA-seq of microglia from mice subjected to cuprizone-induced demyelination (in which there is no peripheral infiltration in the CNS parenchyma) showed specific microglial profiles associated with de- and re-myelination[27]. Similarly, CyTOF characterization of microglia in EAE revealed distinct phenotypes associated with the pathology. Two CNS-specific populations were specifically linked to onset and peak stages of the pathology, defined as CD317^{+}MHCII^{−}CD39^{hi}CD86^{+} and CD317^{+}MHCII^{+}CD39^{hi}CD86^{+}CD11c^{+} respectively. The expression of these markers is indicative of an activated, pro-inflammatory phenotype. Interestingly, the frequency of these populations, particularly the peak-EAE-associated population, was significantly decreased in chronic EAE, although still higher than in healthy CNS[18]. A second study, also using CyTOF to phenotype different immune cells in the CNS of EAE mice, found a decrease in microglial homeostatic checkpoint markers (CX3CR1, MerTK and Siglec-H) and an increased expression of phagocytosis-related and activation markers (CD44, CD86, PD-L1, CD11c and MHCII)[38]. While mouse models of MS-related pathologies, such as EAE and the cuprizone model, have proven to be a useful tool to study specific disease mechanisms, the findings must be interpreted with caution, as these models do not replicate the complexity of MS[40]. Nevertheless, similar transcriptional signatures were found in huMG isolated from patients with acute MS[27].

Studies attempting to decipher microglial phenotypes associated with MS are mostly limited to classical immunohistochemical techniques[41–43] and bulk genomic analysis[43,44]. In the few cases of high-dimensional single-cell analysis, only a handful of cases could be analyzed at the genomic level[27]. So far it has been shown that microglia invade the site of lesion, adopt a "foamy" morphology with intracytoplasmic myelin deposits[12], and adopt different

phenotypic programs, mostly downregulating homeostatic markers and increasing expression of pro-phagocytic markers[43], which is somewhat concordant with what has been found in mice models.

The studies mentioned above (both in mouse and human) point to a set of phenotypic changes in microglia that may have specific roles in MS pathology. Understanding these changes is of crucial importance, especially in late stages of the disease in which immune infiltration is low or absent in the CNS parenchyma and thus disease-modifying treatments usually aimed at impeding immune entrance in the parenchyma are not effective. Thus, a deeper look into microglia phenotypes and function at late stages of MS could enable the design of new treatment strategies.

1.4 Single-cell mass cytometry to elucidate myeloid phenotypes

1.4.1 Single-cell mass cytometry – high dimensional cell profiling

Advances in single-cell technologies have shown that specialized cell types in each of our organs are in turn composed by heterogeneous cell subsets, which can acquire different states during homeostasis and disease. Bulk analysis, although useful in some settings, oversimplifies this view by averaging signals from different cells.

For protein-level single-cell analysis, we have relied for many years on flow cytometry, a technique in which cells are labelled with fluorescently-tagged antibodies specific for certain proteins[45]. Flow cytometry carries the advantage of high throughput, little to no cell loss and it can be combined with cell sorting (FACS) which thus enables further analysis of isolated cells[46]. However, flow cytometry can usually measure up to 18 channels (in the BD LSR-II system) due to the spectral overlap between channels. CyTOF was developed to overcome this problem and enable high-dimensional single-cell protein measurement[47]. Briefly, cells in suspension are labelled with antibodies tagged with rare earth metals, typically from the lanthanide series, not usually found in biological conditions. Cells are nebulized into single-cell droplets and ionized using inductively-coupled plasma. Ionized particles are passed

through a quadrupole to remove cell debris and heavy metal ions are quantified in a Time-of-Flight (TOF) mass spectrometer. Thus, a quantification of each ion corresponding to a different isotope is obtained per cell, as output data. CyTOF has a clear advantage over flow cytometry in so far as the usage of rare metal isotopes as antibody tags comes with little overlap between signals, thus allowing for the detection of up to 60 markers simultaneously. Furthermore, the measurement of pooled barcoded samples allows the reduction of technical noise thus increasing sensitivity to detect differences between samples or groups[48].

1.4.2 Imaging CyTOF – single cell atlas on the tissue

While suspension CyTOF has the advantage of being high-dimensional and per-cell, it cannot determine how the different cell phenotypes are distributed within the tissue. To address this question, imaging mass cytometry (IMC) was recently developed by combining standard immunohistochemical techniques (IHC) and mass cytometry[49]. Briefly, tissue samples are mounted on a slide and samples are stained with antibodies tagged with metal isotopes using IHC protocols. Tissue such as fresh-frozen or formalin-fixed paraffin-embedded (FFPE) can be used. Regions of interest from each sample are then selected and ablated with a UV laser at a resolution of 1 μm. The nebulized masses are then passed to a TOF spectrometer and the abundances of each metal per spot are recorded. The system can track back each measurement to a specific coordinate in the original sample, thus creating an artificial image for each marker. Therefore, in IMC the information is not obtained per cell, but correlates with a coordinate on the generated image. This means a cell segmentation step is needed after acquisition in order to perform single cell analysis. IMC enables a more comprehensive analysis of cells within their tissue microenvironment, and can be used to perform morphological, spatial and network analysis of cell subpopulations and obtain detailed descriptions of tissue architecture[48].

2. Hypothesis & Aims of the study

Several immunological studies have explored the roles of myeloid cells in MS pathology at different stages of the disease. Studies using the neuroinflammatory mouse model EAE have shown that monocytes invaded the parenchyma upon immunization and released immune mediators modulating the disease[17]. Furthermore, impeding the entrance of monocytes into the CNS parenchyma dampens the autoimmune response, which prevents progression to severe disease[11]. In late stages of PMS there is little to no contribution of peripheral immune cells to the pathology, instead active demyelinating plaques are dominated by resident microglia and macrophages[41]. Recent studies on EAE mice at the single-cell level have shown specific microglial phenotypes associated to lesion with roles in inflammation, de- and remyelination[18,38]. Despite the clear evidence that myeloid cells play important roles in early and late stages of neuroinflammation and demyelination in mice, there is no study to date giving a proper characterization of these cells in the human pathology. Furthermore, since depression is recognized as one of the major co-morbidity in patients with MS and systemic inflammation has been suggested in patients with MDD, it is more likely that neuroinflammation can be also observed in MDD and it may synergize or drive MS-associated depression, which can worsen or exacerbate the disease outcome.

The main goal of this study was to phenotypically characterize the myeloid cell compartments including peripheral blood monocytes and microglia in early and late stages of MS using single-cell mass cytometry and imaging mass cytometry. Specifically, at the early stages of MS, phenotypic alterations of peripheral immune cells with a focus on monocytes were investigated, whereas the CNS myeloid cell compartment was characterized at the late stages of the disease. Finally, we aimed to investigate whether similar signatures could be found in microglia isolated from different regions of post-mortem brains from patients with MDD.

Identification of phenotypic alteration of myeloid cells in the human MS pathology may lead to better understanding the role of these cells in MS pathogenesis.

3. Materials and Methods

Passages of the following chapter that are similar to methods described previously by the author are italicized.

3.1 Subjects

Human peripheral blood mononuclear cells (PBMCs)

The study was registered and approved by the Ethics Committee of Charité – Universitätsmedizin Berlin. All participants provided written informed consent before any study-related procedures were undertaken. The study has been performed according to the Declaration of Helsinki and to the relevant ethical guidelines for research in humans. PBMCs were isolated from heparinized blood through Biocoll (Biochrom GmbH, Berlin, Germany) density centrifugation at 760 × g for 20 minutes at RT as described before[42]. Cell pellets were resuspended in freezing medium at a concentration of 5 × 10^6 cells/ml, and further stored in liquid nitrogen[50].

Human post-mortem brain tissue and microglia isolation

Post-mortem tissue of brain donors was provided by the Netherlands Brain Bank (NBB, Amsterdam, The Netherlands, www.brainbank.nl). All brain donors gave informed consent to perform autopsies and to use tissue, clinical and neuropathological information for research purposes, approved by the Ethics Committee of VU medical center (Amsterdam, The Netherlands). Microglia were isolated from post-mortem WM tissue using Percoll gradient centrifugation (density of 1.13 g/ml; GE Healthcare, Little Chalfont, UK) and subsequent CD11b magnetic beads (catalogue number #130–049- 601, Miltenyi Biotech) sorting. For CyTOF analysis, CD11b$^+$ cells were incubated for 11 min in fixation/stabilization buffer (Smart Tube Inc., San Carlos, CA, USA) and stored in − 80 °C [51,52].

3.2 CyTOF & IMC staining and acquisition

PBMCs were live-barcoded using combinations of pre-conjugated ^{89}Y-CD45 (HI30, Fluidigm) and in-house conjugated ^{113}In, ^{115}In, ^{195}Pt, ^{196}Pt or ^{198}Pt-CD45 (HI30, Biolegend)[53] antibodies[50]. Isolated CD11b$^+$ brain myeloid cells were barcoded using Cell-ID 20-plex Pd Barcoding Kit (Fluidigm)[51]. All antibodies used were either purchased pre-conjugated to metal isotopes (Fluidigm) or were conjugated in-house using the MaxPar X8 Kit (Fluidigm). After cell barcoding, each set of samples were pooled together and stained with antibody master mixes. For intracellular staining, the cells were incubated in fixation/permeabilization buffer (Fix/Perm Buffer, eBioscience) and permeabilized (permeabilization buffer, eBioscience). The samples were then stained with antibody cocktails and fixed overnight in 4% methanol-free formaldehyde solution. Fixed cells were stained in ^{191}Ir/^{193}Ir intercalator solution (Fluidigm) and kept at 4 °C until CyTOF measurement[51,52].

IMC was used to validate the results obtained from CyTOF on the brain tissue. Paraffin tissue microarray (TMA) blocks were cut into 5 μm-thick sections, deparaffinized and treated by heat-induced antigen retrieval in Tris-EDTA buffer (pH= 9.0) at 95 °C. The sections were then stained with metal-conjugated antibodies overnight. Nuclei were detected using an ^{191}Ir/^{193}Ir DNA-intercalator. Samples were dried and stored at RT until measurement[51].

All CyTOF and IMC analysis were performed in the Flow & Mass Cytometry Core Facility, Charité – Universitätsmedizin Berlin and Berlin Institute of Health (BIH) under supervision of Dr. Désirée Kunkel as described before[50–52].

3.3 CyTOF data analysis

For CyTOF, as a first step all FCS files were transferred to the Cytobank platform (www.cytobank.org) where we performed manual gating and de-barcoding on live single cells according to DNA intercalators ^{191}Ir/^{193}Ir signals and event length. For de-barcoding, Boolean gating was used to deconvolute individual samples according to their barcode combinations. Once the FCS files for individual samples were obtained, all files were compensated for signal spillover using the Bioconductor package *CATALYST*[54] on R[55]. For

dimensionality reduction and visualization, we generated two-dimensional t-distributed stochastic neighbor embedding (tSNE) maps according to the expression levels of all markers in each panel using Cytobank. To visualize marker expression arcsinh transformation was applied to the data. All files, containing the tSNE coordinates for each cell, were then loaded into R for further unsupervised data analysis using an in-house written script based on the workflow suggested by Nowicka and colleagues[56]. For population identification, we performed clustering analysis of the data using the *FlowSOM/ConsensusClusterPlus*[57,58] algorithm. We had slight workflow differences between studies:

In the study on PBMCS (Chapter 4.1)[50] cluster identification was conducted using PBMCs lineage markers: HLA-DR, CD19, CD44, CD4, CD11c, CD16, CD3, CD56, CD14, CD8a, T-bet, CD33, CCR2 and CD11b in the Panel A; and HLA-DR, CD38, CD64, CD68, CD8a, CD33 and CD64 in the Panel B. After this step we manually merged the clusters in order to obtain clusters corresponding to known major PBMC populations including B cells, CD4/CD8-single positive and double-negative T cells (DN), natural killer (NK) cells, and myeloid cells. For high resolution analysis we then subclustered each of the major populations and determined the correct number of clusters based on visual inspection of the cluster-colored tSNE plots and the respective phenotypic heatmaps (we had a cutoff of a minimal mean frequency of 0.1% of parent).

In the study on brain-isolated myeloid cells from PMS and MDD patients (Chapters 4.2 and 4.3)[51,52] cluster identification for MDD and *Experiment I (Exp I)* was performed using all the markers and *Experiments II (Exp II)* and *III (Exp III)* were clustered using only the linage markers (referred to as *TYPE* markers), thus allowing the comparison between experiments. The number of clusters was determined based on delta area under cumulative distribution function curve and k value of the clustering analysis, namely the "elbow-point" criteria, with which one can assess the number of clusters that best fits the complexity of the data[59]. Visual inspection of cluster-colored tSNE plots and respective phenotypic heatmaps were also used to determine the final number of meta-clusters tested in each experiment.

It is important to note that in both cases we used an over-clustering approach, in which clusters are obtained at high resolution (a high number of clusters) which has proven useful for discovery studies. Each cluster, however, may not represent biologically distinct populations, but instead could represent different cell states.

3.4 IMC data analysis

For IMC data analysis, MCD files were then converted to 16-bit image .TIFF files on MCD viewer software version 1.0.056. For visualization only, .TIFF files were transferred to ImageJ and a Gaussian blurr (kernel width, 0.70 pixels) was used for noise reduction on combined channels[51].

For single cell analysis, segmentation was performed for each of the .TIFF files. First, we used Ilastik[60] for pixel classification. The program was trained to identify DNA Iridium intercalator signal as nuclei and $P2Y_{12}$-^{165}Ho signal as membrane, thus each single cell mask contained either only the nuclei or, for $P2Y_{12}^{+}$ cells, also the cytoplasm area. As a result, the Ilastik output of binary masks for each cell in each image was then fed into CellProfiler[61]. CellProfiler in turn creates 16-bit .TIFF single-cell masks with only full cells on each image that can be used in HistoCAT[62]. All original .TIFF images and single-cell masks were loaded into HistoCAT for single cell analysis. The platform offers different analysis options, for instance, we ran two-dimensional tSNE using all markers from all samples and Phenograph clustering analysis (for markers CD11c, CD44, CD45, CD68, HLA-DR, $P2Y_{12}$ and TNF, using k = 50 nearest neighbors). The mean expression and cell frequencies per sample/cluster where then analyzed using R[51].

3.5 Statistical analysis

No randomization and blinding strategies were applied in either of the studies. However, data processing and analysis, as well as statistical testing were carried out in unsupervised manner. Dichotomous variables of the sample cohort were analyzed with Fisher's exact test (GraphPad Prism)[50–52].

Detection of significative differential abundance of clusters between groups was done using generalized linear mixed models (GLMM) using the Diffcyt[63] package, with a false discovery rate (FDR) adjustment (Benjamini-Hochberg (BH) procedure) for multiple hypothesis

testing. A P value < 0.05 (unadjusted) and < 0.05 (FDR-BH adjusted) was considered statistically significant[50–52].

4. Results

4.1 Multi parameter immune profiling of peripheral blood mononuclear cells by multiplexed single-cell mass cytometry in patients with early multiple sclerosis

All results presented here have been previously published in Böttcher, C., et al., 2019[50].

4.1.1 Phenotypic characterization of PBMCs from early MS patients and controls using single-cell mass cytometry.

For in-depth phenotyping of the immune populations of PBMCs present in blood of early MS patients and controls, we stained and measured the cells with two antibody panels (35 antibodies/panel) for single-cell mass cytometry analysis. A schematic illustration of the workflow used can be found in Figure 1.
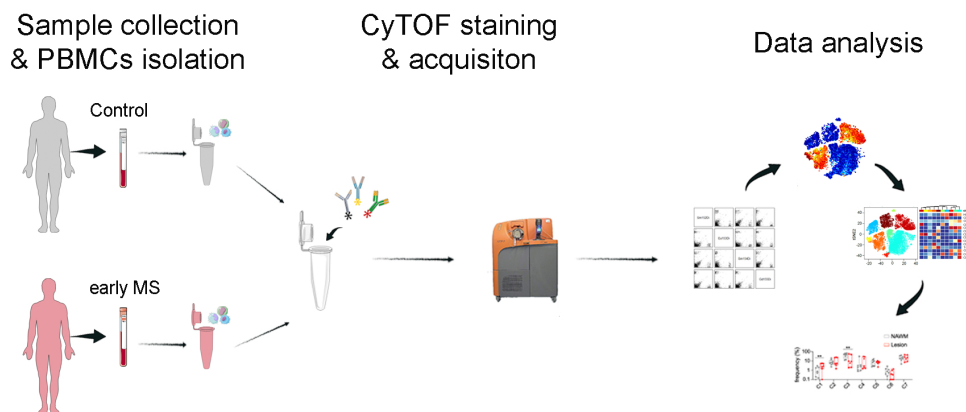
Figure 1. *PBMCs phenotypes from control and early MS patients analyzed using CyTOF. Whole blood was obtained from both donor groups followed by PBMCs isolation and sample storage. At the time of measurement all samples were barcoded and pooled together for CyTOF staining. Data analysis included de-barcoding, spillover compensation, dimensionality reduction visualization, unsupervised clustering and statistical testing.*

First, in order to visualize the high-dimensional data, we performed dimensionality reduction using the two-dimensional tSNE algorithm and obtained plots for both panels (Fig 2 A and D). Next, to better understand the cell composition in each sample, we identified six canonical PBMC populations: B cells, $CD4^+$ T cells, $CD8^+$ T cells, DN T cells, NK cells and myeloid cells and one population of $CD3^-CD4^+HLA-DR^+$ cells for Panel A (Fig 2 A-C). Panel B was designed with a focus on myeloid cell markers, and we used it to identify four major populations: myeloid cells, $HLA-DR^+$ lymphocytes, $CD4^+$ T cells and NK cells and $CD8^+$ cells (Fig 2 D-F). No difference in abundance of these major populations was found between conditions in either Panel A or Panel B (data not shown). For high resolution analysis of cell sub-populations, we performed clustering within each of this major PBMC populations.
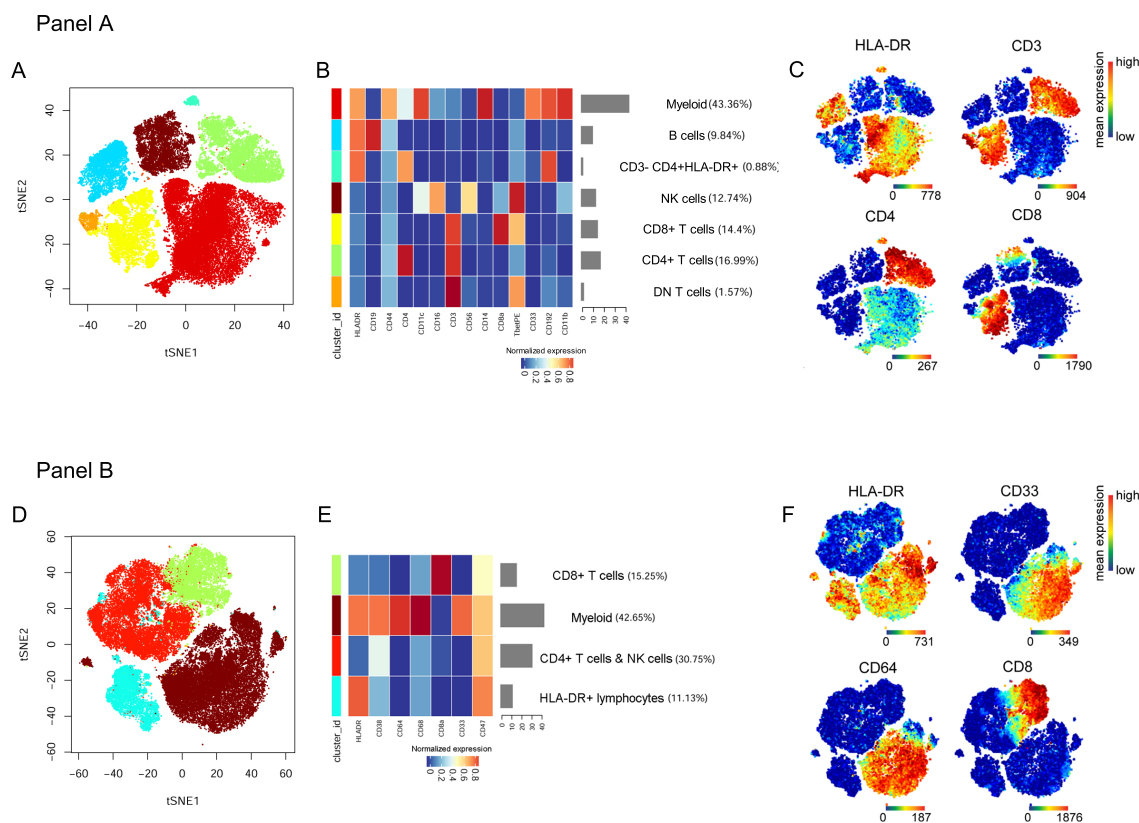
Figure 2. *Phenotypic characterization of PBMC populations using CyTOF.* ***A and D.*** *2D-tSNE representations (from a healthy control) from Panel A and Panel B respectively, each dot represents a cell, plots are colored according to marker expression.* ***B and E.*** *2D-tSNE plots colored for cluster identities form Panel A and B respectively.* ***C and F.*** *Heatmaps showing overall expression levels of markers used for cluster embedding (% of total cells) from Panel A and B respectively. Adapted from Böttcher C., et al. 2019[50].*

4.1.2 Detailed analysis of the lymphoid compartment in early MS reveals phenotypic alterations.

We subclustered each of the major populations from the lymphoid compartment previously identified. Within the CD4$^+$ T cells measured with Panel A, we identified two clusters that had a significantly different abundance between early MS patients and control donors: **CD4$^+$-C1** and **CD4$^+$-C13**. **CD4$^+$-C1** had a lower abundance in early MS than controls and was characterized as CCR7^{lo}NFAT1^{hi}T-bet^{hi}, indicative of T helper 1 (Th1) phenotype. **CD4$^+$-C13** was more abundant in early MS than controls and was characterized as CCR7^{hi}CD95^{lo}NFAT1^{lo} (when compared with the remaining CD4$^+$ lymphoid clusters) indicating naïve T cell phenotype (Fig 3-A). With Panel B we found a small population of IL-6^{hi} within the mixed NK and CD4$^+$ T cell cluster that was significantly more abundant in early MS. Interestingly, IL-6 signaling in T cells has been linked to the induction of Th17 differentiation, which in turn has been proposed to have a crucial role in development of EAE and MS[64], however we did not have enough markers in our panels to discern the Th17 phenotype (Fig 3-B). In the CD8$^+$ T cell compartment, cluster **CD8$^+$-C5** had a significantly higher abundance in early MS and was characterized as CCR7^{hi}CD62L^{hi}NFAT1^{lo}T-bet^{lo} when compared with the rest of the CD8$^+$ T cell clusters, suggesting that it is composed of naïve T cells (Fig 3-C). Within the DN T cell population two clusters had difference in abundance: **DN-C2** ADRP^{lo}T-bet^{lo} (higher abundance in early MS) and **DN-C3** T-bet^{hi}(lower abundance in early MS) which differed from the rest of DN clusters by ADRP and T-bet expression(Fig 3-D).

As to the B cell compartment, we identified a small subpopulation, **CD19-C2** with high expression of CD62L, which was enriched in MS patients (Fig 3-E). And a small subpopulation of the HLA-DR$^+$ lymphocytes with high expression of MIPβ^{hi} (**HLA-DR$^+$-C7**), presumably containing B cells, was found to be significantly lower in early MS patients (Fig 3-F).
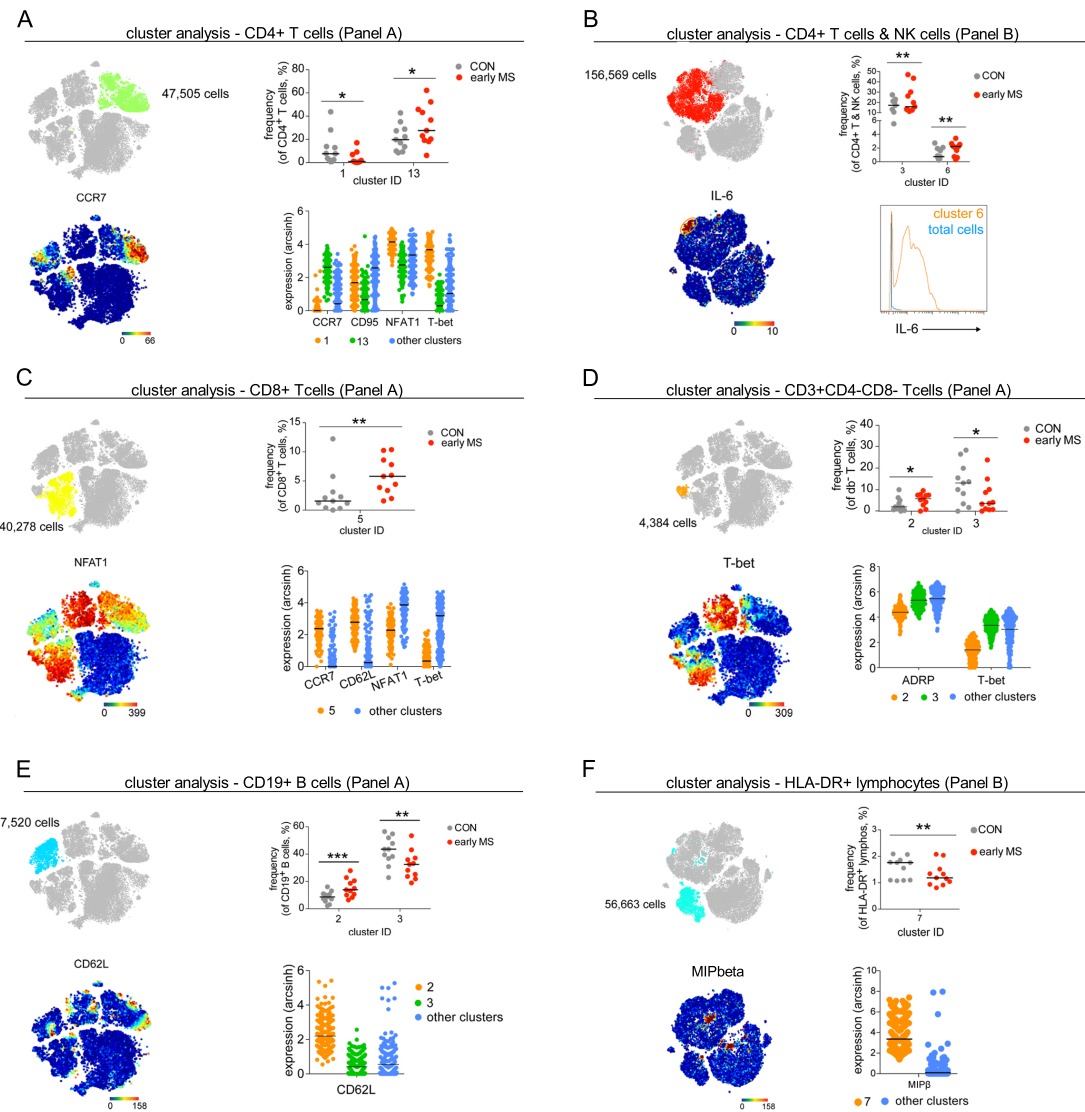
Figure 3. *Phenotypic changes in the lymphoid compartment. Subclustering analysis of the main PBMCs populations. For all panels, top-right 2D-tSNE plots colored for the cluster identity of the main PBMC population and representative marker expression (left plots, top and lower respectively). Frequencies for the significantly different abundance in subclusters between groups and median marker expression levels between the significantly different clusters and all other clusters (right plots, top and lower respectively). A P value < 0.05 at 10% FDR was considered statistically significant, determined using GLMM (*P < 0.05; **P < 0.01, unadjusted). Adapted from Böttcher C., et al. 2019[50].*

4.1.3 Small phenotypic changes in the myeloid cell composition in patients with early MS

Subclustering analysis of the major myeloid populations revealed no change in any cluster identified by Panel A. Panel B, which had markers specifically directed at detecting changes in the myeloid population, revealed a small subpopulation (**MC-C13**) of CD141^{hi}CD64$^-$CD68^{lo}CXCR3$^+$IRF8^{hi} dendritic cells (DCs) which was present at a significantly lower abundance in early MS as compared with controls. Interestingly, IRF8 expression in CD141$^+$ cells has been associated with a tolerogenic phenotype in mice[65].

4.2 Single-cell mass cytometry reveals complex myeloid cell composition in active lesions of progressive multiple sclerosis.

All results presented here have been previously published in Böttcher, C., et al. 2020[51].

4.2.1 Distinct composition of myeloid cells from active lesions and NAWM.

In this study we focused on determining the phenotypes of myeloid cells in active lesions and NAWM of patients with progressive MS. Each region was dissected by a neuropathologist under MRI guidance. Active lesion tissue was dissected based on macroscopic appearance. Myeloid cells were then isolated using a Percoll gradient followed by CD11b$^+$ MACS sorting, as established before[66]. In order to determine the different myeloid phenotypes present in the samples, we performed three different CyTOF experiments, analyzing a total of 74 antibodies. A schematic summary of the workflow used can be found in Figure 4.
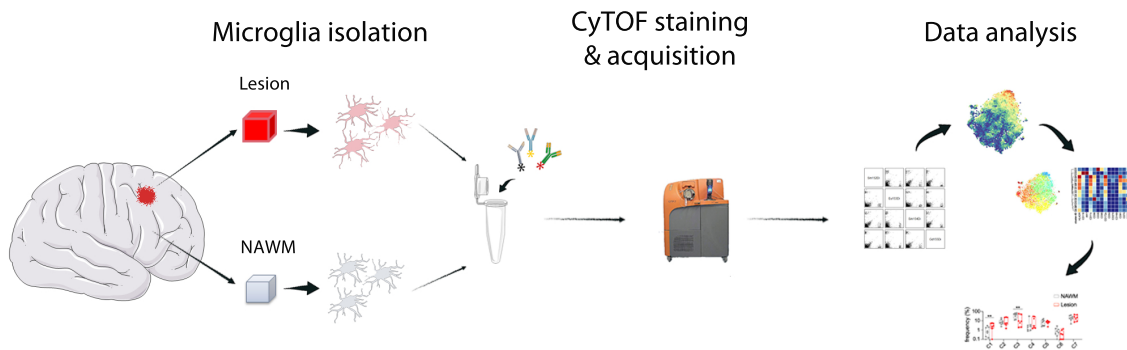
Figure 4. *Brain myeloid cell phenotyping using CyTOF. Myeloid cells were isolated from post-mortem human brain samples using CD11b MACS sorting. All cells were barcoded and pooled together for CyTOF staining and acquisition in three different experiments. Data analysis included sample de-barcoding, spillover compensation, 2D-tSNE plots for visualization, unsupervised clustering analysis and statistical testing.*

In *Exp-I* we used a panel of 36 antibodies, which were selected to characterize microglia and to detect the major circulating immune cell subsets including myeloid cells, T, B, and NK cells that may have remained after the CD11b enrichment. First, we pooled all cells from both groups and obtained 2D tSNE plots for visualization (Fig 5 A-B). We then performed unsupervised clustering analysis which revealed 12 clusters with distinct phenotypes (Fig 5 B and C).
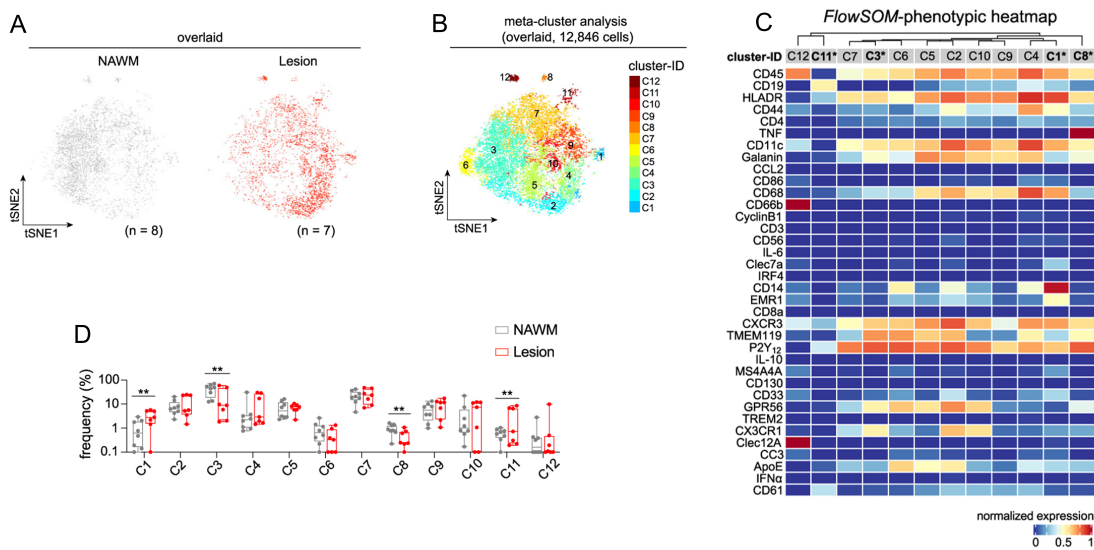
Figure 5. *Phenotypic characterization of myeloid cells from NAWM and active lesions of PMS patients. **A** Overlaid 2D-tSNE plots with cells from all donors from NAWM and active lesion, each dot represents a cell,*

As expected, most clusters showed typical microglial marker expression such as $P2Y_{12}$, TMEM119, CX3CR1, GPR56, HLA-DR^{dim} and CD11c^{dim} (Fig 5 C). Only 2 out of 12 clusters showed negative or lower expression of these markers. The first non-microglial cluster, **C12,** was defined as CD45$^+$CD66b^{hi}Clec12A^{hi}P2Y$_{12}^-$TMEM119$^-$ (Fig 5 C). The mixed expression of CD66b, a neutrophil marker, and Clec12A, a marker for peripheral myeloid cells, suggests that this population is comprised of a mixture of infiltrating immune cells. This cluster was found at a similar frequency between NAWM and active lesions (Fig 5 D). The other non-microglial cluster, **C11**, defined as P2Y$_{12}^{dim}$TMEM119$^-$CD19^{dim}HLA-DR$^+$CXCR3^{dim}CD62$^+$ (Fig 6 B-C) was a myeloid cluster with higher frequency in active lesion as compared with NAWM.

From the microglial compartment, we identified a cluster of homeostatic microglia **hoMG-C3** (Fig 6 A), defined by its expression of homeostatic markers, P2Y$_{12}^+$TMEM119$^+$CD11c^{dim}HLA-DR^{dim}CxCR3$^+$GPR56$^+$CX3CR1$^+$CD68^{dim}. **hoMG-C3** was either dim or negative for most of the other markers (Fig 6 C) and showed higher frequency than other clusters in NAWM although it was significantly lower in active lesion (Fig 6 A). **C8** was also significantly lower in active lesions as compared to NAWM and had a similar phenotype to the **hoMG-C3** cluster, except for a significative increase in TNF expression and a slight decrease in TMEM119 (Fig 6 A and C). **C1** was present at a higher abundance in active lesions and was further characterized as P2Y$_{12}^+$TEM119^{dim}CD11c$^+$ HLA-DR^{hi}CXCR3$^+$CD68^{hi}CD14^{hi}. High expression of CD68, HLA-DR[42] and CD14[67] clearly indicated an activated microglia phenotype[42].
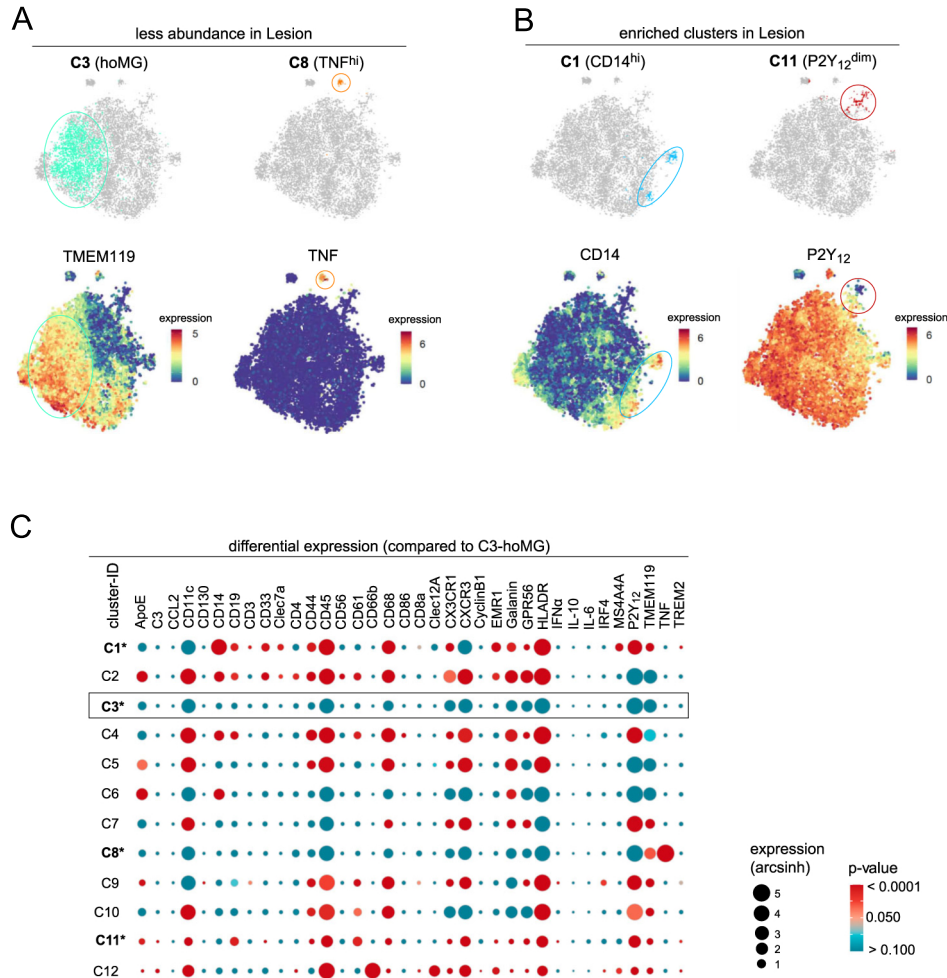
Figure 6. *Differences in abundance of myeloid clusters in Exp-I. **A** 2D-tSNE plots of the less abundant cluster in lesion (hoMG-C3 and C8) colored for cluster identities and for marker expression. **B** 2D-tSNE plots of the lesion-associated clusters (C1 and C11) colored for cluster identities and for marker expression. **C** Balloon plot showing expression of all markers across all clusters in comparison to hoMG-C3. Tile size denotes expression level (arcsinh) and heat colors show p-value (range from < 0.0001 (red) to > 0.100 (green)). Adapted from Böttcher C., et al. 2020[51].*

To better characterize the phagocytic and inflammatory properties of myeloid cells from both regions we performed *Exp-II* and *III,* which included markers common to both experiments, referred to as *TYPE* markers, used to identify myeloid populations and to facilitate comparison between experiments. The rest of the markers, referred to as *STATE* markers, were included to detect different phagocytosis and inflammation-associated phenotypes in

the myeloid cells. Unsupervised clustering resulted in 12 distinct clusters per experiment and statistical testing for difference in cluster abundance between conditions identified three differentially abundant clusters per experiment (Fig 7 A-D). The homeostatic microglial clusters were identified as **hoMG-C6** (*Exp-II)* and **hoMG-C9** *(Exp-III),* as in *Exp-I,* both clusters had a significantly lower abundance in active lesions when compared with NAWM. Given the limitations in metal-channel availability to include the typical microglial markers $P2Y_{12}$ and TMEM119, both homeostatic clusters were identified as HLA-$DR^{dim}CD11c^{dim}CCR2^{lo/-}$. **C5** and **C1** (*Exp-II)* and **C3** and **C1** *(Exp-III)* (Fig 7 E-H) were enriched in active lesions and were characterized by *TYPE* makers as having positive to high expression of: HLA-DR, CD11c (indicative of an activated phenotype[42]) CD172a, CD91 and CD47. CD172a (SIRPα),the ligand of CD47, is identified as part of the "don't-eat-me" signal regulating myeloid inhibition[68]. CD91 in turn, is a scavenger-receptor involved in myelin clearance in MS[69]. In *Exp-II* both lesion-enriched clusters (**C3** and **C1**) showed positive to high expression of the *STATE* markers ABCA7, Galanin, CD56, NFAT, GLUT5, CD44 and AXL, among others (Fig 7 G). In *Exp-III*, both clusters showed positive to high expression of ABCA7, CD14, CD56, CD64, NFAT, and GATA6 among others (Fig. 7 H).
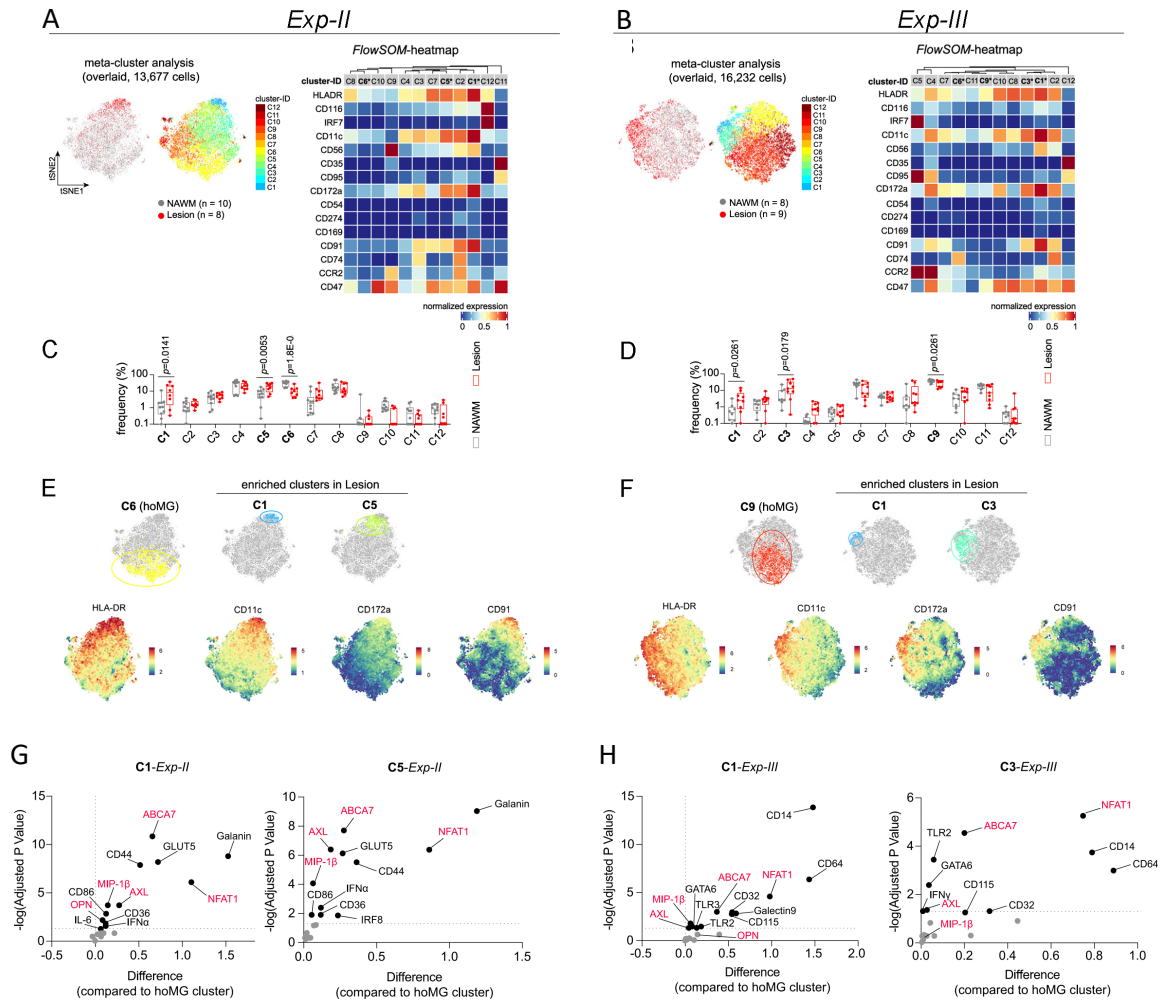
Figure 7. *Differences in abundance of myeloid clusters in Exp-II and Exp-III.* **A-B** *overlaid 2D-tSNE plots with all cells colored by group (NAWM and Lesion) or by cluster identities. Phenotypic heatmaps with overall marker expression per cluster. Asterisk denotes differentially abundant clusters.* **C-D** *Statistical analysis of cluster frequencies between NAWM and Lesion. An FDR-adjusted p value < 0.05 was considered statistically significant, determined using GLMM (*p <0.05; **p < 0.01, adjusted).* **E-F** *2D-tSNE plots of differentially abundant clusters colored by cluster ID and marker expression.* **G-H** *Volcano plots show differential expression (in comparison to hoMG) of STATE markers in significantly enriched microglial clusters. Black dots indicate significantly different expressed markers, whereas the grey dots are non-significant markers. Markers labelled in red are determined in both Exp-II and Exp-III. Two-tailed, unpaired t-test followed a correction for multiple comparisons using the Holm-Šídák method. p-value < 0.05 is considered statistically significant. The X axis plots the difference in mean expression between the significantly enriched clusters and the hoMG cluster. A dotted grid line is shown at X = 0, no difference. The Y axis plots the multiplicity adjusted p-value (−log) tested using two-tailed, unpaired t-test. A dotted grid line is shown at Y = −log (0.05), no statistical significance. Adapted from Böttcher C., et al. 2020[51].*

4.2.2 IMC partially corroborates myeloid diversity in active lesions

In order to validate the results obtained with CyTOF, we performed IMC on FFPE-TMA's from the same donors. IMC was performed using a panel of 13 antibodies, including those analyzed in *Exp-I,* on 1-3 sections per sample from all samples, from which $1mm^2$ per sample was acquired and analyzed. A schematic representation of the workflow used is depicted in Figure 8.
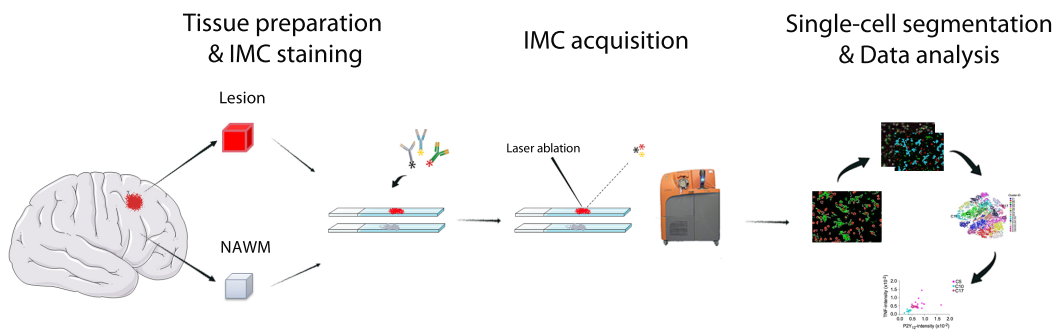
Figure 8. *Schematic representation of IMC analysis. For IMC analysis tissue blocks were embedded in paraffin and cut at a thickness of 5 µm with a microtome. Tissue sections were stained with metal-labelled antibodies following typical immunohistochemical protocols and measured. Data analysis included single-cell segmentation, high-dimensional image visualization, unsupervised clustering and statistical testing.*

After single-cell segmentation and phenograph clustering (Fig 9 B), we tested the difference in abundance of the different clusters between NAWM and Lesion (Fig 9 C). We observed a higher abundance of $TNF^+P2Y_{12}^+$ microglia in NAWM as compared with active lesion samples (Fig 9 D), confirming the results from **C8** in *Exp-I*. Among the five clusters that were significantly different in abundance between conditions we noted a higher abundance of clusters expressing $CD45^{+/hi}CD68^{+/hi}$ in active lesions as compared with NAWM (Fig 9 D), thus with a similar phenotype from that of **C1** from *Exp-I*. Of note, those clusters did not show a higher expression of HLA-DR, CD44, CD11c or CD14 as seen in the solution CyTOF experiments, but had a similar phenotype as that of **C11** from *Exp-I*. These results indicate that the clusters identified with IMC may be composed of mixed cells from both clusters.
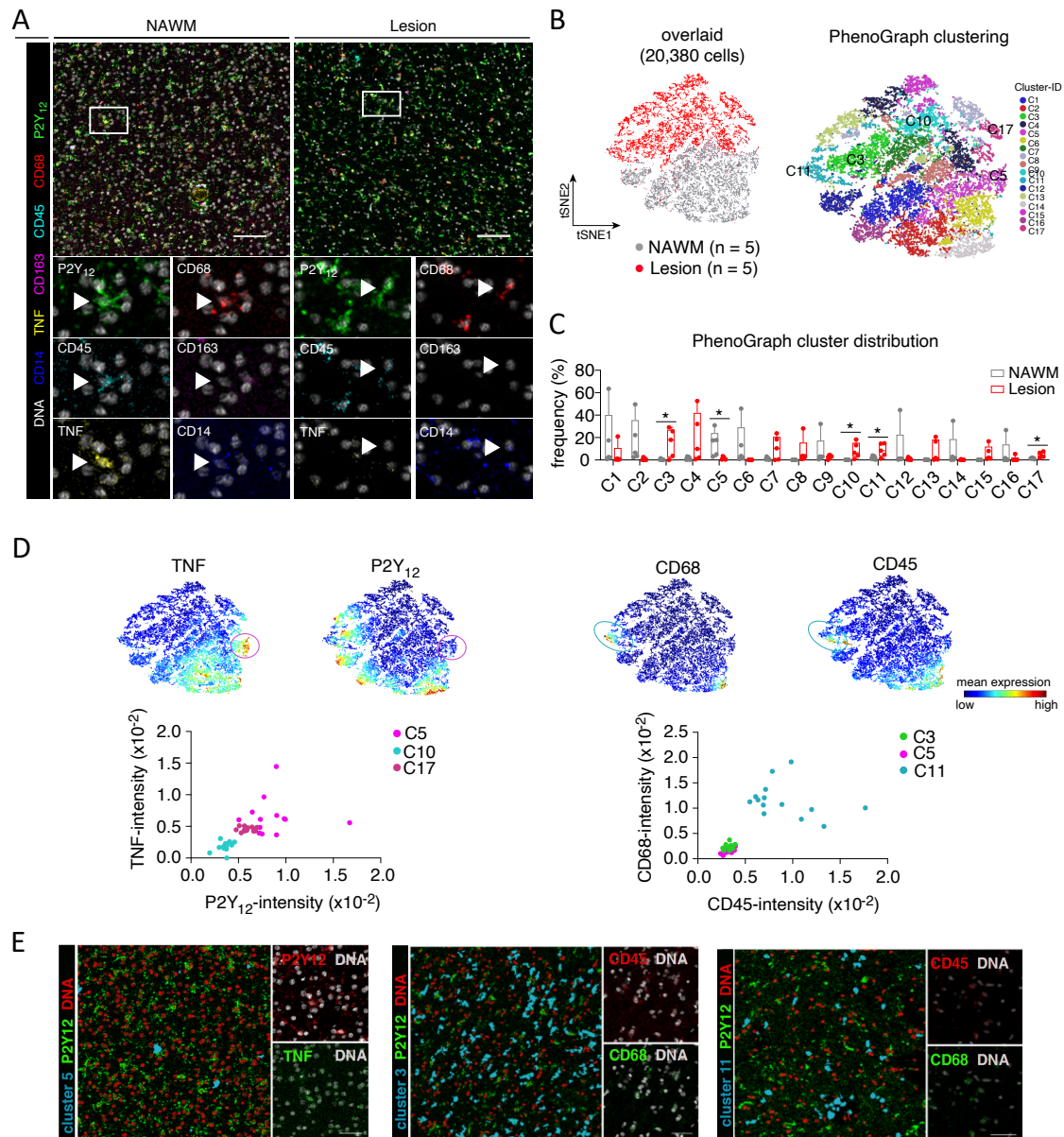
Figure 9. *IMC analysis results.* ***A*** *Representative images from imaging mass cytometry measurements on post-mortem human brain tissue from NAWM and Lesion from PMS patients (scale bar = 100 μm). Arrow head indicates P2Y$_{12}$$^+$ microglia, which are positive or negative for TNF.* ***B*** *Overlaid 2D-tSNE plot with all cells from all samples colored by group or cluster IID as determined by Phenograph clustering analysis.* ***C*** *Cluster frequencies between NAWM and Lesion. Five differentially abundant clusters (C3, C5, C10, C11 and C17) in lesions, compared to NAWM samples, were labelled with asterisk. Boxes extend from the 25th to 75th percentiles. Whisker plots show the min (smallest) and max (largest) values. The line in the box denotes the median. Each dot represents the value of each sample. Two-tailed, unpaired t-test. p-value < 0.05 (*) is considered statistically significant.* ***D*** *2D-tSNE plots with expression of different markers. Dot plot in the left showing correlations between TNF and P2Y$_{12}$ signal intensities of C5, C10 and C17. Right dot plot shows correlations between CD68 and CD45 signal intensities of C5, C3 and C11.* ***E*** *Representative IMC images of five differentially abundant clusters detected in lesion WM (scale bar = 50 μm). Adapted from Böttcher C., et al. 2020[51].*

4.3. Increased homeostatic phenotypic signature in microglia from major depressive disorder (MDD) patients

All results presented here have been previously published in Böttcher, C. et al. 2020[52]

4.3.1 Microglial homeostatic signatures are maintained in different brain regions of MDD patients

To elucidate the different myeloid profiles from post-mortem brains of patients with MDD we performed CyTOF analysis with two antibody panels comprising 35 antibodies/panel. We used isolated myeloid cells from four different brain regions: subventricular zone (SVZ), thalamus (THA), temporal lobe (GTS) and frontal lobe (GFM). Panel A was designed to identify the major immune populations from CNS cells and included a set of cytokine, chemokine, and other inflammatory markers. Panel B, instead, was designed to analyze functional and activity changes in the microglial subsets (in here only Panel A is shown). First, we checked for regional differences in myeloid signatures and, concordant with a previous study by our group[28], we observed distinct phenotypes from SVZ microglia as compared with THA, GFM and GTS (Fig 10). Mainly, we found an overall increased expression of HLA-DR, CD11c and CX3CR1 in SVZ from control donors (Fig 10 B). These changes were also detected in cells from MDD patients, except for lower levels of HLA-DR from SVZ on MDD patients, thus suggesting non-inflammatory profile in MDD myeloid cells.
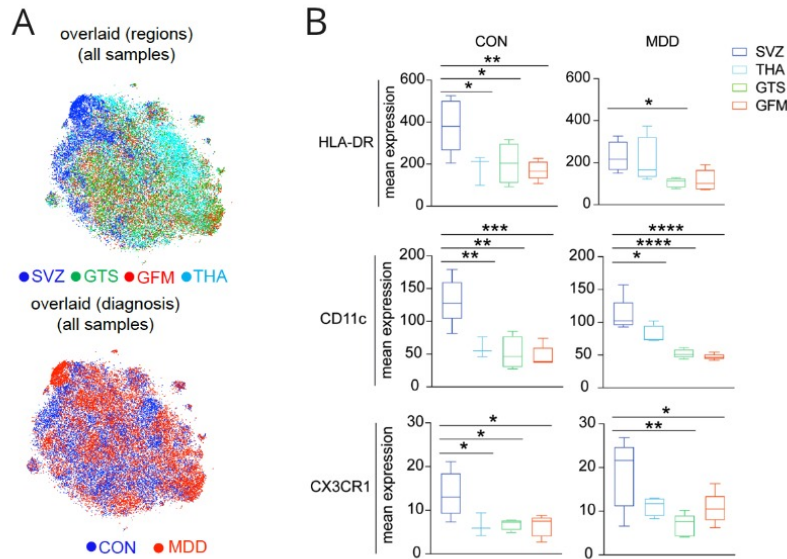
Figure 10. *CyTOF analysis of isolated myeloid cells from MDD patients and control donors. **A** 2D t-SNE plots from all cells, in the upper panel colored by region; in the lower panel colored by condition. **B** Boxplots show mean expression levels of selected markers in different brain regions for huMG from CON and MDD cases. Boxes extend from the 25th to 75th percentiles. Whisker plots show the min (smallest) and max (largest) values. The line in the box denotes the median. *P < 0.05, **P < 0.01, ***P < 0.001, ****P < 0.0001, one-way ANOVA testing with Dunnett correction for multiple comparisons. Adapted from Böttcher C., et al. 2020[52].*

For a more detailed characterization of the four different brain regions and to further understand possible phenotypic changes during MDD we performed unbiased clustering analysis (Fig 11). From the 8 clusters obtained, there was no difference in cluster abundance between MDD and controls, and only two clusters showed difference in abundance between SVZ and other regions. We recognized **C2**, low abundant in SVZ, as the main microglial cluster by the high expression of $P2Y_{12}$ and TMEM119 and low expression of HLA-DR and CD68 (Fig 11 A). **C3**, composed of cells with high expression of $P2Y_{12}$, TMEM119, HLA-DR and CD68, indicative of an activated phenotype, was enriched in SVZ. Thus, we could further confirm heterogeneity of microglial phenotypes between brain regions. In both **C2** and **C3** expression of $P2Y_{12}$ and TMEM119 was higher in MDD and expression of HLA-DR and CD68 was lower in MDD as compared with controls, showing an increased homeostatic signature in microglial cells from MDD patients (Fig 11 C). Interestingly, we also found increased levels of CD195 (CCR5) in MDD as compared with controls. In contrast, the macrophage cluster **C8** identified as $CD206^{hi}P2Y_{12}^{lo}TMEM119^{lo}$, showed an increase in expression of HLA-DR, TMEM119 and CD91 (low-density lipoprotein receptor-related protein 1 [LRP1]) in MDD cases as compared with controls (Fig 11 C). Furthermore, all

clusters showed comparable levels of other inflammatory markers such as IL-1β, IL-6, TNF, MIP- 1β (CCL4), IL-10, and MCP-1 (CCL2) between MDD and controls (Fig 11 C).
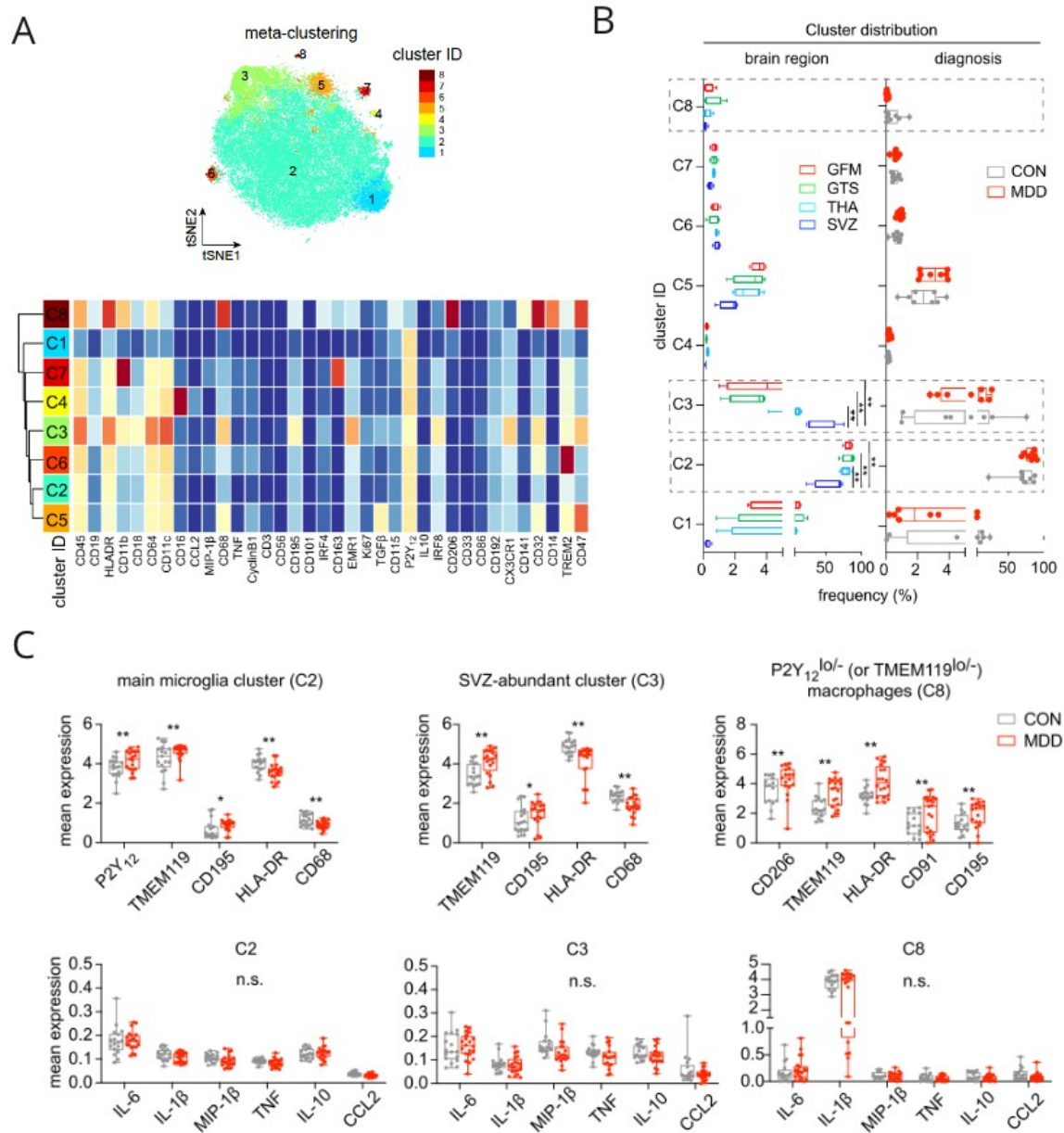
Figure 11. Unsupervised clustering analysis. A Overlaid 2D-tSNE plots colored by cluster identity and the corresponding phenotypic heatmaps. B Boxplots showing cluster distribution across regions (SVZ, THA, GTS and GFM) and between conditions (CON and MDD). Whisker plots show the min (smallest) and max (largest) values. A dot indicates the frequency (%) of an individual sample. The line in the box denotes the median. **P < 0.01, multiple t-test with FDR adjustment (at 10% using the Benjamini–Krieger–Yekutieli procedure). C Boxplots showing markers with differential expression (arcsinh) between CON and MDD for clusters C2, C3 and CD8. A dot indicates the mean expression of an individual sample. *P < 0.05, **P < 0.01, multiple t-test with FDR adjustment (at 10% using the Benjamini-Krieger-Yekutieli procedure. Adapted from Böttcher C., et al. 2020[52].

Overall we have shown a strong homeostatic signature in microglia from MDD patients, which is in contrast with the changes seen in microglia isolated from PMS patients[51]. Furthermore, we have confirmed the regional microglial differences between SVZ and THA, GTS and GFM and we have seen that these regional differences remain unchanged during MDD.

5. Discussion

In the three studies presented here, single-cell mass cytometry was used to deeply characterize the protein phenotypes of myeloid cells from patients at early and late stages of MS and in MDD. The results shown here have demonstrated the complexity of the disease and the heterogeneity of myeloid phenotypes in MS patients which can help understand the role of these cells in the disease. Furthermore, we have shown that myeloid cells in the brains of MDD patients display a homeostatic signature, in contrast with previous reports suggesting a neuroinflammatory signature during MDD.

5.1 Phenotypical changes in PBMCs in early MS

The study of PBMC phenotypes using CyTOF led to the discovery of several changes in composition of the lymphoid compartment from early MS patients as compared with control donors. These changes were more prominent in several T cell subsets, underscoring the high impact of these cells in the pathology. Among our results, we show an overall increase in $CCR7^+CD4^+$ and $CCR7^+CD62L^+CD8^+$ T cell clusters in early MS. CCR7 and CD62L are recognized homing receptors for secondary lymphoid organs and markers of naïve T cell phenotype[70]. Both markers have also been recognized as part of the central memory T cell (T_{CM}) phenotype[71], however, markers to distinguish between this two populations such as CD45RA and CD45RO were missing in our panels. T_{CM} are key players of the adaptive immune system by conferring immediate response upon antigenic stimulation, they rapidly home to secondary lymphoid organs where they proliferate and differentiate into effector

cells[72]. Higher levels of T_{CM} have been reported in blood from MS patients and it is speculated that increase of T_{CM} is a mechanism of maintenance of MS[73]. Interestingly, depletion of CCR7 in CD4+ T cells in EAE mice leads to impaired induction of autoimmunity[74]. We also saw an overall decrease in NFAT^hiT-bet^hi CD4+ T cells in patients with early MS. NFAT is an important regulator of T cell immune responses, among its target genes is the regulation of the lineage specific transcription factor T-bet which in turn regulates transition to T helper 1 lineage[75]. Th1 CD4+ T cells have been strongly correlated with MS, these cells typically secrete IFN -γ and TNF which is believed to increase immune activation in the CNS by inducing further release of pro-inflammatory mediators and enhancing antigen presentation[76]. Furthermore, NFAT has been identified as a target for autoimmune disease treatment, and it has been reported that pharmaceutical inhibition of NFAT ameliorated EAE by inhibiting Th1 and Th17 cells but not Treg cells[77]. We also detected an increase in a mixed NK - T cell cluster with high expression of IL-6 in early MS patients. IL-6 is a known modulator of immune responses although mainly secreted by antigen presenting cells. Elevated levels of IL-6 have been observed in CSF[78] and plasma[79] of patients with MS, even from an early stage in the disease, and have shown positive correlation with disease severity[78].

As for the myeloid compartment, even though antibody Panel B was specifically designed to detect major changes in the myeloid population, we only detected one minor change within the DC population. These results are concordant with other studies showing low variations in the overall population of monocytes between patients at different stages of MS (including CIS) and controls[81,82]. Nonetheless, these studies report changes in marker expression within the non-classical monocyte subsets, such as lower HERVs (not present in our panels) and changes in the abundance of non-classical monocytes at later stages of the disease[81,82]. The lower abundance of CD141+DCs found in our study is in contrast with one previous study showing increased abundance of these cells in PBMCs from CIS patients using flow cytometry[83]. In order to address the suitability of our panel design to detect changes in myeloid subsets we also measured samples from patients with Crohn's disease[84] which showed a strong inflammatory phenotype in the myeloid compartment as compared with MS and control samples, concordant with previous reports.

5.2 Myeloid phenotypes in active lesions of PMS patients and MDD patients

In the second study, we have characterized the protein phenotypes of myeloid cells from active lesions vs. NAWM from PMS patients at the single-cell level using mass cytometry. Our results show an abundance of microglia in both lesion and NAWM and a shift from homeostatic microglia in NAWM to more activated profiles in active lesion. Cells present in lesion-associated clusters expressed markers related with myelin clearance and remyelination as well as markers related with inflammation. We consistently detected the same results along the three experiments, thus proving the reproducibility and consistency of the technique. The unsupervised data analysis approach enabled identification of 12 clusters with distinct phenotypic signatures, the multiplicity of microglial phenotypes identified possibly relates to a large array of functions for these cells in the disease.

In *Exp I*, we used two markers that enabled distinction between microglia and resident macrophages, $P2Y_{12}$[85] and TMEM119[86], the positivity for these two markers in the major population in both NAWM and active lesion indicates a majority of microglia present in both. However, there was an overall decrease in expression of these markers in lesions, as shown by a lower frequency of homeostatic microglia in lesion and a lower expression of TMEM119, $P2Y_{12}$, CX3CR1 and GPR56 in lesion-associated clusters, consistent with previous reports in MS[27,43,85] and mouse models of demyelination[27] and neurodegeneration[32]. In *Exp II* and *III,* we did not use specific microglia markers but microglia/macrophage markers HLA-DR, CD11c or CD172a, thus it was not possible to properly discern between the cell types. However, we can extract from the data in *Exp I* that the main populations were mostly composed of microglia cells.

We found that cells in lesion-associated clusters had an increased expression of markers involved in phagocytosis and pro-inflammatory signals including typical markers of microglia activation such as HLA-DR, CD68 or CD11c. Phagocytosis is a complex cell process that needs the tight regulation and cooperation of different types of receptors and signaling pathways, in the CNS it is mostly performed by resident macrophages and microglia. In the context of MS, phagocytosis ensures the proper clearing of myelin debris which is of key importance to allow axonal and oligodendrocyte regeneration[87]. Phagocytosis

and processing of different cholesterol products (such as those composing myelin) are also known to induce a pro-inflammatory phenotype in mciroglia[88]. Our results show high expression of phagocytosis-related molecules in cells from lesion-associated clusters including CD68, TLRs, HLA-DR, CD74, CD14, CD91 and ABCA7. TLR stimulation in mouse microglia induces activation and up-regulation of several molecules, including cytokines, co-stimulatory molecules and MHC-class II receptors[90]. HLA-DR (MHC-class II receptor) is typically used by APCs to present antigens to T cells and thus stimulates the adaptive arm of the immune response. Microglia express low levels of HLA-DR in homeostatic conditions, an upregulation in the expression of this molecule is a typical response to inflammation and usually considered as a marker of activation in many CNS pathologies including MS[27,44,91]. Furthermore, different HLA-DR haplotypes have been strongly associated with MS in genome wide studies[3,92]. A role for HLA-DR in antigen presentation by microglia in the context of MS has been challenged by recent studies in mice in which induction of EAE in mice harboring MHC class II-deficient microglia remained unaltered[93]. Furthermore, MHC class II molecules where also upregulated in the cuprizone demyelination mice model[94], which lacks T cell involvement, but had no apparent effect on the pathology, as MHC class II deficiency in microglia do not seem to affect de- or remyelination[94]. Interestingly, in the de and re-myelination associated microglia described with the cuprizone model, upregulation of MHC class II molecules is accompanied by increase in CD74 but no other co-stimulatory molecules such as CD80 or CD86[27,94], a pattern similar to that seen in our lesion-associated microglia, which show higher expression of HLA-DR and CD74 but no change in CD86 expression.

In *Exp II* and *III*, CD91 was shown to be upregulated in all lesion-associated clusters. CD91 (LRP1 or APOE receptor), is a scavenger receptor that is involved in myelin clearance and inflammatory response in MS[69]. We also saw increased expression in lesion of CD14 and ABCA7, a molecule associated with lipid metabolism and part of the cuprizone reacting microglial signature[94]. ABCA7's primary function is to regulate the transport of phospholipids and cholesterol but it is also involved in maintaining the homeostasis of the immune system. CD14 is also known for being the coreceptor of TLR4[67] and TLR2[96]. CD14 expression in microglia provides them with high sensitivity to LPS, more than other macrophages tested, and is known to induce cytokine secretion but also to prevent excessive

inflammatory reactions in the mouse CNS[67]. It is important to note that although TREM2 and ApoE have been suggested as the main mediators in the switch from homeostatic to neurodegenerative microglia in mice models of AD, ALS and MS[31,32] we did not see any changes in the expression of TREM2 or ApoE in any of the lesion-associated clusters.

Activation of phagocytosis is tightly linked with activation of the immune response in microglia. In our study we found up-regulation of several immune mediators in lesion-associated clusters, among them NFAT, AXL, SPP1, CD44, CD115 or CD172a. These results partially correlate with the DAM phenotype found in mouse models of neurodegeneration[32]. AXL is a member of the family of receptor tyrosine kinases with a role in regulation of the immune response, including regulation of cytokine secretion and in promoting the clearance of debris[98]. Studies in mice have evidenced that the levels of *Axl* expression rise when CNS homeostasis is broken, as in EAE or in cuprizone treated mice[99], where it regulates cytokine release and the clearance of debris[98]. The expression of AXL was also found higher in homogenates from MS lesions[99], concordant with our results. Furthermore, a recent study testing the potential of antibodies against AXL receptor (enhancing AXL function) for MS treatment showed promising results by decreasing EAE clinical scores as well as diminishing demyelination and inflammatory myeloid cells in the CNS[100]. SPP1 (also named osteopontin [OPN]) is a pro-inflammatory cytokine secreted by many immune cells including activated microglia and macrophages, among its functions in macrophages are regulation of migration, survival, phagocytosis and pro-inflammatory cytokine production[101]. High levels of SPP1 in CNS-resident myeloid cells have been found in different CNS conditions, including mouse models of neuroinflammation[27,39,102] and neurodegeneration[32,103], as well as in AD[104] and brains[102] , blood and CSF from MS patients correlating with disease severity[105]. Despite this, we did not detect changes in expression of some pro-inflammatory mediators usually linked to neuroinflammation such as CCL2 or IL-1β. We only found a small increase in expression in IL-6 in one of the lesion-associated clusters. We did see, however, a high increase in TNF expression in a NAWM-associated cluster. This result might be linked to a response of microglia in non-affected areas and a failure of lesion-associated microglia to promote remyelination in active lesions at late stages

of the disease, given the reports of TNF produced by microglia to promote oligodendrocyte proliferation and remyelination[106].

In addition to CyTOF, we also used IMC as a validation tool of our results. The IMC analysis in this thesis is among the first to apply the newly developed IMC technology to brain samples and the first to apply IMC in a larger cohort, as the two previous studies consisted of either one[107] or two samples[108]. We could confirm in-situ many of the findings resulted from the solution CyTOF experiments. For instance, we also saw an increased abundance of TNF$^+$ microglia in NAWM as compared with lesion and we observed an increase in frequency of activated microglia in lesion. It is important to note, however, that a direct comparison of the results between both technologies is still technically challenging.

Taken together our results suggest a multiplicity of myeloid responses in active lesions of PMS. The markers found to be highly expressed in cells from lesion-associated clusters are involved in multiple responses that range from mechanisms related to phagocytosis, promotion of inflammation or remyelination. These results indicate the coexistence of different cell populations, or cells in different activation states within the lesion milieu. This phenotypic range should be considered when designing new treatment strategies, as the fine modulation of myeloid phenotypes within the CNS could drive towards inflammation resolution but should not hinder the capacity of microglia to dispose of cellular debris needed for proper remyelination.

In contrast with the changes seen in microglia from active lesions of PMS patients we found that microglia from MDD patients have a non-inflammatory phenotypic signature, and furthermore all the microglial populations showed increased homeostatic signatures an even a decreased expression of HLA-DR and CD68 in the main microglia cluster in MDD as compared with controls. To our knowledge this is the first study to analyze microglia from MDD patients at the single-cell level using high-dimensional profiling. Although further studies with a bigger cohort are needed, our results challenge previews reports that suggested an increased microglial activation in brains of MDD patients, mainly relaying on TSPO ligand binding measured with PET[36] but are in-line with a recent microarray transcriptomic study showing no significant changes in MDD gene expression[109].

5.3 Future directions

It is important to note that the three studies described in this thesis consist of a snapshot in time and space of the myeloid cell compartments present in MS patients. The precise function and biological relevance of the populations ifound associated with MS remain to be investigated. In the first study on PBMCs in early MS, we could not detect major changes within the myeloid populations. This could be due to lack of specific antibodies to detect those changes or that changes in myeloid cells are not happening at such an early stage. Therefore, follow-up studies with expanded antibody panels or at later stages of the disease might provide relevant information and establish specific associations of these cells during disease progression. Nevertheless, it remains also to be determined whether or not these cells are more susceptible to insults. *Ex vivo* functional analysis will be required to investigate their responses under stimulation.

Regarding the results obtained on our second study, an assessment of a larger cohort could be useful in proving the extent of the changes shown here. Even though IMC is still a young technology, the possibilities of high-dimensional imaging acquisition could expand the understanding of how the different immune phenotypes studied here correlate and interact with their tissue microenvironment. Hence, further studies on PPMS patient samples using IMC including markers for other cell types with proposed roles in the disease could shed some light as to their function in disease progression. Lastly, a combination of different omics tools, testing the transcriptomic, proteomic and spatial relationships of myeloid cells at different disease stages would provide important information as to how these cells are regulated and cooperate with their specific environment at different pathological stages.

Bibliography

1. Filippi, M., Bar-Or, A., Piehl, F., Preziosa, P., Solari, A., Vukusic, S. & Rocca, M. A. Multiple sclerosis. *Nat. Rev. Dis. Prim.* **4**, 1–27 (2018).
2. Zalc, B. One hundred and fifty years ago Charcot reported multiple sclerosis as a new neurological disease. *Brain* **141**, 3482–3488 (2018).
3. Beecham, A. H., Patsopoulos, N. A., Xifara, D. K., Davis, M. F., Kemppinen, A., Cotsapas, C., Shah, T. S., McCauley, J. L., *et al.* Analysis of immune-related loci identifies 48 new susceptibility variants for multiple sclerosis. *Nat. Genet.* **45**, 1353–1362 (2013).
4. Dendrou, C. A., Fugger, L. & Friese, M. A. Immunopathology of multiple sclerosis. *Nat. Rev. Immunol.* **15**, 545–558 (2015).
5. Miller, D. H., Grossman, R. I., Reingold, S. C. & McFarland, H. F. The role of magnetic resonance techniques in understanding and managing multiple sclerosis. *Brain* **121**, 3–24 (1998).
6. Mahad, D. H., Trapp, B. D. & Lassmann, H. Pathological mechanisms in progressive multiple sclerosis. *Lancet Neurol.* **14**, 183–193 (2015).
7. Thompson, A. J., Banwell, B. L., Barkhof, F., Carroll, W. M., Coetzee, T., Comi, G., Correale, J., Fazekas, F., Filippi, M., Freedman, M. S., Fujihara, K., Galetta, S. L., Hartung, H. P., Kappos, L., Lublin, F. D., Marrie, R. A., Miller, A. E., Miller, D. H., Montalban, X., Mowry, E. M., Sorensen, P. S., Tintoré, M., Traboulsee, A. L., Trojano, M., Uitdehaag, B. M. J., Vukusic, S., Waubant, E., Weinshenker, B. G., Reingold, S. C. & Cohen, J. A. Diagnosis of multiple sclerosis: 2017 revisions of the McDonald criteria. *Lancet Neurol.* **17**, 162–173 (2018).
8. Comi, G. C. Early treatment. *Neurol. Sci.* **27**, 8–12 (2006).
9. Kuhlmann, T., Ludwin, S., Prat, A., Antel, J., Brück, W. & Lassmann, H. An updated histological classification system for multiple sclerosis lesions. *Acta Neuropathol.* **133**, 13–24 (2017).
10. Machado-Santos, J., Saji, E., Tröscher, A. R., Paunovic, M., Liblau, R., Gabriely, G., Bien, C. G., Bauer, J. & Lassmann, H. The compartmentalized inflammatory response in the multiple sclerosis brain is composed of tissue-resident CD8+ T lymphocytes and B cells. *Brain* **141**, 2066–2082 (2018).
11. Ajami, B., Bennett, J. L., Krieger, C., McNagny, K. M. & Rossi, F. M. V. Infiltrating monocytes trigger EAE progression, but do not contribute to the resident microglia pool. *Nat. Neurosci.* **14**, 1142–9 (2011).
12. Lassmann, H., Brück, W. & Lucchinetti, C. Heterogeneity of multiple sclerosis pathogenesis: Implications for diagnosis and therapy. *Trends Mol. Med.* **7**, 115–121 (2001).
13. Geissmann, F., Jung, S. & Littman, D. R. Blood Monocytes Consist of Two Principal Subsets with Distinct Migratory Properties. *Immunity* **19**, 71–82 (2003).
14. Guilliams, M., Mildner, A. & Yona, S. Developmental and Functional Heterogeneity of Monocytes. *Immunity* **49**, 595–613 (2018).
15. Mildner, A., Yona, S. & Jung, S. *A Close Encounter of the Third Kind. Monocyte-Derived Cells*. *Advances in Immunology* vol. 120 (Elsevier Inc., 2013).
16. Prinz, M. & Priller, J. Tickets to the brain: Role of CCR2 and CX3CR1 in myeloid cell entry in the CNS. *J. Neuroimmunol.* **224**, 80–84 (2010).

17. Mildner, A., MacK, M., Schmidt, H., Brück, W., Djukic, M., Zabel, M. D., Hille, A., Priller, J. & Prinz, M. CCR2 + Ly-6C hi monocytes are crucial for the effector phase of autoimmunity in the central nervous system. *Brain* **132**, 2487–2500 (2009).

18. Ajami, B., Samusik, N., Wieghofer, P., Ho, P. P., Crotti, A., Bjornson, Z., Prinz, M., Fantl, W. J., Nolan, G. P. & Steinman, L. Single-cell mass cytometry reveals distinct populations of brain myeloid cells in mouse neuroinflammation and neurodegeneration models. *Nat. Neurosci.* (2018) doi:10.1038/s41593-018-0100-x.

19. Prinz, M., Jung, S. & Priller, J. Microglia Biology: One Century of Evolving Concepts. *Cell* **179**, 292–311 (2019).

20. Sierra, A., de Castro, F., del Río-Hortega, J., Rafael Iglesias-Rozas, J., Garrosa, M. & Kettenmann, H. The "Big-Bang" for modern glial biology: Translation and comments on Pío del Río-Hortega 1919 series of papers on microglia. *Glia* **64**, 1801–1840 (2016).

21. Ginhoux, F., Greter, M., Leboeuf, M., Nandi, S., See, P., Gokhan, S., Mehler, M. F., Conway, S. J., Ng, L. G., Stanley, E. R., Samokhvalov, I. M. & Merad, M. Primitive Macrophages. *Science (80-.).* **701**, 841–845 (2010).

22. Réu, P., Khosravi, A., Bernard, S., Mold, J. E., Salehpour, M., Alkass, K., Perl, S., Tisdale, J., Possnert, G., Druid, H. & Frisén, J. The Lifespan and Turnover of Microglia in the Human Brain. *Cell Rep.* **20**, 779–784 (2017).

23. Sierra, A., Encinas, J. M., Deudero, J. J. P., Chancey, J. H., Enikolopov, G., Overstreet-Wadiche, L. S., Tsirka, S. E. & Maletic-Savatic, M. Microglia shape adult hippocampal neurogenesis through apoptosis-coupled phagocytosis. *Cell Stem Cell* **7**, 483–495 (2010).

24. Paolicelli, R. C., Bolasco, G., Pagani, F., Maggi, L., Scianni, M., Panzanelli, P., Giustetto, M., Ferreira, T. A., Guiducci, E., Dumas, L., Ragozzino, D. & Gross, C. T. Synaptic pruning by microglia is necessary for normal brain development. *Science (80-.).* **333**, 1456–1458 (2011).

25. Hong, S., Dissing-Olesen, L. & Stevens, B. New insights on the role of microglia in synaptic pruning in health and disease. *Curr. Opin. Neurobiol.* **36**, 128–134 (2016).

26. Grabert, K., Michoel, T., Karavolos, M. H., Clohisey, S., Kenneth Baillie, J., Stevens, M. P., Freeman, T. C., Summers, K. M. & McColl, B. W. Microglial brain regionâ 'dependent diversity and selective regional sensitivities to aging. *Nat. Neurosci.* **19**, 504–516 (2016).

27. Masuda, T., Sankowski, R., Staszewski, O., Böttcher, C., Amann, L., Scheiwe, C., Nessler, S., Kunz, P., van Loo, G., Coenen, V. A., Reinacher, P. C., Michel, A., Sure, U., Gold, R., Priller, J., Stadelmann, C. & Prinz, M. Spatial and temporal heterogeneity of mouse and human microglia at single-cell resolution. *Nature* **566**, 388–392 (2019).

28. Böttcher, C., Schlickeiser, S., Sneeboer, M. A. M., Kunkel, D., Knop, A., Paza, E., Fidzinski, P., Kraus, L., Snijders, G. J. L., Kahn, R. S., Schulz, A. R., Mei, H. E., Hol, E. M., Siegmund, B., Glauben, R., Spruth, E. J., de Witte, L. D. & Priller, J. Human microglia regional heterogeneity and phenotypes determined by multiplexed single-cell mass cytometry. *Nat. Neurosci.* **22**, 78–90 (2019).

29. Ransohoff, R. M. A polarizing question: do M1 and M2 microglia exist? *Nat. Neurosci.* **19**, 987–91 (2016).

30. del Río-Hortega, P. El 'tercer elemento' de los centros nerviosos. I. La microglia en estado normal. *Bol Soc Esp Biol* **1919**, 67–82.

31.   Keren-Shaul, H., Spinrad, A., Weiner, A., Matcovitch-Natan, O., Dvir-Szternfeld, R., Ulland, T. K., David, E., Baruch, K., Lara-Astaiso, D., Toth, B., Itzkovitz, S., Colonna, M., Schwartz, M. & Amit, I. A Unique Microglia Type Associated with Restricting Development of Alzheimer's Disease. *Cell* **169**, 1276-1290.e17 (2017).

32.   Krasemann, S., Madore, C., Cialic, R., Baufeld, C., Calcagno, N., El Fatimy, R., Beckers, L., O'Loughlin, E., Xu, Y., Fanek, Z., Greco, D. J., Smith, S. T., Tweet, G., Humulock, Z., Zrzavy, T., Conde-Sanroman, P., Gacias, M., Weng, Z., Chen, H., Tjon, E., Mazaheri, F., Hartmann, K., Madi, A., Ulrich, J. D., Glatzel, M., Worthmann, A., Heeren, J., Budnik, B., Lemere, C., Ikezu, T., Heppner, F. L., Litvak, V., Holtzman, D. M., Lassmann, H., Weiner, H. L., Ochando, J., Haass, C. & Butovsky, O. The TREM2-APOE Pathway Drives the Transcriptional Phenotype of Dysfunctional Microglia in Neurodegenerative Diseases. *Immunity* **47**, 566-581.e9 (2017).

33.   Consortium, T. N. and P. A. S. of the P. G. Psychiatric genome-wide association study analyses implicate neuronal, immune and histone pathways. *Nat. Neurosci.* **18**, 199–209 (2015).

34.   Wray, N. R., Ripke, S., Mattheisen, M., Trzaskowski, M., Byrne, E. M., Abdellaoui, A., Adams, M. J., Sullivan, P. F., *et al.* Genome-wide association analyses identify 44 risk variants and refine the genetic architecture of major depression. *Nat. Genet.* **50**, 668–681 (2018).

35.   Steiner, J., Bielau, H., Brisch, R., Danos, P., Ullrich, O., Mawrin, C., Bernstein, H. G. & Bogerts, B. Immunological aspects in the neurobiology of suicide: Elevated microglial density in schizophrenia and depression is associated with suicide. *J. Psychiatr. Res.* **42**, 151–157 (2008).

36.   Setiawan, E., Wilson, A. A., Mizrahi, R., Rusjan, P. M., Miler, L., Rajkowska, G., Suridjan, I., Kennedy, J. L., Rekkas, V., Houle, S. & Meyer, J. H. Increased Translocator Protein Distribution Volume, A Marker of Neuroinflammation, in the Brain During Major Depressive Episodes. *JAMA Psychiatry* **72**, 268–275 (2016).

37.   Hasselmann, H., Bellmann-Strobl, J., Ricken, R., Oberwahrenbrock, T., Rose, M., Otte, C., Adli, M., Paul, F., Brandt, A. U., Finke, C. & Gold, S. M. Characterizing the phenotype of multiple sclerosis-associated depression in comparison with idiopathic major depression. *Mult. Scler.* **22**, 1476–1484 (2016).

38.   Mrdjen, D., Pavlovic, A., Hartmann, F. J., Schreiner, B., Utz, S. G., Leung, B. P., Lelios, I., Heppner, F. L., Kipnis, J., Merkler, D., Greter, M. & Becher, B. High-Dimensional Single-Cell Mapping of Central Nervous System Immune Cells Reveals Distinct Myeloid Subsets in Health, Aging, and Disease. *Immunity* **48**, 380-395.e6 (2018).

39.   Jordão, M. J. C., Sankowski, R., Brendecke, S. M., Sagar, Locatelli, G., Tai, Y. H., Tay, T. L., Schramm, E., Armbruster, S., Hagemeyer, N., Groß, O., Mai, D., Çiçek, Ö., Falk, T., Kerschensteiner, M., Grün, D. & Prinz, M. Neuroimmunology: Single-cell profiling identifies myeloid cell subsets with distinct fates during neuroinflammation. *Science (80-.).* **363**, (2019).

40.   Davis, M. M. & Brodin, P. Rebooting Human Immunology. *Annu. Rev. Immunol.* **36**, 843–864 (2018).

41.   Lucchinetti, C., Bruck, W., Parisi, J., Scheithauer, B., Rodriguez, M. & Lassmann, H. Heterogeneity of multiple sclerosis lesions. *Ann. Neurol.* **47**, 707–717 (2000).

42.   Hendrickx, D. A. E., van Eden, C. G., Schuurman, K. G., Hamann, J. & Huitinga, I.

Staining of HLA-DR, Iba1 and CD68 in human microglia reveals partially overlapping expression depending on cellular morphology and pathology. *J. Neuroimmunol.* **309**, 12–22 (2017).

43. Zrzavy, T., Hametner, S., Wimmer, I., Butovsky, O., Weiner, H. L. & Lassmann, H. Loss of 'homeostatic' microglia and patterns of their activation in active multiple sclerosis. *Brain* **140**, 1900–1913 (2017).

44. Hendrickx, D. A. E., van Scheppingen, J., van der Poel, M., Bossers, K., Schuurman, K. G., van Eden, C. G., Hol, E. M., Hamann, J. & Huitinga, I. Gene expression profiling of multiple sclerosis pathology identifies early patterns of demyelination surrounding chronic active lesions. *Front. Immunol.* **8**, (2017).

45. Chattopadhyay, P. K., Hogerkorp, C. M. & Roederer, M. A chromatic explosion: The development and future of multiparameter flow cytometry. *Immunology* **125**, 441–449 (2008).

46. Herzenberg, L. A., Parks, D., Sahaf, B., Perez, O., Roederer, M. & Herzenberg, L. A. The history and future of the Fluorescence Activated Cell Sorter and flow cytometry: A view from Stanford. *Clin. Chem.* **48**, 1819–1827 (2002).

47. Bendall, S. C., Simonds, E. F., Qiu, P., Amir, E. D., Krutzik, P. O., Finck, R., Bruggner, R. V, Melamed, R., Trejo, A., Ornatsky, O. I., Balderas, R. S., Plevritis, S. K., Sachs, K., Pe, D., Tanner, S. D. & Nolan, G. P. Single-Cell Mass Cytometry of Differential. *Science (80-.).* **332**, 687–695 (2011).

48. Fernández-Zapata, C., Leman, J. K. H., Priller, J. & Böttcher, C. The use and limitations of single-cell mass cytometry for studying human microglia function. *Brain Pathol.* 1–14 (2020) doi:10.1111/bpa.12909.

49. Giesen, C., Wang, H. A. O., Schapiro, D., Zivanovic, N., Jacobs, A., Hattendorf, B., Schüffler, P. J., Grolimund, D., Buhmann, J. M., Brandt, S., Varga, Z., Wild, P. J., Günther, D. & Bodenmiller, B. Highly multiplexed imaging of tumor tissues with subcellular resolution by mass cytometry. *Nat. Methods* **11**, 417–422 (2014).

50. Böttcher, C., Fernández-Zapata, C., Schlickeiser, S., Kunkel, D., Schulz, A. R., Mei, H. E., Weidinger, C., Gieß, R. M., Asseyer, S., Siegmund, B., Paul, F., Ruprecht, K. & Priller, J. Multi-parameter immune profiling of peripheral blood mononuclear cells by multiplexed single-cell mass cytometry in patients with early multiple sclerosis. *Sci. Rep.* **9**, 1–14 (2019).

51. Böttcher, C., Poel, M. Van Der, Fernández-zapata, C., Schlickeiser, S., Leman, J. K. H., Hsiao, C., Mizee, M. R., Vincenten, M. C. J. & Kunkel, D. Single-cell mass cytometry reveals complex myeloid cell composition in active lesions of progressive multiple sclerosis. **8**, 1–18 (2020).

52. Böttcher, C., Fernández-zapata, C., Snijders, G. J. L., Schlickeiser, S., Sneeboer, M. A. M., Kunkel, D., Witte, L. D. De & Priller, J. Single-cell mass cytometry of microglia in major depressive disorder reveals a non-in fl ammatory phenotype with increased homeostatic marker expression. *Transl. Psychiatry* 1–11 (2020) doi:10.1038/s41398-020-00992-2.

53. Böttcher, C., Fernández-Zapata, C., Schlickeiser, S., Kunkel, D., Schulz, A. R., Mei, H. E., Weidinger, C., Gieß, R. M., Asseyer, S., Siegmund, B., Paul, F., Ruprecht, K. & Priller, J. Multi-parameter immune profiling of peripheral blood mononuclear cells by multiplexed single-cell mass cytometry in patients with early multiple sclerosis. *Sci. Rep.* **9**, 19471 (2019).

54. Chevrier, S., Crowell, H. L., Zanotelli, V. R. T., Engler, S., Robinson, M. D. &

Bodenmiller, B. Compensation of Signal Spillover in Suspension and Imaging Mass Cytometry. *Cell Syst.* **6**, 612-620.e5 (2018).

55. (2013), R. C. T. R: A language and environment for statistical computing.

56. Nowicka, M., Krieg, C., Weber, L. M., Hartmann, F. J., Guglietta, S., Becher, B., Levesque, M. P., Robinson, M. D. & Finak, G. CyTOF workflow : differential discovery in high-throughput high-dimensional cytometry datasets [version 2 ; referees : 2 approved] Referee Status : (2017) doi:10.12688/f1000research.11622.1.

57. Van Gassen, S., Callebaut, B., Van Helden, M. J., Lambrecht, B. N., Demeester, P., Dhaene, T. & Saeys, Y. FlowSOM: Using self-organizing maps for visualization and interpretation of cytometry data. *Cytom. Part A* **87**, 636–645 (2015).

58. Wilkerson, M. D. & Hayes, D. N. ConsensusClusterPlus: A class discovery tool with confidence assessments and item tracking. *Bioinformatics* **26**, 1572–1573 (2010).

59. Monti, S., Tamayo, P., Mesirov, J. & Golub, T. Consensus clustering: A resampling-based method for class discovery and visualization of gene expression microarray data. *Mach. Learn.* **52**, 91–118 (2003).

60. Berg, S., Kutra, D., Kroeger, T., Straehle, C. N., Kausler, B. X., Haubold, C., Schiegg, M., Ales, J., Beier, T., Rudy, M., Eren, K., Cervantes, J. I., Xu, B., Beuttenmueller, F., Wolny, A., Zhang, C., Koethe, U., Hamprecht, F. A. & Kreshuk, A. Ilastik: Interactive Machine Learning for (Bio)Image Analysis. *Nat. Methods* **16**, 1226–1232 (2019).

61. Carpenter, A. E., Jones, T. R., Lamprecht, M. R., Clarke, C., Kang, I. H., Friman, O., Guertin, D. A., Chang, J. H., Lindquist, R. A., Moffat, J., Golland, P. & Sabatini, D. M. CellProfiler: Image analysis software for identifying and quantifying cell phenotypes. *Genome Biol.* **7**, (2006).

62. Schapiro, D., Jackson, H. W., Raghuraman, S., Fischer, J. R., Zanotelli, V. R. T., Schulz, D., Giesen, C., Catena, R., Varga, Z. & Bodenmiller, B. HistoCAT: Analysis of cell phenotypes and interactions in multiplex image cytometry data. *Nat. Methods* **14**, 873–876 (2017).

63. Weber, L. M., Nowicka, M., Soneson, C. & Robinson, M. D. diffcyt: Differential discovery in high-dimensional cytometry via high-resolution clustering. *bioRxiv* 349738 (2019) doi:10.1101/349738.

64. Dos Passos, G. R., Sato, D. K., Becker, J. & Fujihara, K. Th17 Cells Pathways in Multiple Sclerosis and Neuromyelitis Optica Spectrum Disorders: Pathophysiological and Therapeutic Implications. *Mediators Inflamm.* **2016**, (2016).

65. Orabona, C., Puccetti, P., Vacca, C., Bicciato, S., Luchini, A., Fallarino, F., Bianchi, R., Velardi, E., Perruccio, K., Velardi, A., Bronte, V., Fioretti, M. C. & Grohmann, U. Toward the identification of a tolerogenic signature in IDO-competent dendritic cells. *Blood* **107**, 2846–2854 (2006).

66. Mizee, M. R., Miedema, S. S. M., van der Poel, M., Adelia, Schuurman, K. G., van Strien, M. E., Melief, J., Smolders, J., Hendrickx, D. A., Heutinck, K. M., Hamann, J. & Huitinga, I. Isolation of primary microglia from the human post-mortem brain: effects of ante- and post-mortem variables. *Acta Neuropathol. Commun.* **5**, 16 (2017).

67. Janova, H., Böttcher, C., Holtman, I. R., Regen, T., van Rossum, D., Götz, A., Ernst, A. S., Fritsche, C., Gertig, U., Saiepour, N., Gronke, K., Wrzos, C., Ribes, S., Rolfes, S., Weinstein, J., Ehrenreich, H., Pukrop, T., Kopatz, J., Stadelmann, C., Salinas-Riester, G., Weber, M. S., Prinz, M., Brück, W., Eggen, B. J. L., Boddeke,

H. W. G. M., Priller, J. & Hanisch, U. K. CD14 is a key organizer of microglial responses to CNS infection and injury. *Glia* **64**, 635–649 (2016).

68. Barclay, A. N. & Van Den Berg, T. K. The interaction between signal regulatory protein alpha (SIRPα) and CD47: Structure, function, and therapeutic target. *Annu. Rev. Immunol.* **32**, 25–50 (2014).

69. Chuang, T. Y., Guo, Y., Seki, S. M., Rosen, A. M., Johanson, D. M., Mandell, J. W., Lucchinetti, C. F. & Gaultier, A. LRP1 expression in microglia is protective during CNS autoimmunity. *Acta Neuropathol. Commun.* **4**, 68 (2016).

70. Britschgi, M. R., Link, A., Lissandrin, T. K. A. & Luther, S. A. Dynamic Modulation of CCR7 Expression and Function on Naive T Lymphocytes In Vivo. *J. Immunol.* **181**, 7681–7688 (2008).

71. Unsoeld, H. & Pircher, H. Complex Memory T-Cell Phenotypes Revealed by Coexpression of CD62L and CCR7. *J. Virol.* **79**, 4510–4513 (2005).

72. Sallusto, F., Geginat, J. & Lanzavecchia, A. Central memory and effector memory T cell subsets: Function, generation, and maintenance. *Annu. Rev. Immunol.* **22**, 745–763 (2004).

73. Liu, G. Z., Fang, L. B., Hjelmström, P. & Gao, X. G. Increased CD8+ central memory T cells in patients with multiple sclerosis. *Mult. Scler.* **13**, 149–155 (2007).

74. Belikan, P., Bühler, U., Wolf, C., Pramanik, G. K., Gollan, R., Zipp, F. & Siffrin, V. CCR7 on CD4 + T Cells Plays a Crucial Role in the Induction of Experimental Autoimmune Encephalomyelitis . *J. Immunol.* **200**, 2554–2562 (2018).

75. Hermann-Kleiter, N. & Baier, G. NFAT pulls the strings during CD4+ T helper cell effector functions. *Blood* **115**, 2989–2997 (2010).

76. Kaskow, B. J. & Baecher-Allan, C. Effector t cells in multiple sclerosis. *Cold Spring Harb. Perspect. Med.* **8**, 1–14 (2018).

77. Lee, H. G., Kim, L. K. & Choi, J. M. NFAT-Specific Inhibition by dNP2-VIVITAmeliorates Autoimmune Encephalomyelitisby Regulation of Th1 and Th17. *Mol. Ther. - Methods Clin. Dev.* **16**, 32–41 (2020).

78. Stampanoni Bassi, M., Iezzi, E., Drulovic, J., Pekmezovic, T., Gilio, L., Furlan, R., Finardi, A., Marfia, G. A., Sica, F., Centonze, D. & Buttari, F. IL-6 in the Cerebrospinal Fluid Signals Disease Activity in Multiple Sclerosis. *Front. Cell. Neurosci.* **14**, 1–7 (2020).

79. Krei, K., Fredrikson, S., Fontana, A. & Link, H. Interleukin-6 is elevated in plasma in multiple sclerosis. *J. Neuroimmunol.* **31**, 147–153 (1991).

80. Krzysiek, R., Lefèvre, E. A., Zou, W., Foussat, A., Bernard, J., Portier, A., Galanaud, P. & Richard, Y. Antigen receptor engagement selectively induces macrophage inflammatory protein-1α (MIP-1α) and MIP-1β chemokine production in human B cells. *J. Immunol.* **162**, 4455–4463 (1999).

81. Carstensen, M., Christensen, T., Stilund, M., Møller, H. J., Petersen, E. L. & Petersen, T. Activated monocytes and markers of inflammation in newly diagnosed multiple sclerosis. *Immunol. Cell Biol.* **98**, 549–562 (2020).

82. Gjelstrup, M. C., Stilund, M., Petersen, T., Møller, H. J., Petersen, E. L. & Christensen, T. Subsets of activated monocytes and markers of inflammation in incipient and progressed multiple sclerosis. *Immunol. Cell Biol.* **96**, 160–174 (2018).

83. Trend, S., Jones, A. P., Geldenhuys, S., Byrne, S. N., Fabis-Pedrini, M. J., Nolan, D., Booth, D. R., Carroll, W. M., Lucas, R. M., Kermode, A. G. & Hart, P. H. Evolving identification of blood cells associated with clinically isolated syndrome: Importance

of time since clinical presentation and diagnostic MRI. *Int. J. Mol. Sci.* **18**, (2017).

84. Ziegler, J. F., Böttcher, C., Letizia, M., Yerinde, C., Wu, H., Freise, I., Rodriguez-Sillke, Y., Stoyanova, A. K., Kreis, M. E., Asbach, P., Kunkel, D., Priller, J., Anagnostopoulos, I., Kühl, A. A., Miehle, K., Stumvoll, M., Tran, F., Fredrich, B., Forster, M., Franke, A., Bojarski, C., Glauben, R., Löscher, B. S., Siegmund, B. & Weidinger, C. Leptin induces TNFα-dependent inflammation in acquired generalized lipodystrophy and combined Crohn's disease. *Nat. Commun.* **10**, (2019).

85. Mildner, A., Huang, H., Radke, J., Stenzel, W. & Priller, J. P2Y12 receptor is expressed on human microglia under physiological conditions throughout development and is sensitive to neuroinflammatory diseases. *Glia* **65**, 375–387 (2017).

86. Bennett, M. L., Bennett, F. C., Liddelow, S. A., Ajami, B., Zamanian, J. L., Fernhoff, N. B., Mulinyawe, S. B., Bohlen, C. J., Adil, A., Tucker, A., Weissman, I. L., Chang, E. F., Li, G., Grant, G. A., Hayden Gephart, M. G. & Barres, B. A. New tools for studying microglia in the mouse and human CNS. *Proc. Natl. Acad. Sci. U. S. A.* **113**, E1738–E1746 (2016).

87. Hendrickx, D. A. E., Koning, N., Schuurman, K. G., Van Strien, M. E., Van Eden, C. G., Hamann, J. & Huitinga, I. Selective upregulation of scavenger receptors in and around demyelinating areas in multiple sclerosis. *J. Neuropathol. Exp. Neurol.* **72**, 106–118 (2013).

88. Loving, B. A. & Bruce, K. D. Lipid and Lipoprotein Metabolism in Microglia. *Front. Physiol.* **11**, 1–20 (2020).

89. Chistiakov, D. A., Killingsworth, M. C., Myasoedova, V. A., Orekhov, A. N. & Bobryshev, Y. V. CD68/macrosialin: Not just a histochemical marker. *Lab. Investig.* **97**, 4–13 (2017).

90. Olson, J. K. & Miller, S. D. Microglia Initiate Central Nervous System Innate and Adaptive Immune Responses through Multiple TLRs. *J. Immunol.* **173**, 3916–3924 (2004).

91. Hendrickx, D. A. E., van Eden, C. G., Schuurman, K. G., Hamann, J. & Huitinga, I. Staining of HLA-DR, Iba1 and CD68 in human microglia reveals partially overlapping expression depending on cellular morphology and pathology. *J. Neuroimmunol.* **309**, 12–22 (2017).

92. Fong, P., Boss, D., Yap, T., Tutt, A., Wu, P. & Mergui-Roelvink, M. Risk Alleles for Multiple Sclerosis Identified by a Genomewide Study. *N. Engl. J. Med.* **357**, 851–862 (2007).

93. Wolf, Y., Shemer, A., Levy-Efrati, L., Gross, M., Kim, J. S., Engel, A., David, E., Chappell-Maor, L., Grozovski, J., Rotkopf, R., Biton, I., Eilam-Altstadter, R. & Jung, S. Microglial MHC class II is dispensable for experimental autoimmune encephalomyelitis and cuprizone-induced demyelination. *Eur. J. Immunol.* **48**, 1308–1318 (2018).

94. Olah, M., Amor, S., Brouwer, N., Vinet, J., Eggen, B., Biber, K. & Boddeke, H. W. G. M. Identification of a microglia phenotype supportive of remyelination. *Glia* **60**, 306–321 (2012).

95. Aikawa, T., Ren, Y., Yamazaki, Y., Tachibana, M., Johnson, M. R., Anderson, C. T., Martens, Y. A., Holm, M. L., Asmann, Y. W., Saito, T., Saido, T. C., Fitzgerald, M. L., Bu, G. & Kanekiyo, T. ABCA7 haplodeficiency disturbs microglial immune responses in the mouse brain. *Proc. Natl. Acad. Sci. U. S. A.* **116**, 23790–23796

(2019).

96. Reed-Geaghan, E. G., Savage, J. C., Hise, A. G. & Landreth, G. E. CD14 and toll-like receptors 2 and 4 are required for fibrillar Aβ-stimulated microglial activation. *J. Neurosci.* **29**, 11982–11992 (2009).

97. Ma, B., Yu, J., Xie, C., Sun, L., Lin, S., Ding, J., Luo, J. & Cai, H. Toll-like receptors promote mitochondrial translocation of nuclear transcription factor nuclear factor of activated T-cells in prolonged microglial activation. *J. Neurosci.* **35**, 10799–10814 (2015).

98. Ray, A. K., DuBois, J. C., Gruber, R. C., Guzik, H. M., Gulinello, M. E., Perumal, G., Raine, C., Kozakiewicz, L., Williamson, J. & Shafit-Zagardo, B. Loss of Gas6 and Axl signaling results in extensive axonal damage, motor deficits, prolonged neuroinflammation, and less remyelination following cuprizone exposure. *Glia* **65**, 2051–2069 (2017).

99. Weinger, J. G., Brosnan, C. F., Loudig, O., Goldberg, M. F., Macian, F., Arnett, H. A., Prieto, A. L., Tsiperson, V. & Shafit-Zagardo, B. Loss of the receptor tyrosine kinase Axl leads to enhanced inflammation in the CNS and delayed removal of myelin debris during Experimental Autoimmune Encephalomyelitis. *J. Neuroinflammation* **8**, 1–18 (2011).

100. Dubois, J. C., Ray, A. K., Davies, P. & Shafit-zagardo, B. Anti-Axl antibody treatment reduces the severity of experimental autoimmune encephalomyelitis. **3**, 1–14 (2020).

101. Lund, S. A., Giachelli, C. M. & Scatena, M. The role of osteopontin in inflammatory processes. *J. Cell Commun. Signal.* **3**, 311–322 (2009).

102. Chabas, D. The Influence of the Proinflammatory Cytokine, Osteopontin, on Autoimmune Demyelinating Disease. *Science (80-.).* **294**, 1731–1735 (2001).

103. Sala Frigerio, C., Wolfs, L., Fattorelli, N., Thrupp, N., Voytyuk, I., Schmidt, I., Mancuso, R., Chen, W. T., Woodbury, M. E., Srivastava, G., Möller, T., Hudry, E., Das, S., Saido, T., Karran, E., Hyman, B., Perry, V. H., Fiers, M. & De Strooper, B. The Major Risk Factors for Alzheimer's Disease: Age, Sex, and Genes Modulate the Microglia Response to Aβ Plaques. *Cell Rep.* **27**, 1293-1306.e6 (2019).

104. Johnson, E. C. B., Dammer, E. B., Duong, D. M., Ping, L., Zhou, M., Yin, L., Higginbotham, L. A., Guajardo, A., White, B., Troncoso, J. C., Thambisetty, M., Montine, T. J., Lee, E. B., Trojanowski, J. Q., Beach, T. G., Reiman, E. M., Haroutunian, V., Wang, M., Schadt, E., Zhang, B., Dickson, D. W., Ertekin-Taner, N., Golde, T. E., Petyuk, V. A., De Jager, P. L., Bennett, D. A., Wingo, T. S., Rangaraju, S., Hajjar, I., Shulman, J. M., Lah, J. J., Levey, A. I. & Seyfried, N. T. Large-scale proteomic analysis of Alzheimer's disease brain and cerebrospinal fluid reveals early changes in energy metabolism associated with microglia and astrocyte activation. *Nat. Med.* **26**, 769–780 (2020).

105. Agah, E., Zardoui, A., Saghazadeh, A., Ahmadi, M., Tafakhori, A. & Rezaei, N. Osteopontin (OPN) as a CSF and blood biomarker for multiple sclerosis: A systematic review and meta-analysis. *PLoS One* **13**, 1–18 (2018).

106. Arnett, H. A., Mason, J., Marino, M., Suzuki, K., Matsushima, G. K. & Ting, J. P. Y. TNFα promotes proliferation of oligodendrocyte progenitors and remyelination. *Nat. Neurosci.* **4**, 1116–1122 (2001).

107. Ramaglia, V., Sheikh-Mohamed, S., Legg, K., Park, C., Rojas, O. L., Zandee, S., Fu, F., Ornatsky, O., Swanson, E. C., Pitt, D., Prat, A., McKee, T. D. & Gommerman, J.

L. Multiplexed imaging of immune cells in staged multiple sclerosis lesions by mass cytometry. *Elife* **8**, 1–29 (2019).

108. Park, C., Ponath, G., Levine-Ritterman, M., Bull, E., Swanson, E. C., De Jager, P. L., Segal, B. M. & Pitt, D. The landscape of myeloid and astrocyte phenotypes in acute multiple sclerosis lesions. *Acta Neuropathol. Commun.* **7**, 130 (2019).

109. Gandal, M. J., Zhang, P., Hadjimichael, E., Walker, R. L., Chen, C., Liu, S., Won, H., Van Bakel, H., Varghese, M., Wang, Y., Shieh, A. W., Haney, J., Parhami, S., Belmont, J., Kim, M., Losada, P. M., Khan, Z., Mleczko, J., Xia, Y., Dai, R., Wang, D., Yang, Y. T., Xu, M., Fish, K., Hof, P. R., Warrell, J., Fitzgerald, D., White, K., Jaffe, A. E., Peters, M. A., Gerstein, M., Liu, C., Iakoucheva, L. M., Pinto, D. & Geschwind, D. H. Transcriptome-wide isoform-level dysregulation in ASD, schizophrenia, and bipolar disorder. *Science (80-.).* **362**, (2018).

Statutory Declaration

I, María Camila Fernández Zapata, by personally signing this document in lieu of an oath, hereby affirm that I prepared the submitted dissertation on the topic Heterogeneity of myeloid cells in multiple sclerosis as evidenced by single-cell mass cytometry (Heterogenität der myeloiden Zellen bei Multipler Sklerose mittels Einzelzell-Massenzytometrie), independently and without the support of third parties, and that I used no other sources and aids than those stated. All parts which are based on the publications or presentations of other authors, either in letter or in spirit, are specified as such in accordance with the citing guidelines. The sections on methodology (in particular regarding practical work, laboratory regulations, statistical processing) and results (in particular regarding figures, charts and tables) are exclusively my responsibility.

Furthermore, I declare that I have correctly marked all of the data, the analyses, and the conclusions generated from data obtained in collaboration with other persons, and that I have correctly marked my own contribution and the contributions of other persons (cf. declaration of contribution). I have correctly marked all texts or parts of texts that were generated in collaboration with other persons.

My contributions to any publications to this dissertation correspond to those stated in the below joint declaration made together with the supervisor. All publications created within the scope of the dissertation comply with the guidelines of the ICMJE (International Committee of Medical Journal Editors; www.icmje.org) on authorship. In addition, I declare that I shall comply with the regulations of Charité – Universitätsmedizin Berlin on ensuring good scientific practice.

I declare that I have not yet submitted this dissertation in identical or similar form to another Faculty.

The significance of this statutory declaration and the consequences of a false statutory declaration under criminal law (Sections 156, 161 of the German Criminal Code) are known to me."

Date   Signature

Declaration of own contribution

María Camila Fernández Zapata contributed the following to the below listed publication:

Publication 1: Böttcher, C*., Fernández-Zapata, C*., Schlickeiser, S*., Kunkel, D., Schulz, A.R., Mei, H. E., Weidinger, C., Gieß, R.M., Asseyer, S., Sigmund, B., Paul, F., Ruprecht, K. & Priller, J. Multi-parameter immune profiling of peripheral blood mononuclear cells by multiplexed single-cell mass cytometry in patients with early multiple sclerosis. *Scientific Reports* 9, 19471, doi.org/10.1038/s41598-019-55852-x (2019).

Contribution in detail: I took part in performing all experiments, together with PD. Dr. rer. nat. Chotima Böttcher. Together with Dr. rer. nat. Stephan Schlickeiser I designed the data analysis workflow. I further performed all data analyses in all figures, under the supervision of PD. Dr. rer. nat. Chotima Böttcher and Dr. rer. nat. Stephan Schlickeiser.

Publication 2: Böttcher, C*., van der Poel, M*., Fernández-Zapata, C*., Schlickeiser, S., Leman J. K. H., Hsiao, C. C., Mizee M. R., Adelia., Vincenten M. C. J., Kunkel, D., Huitinga, I., Hamman, J. & Priller, J. Single-cell mass cytometry reveals complex myeloid cell composition in active lesions of progressive multiple sclerosis. *Acta Neuropathologica Communications* 8, 136, doi.org/10.1186/s40478-020-01010-8 (2020).

Contribution in detail: I performed all mass cytometry experiments, together with PD. Dr. rer. nat. Chotima Böttcher. I performed the data analysis for mass cytometry experiments, under the supervision of PD. Dr. rer. nat. Chotima Böttcher and Dr. rer. nat. Stephan Schlickeiser (Figures 1, 2, 4, Supplementary Figures 4, 8, 9 and 10). I established and performed all imaging CyTOF experiments and data analysis (Figure 3, Supplementary Figure 7). I performed the immunohistochemical experiments and analysis depicted in Supplementary Figures 2d and 3. Furthermore, I took part in the preparation of the figures and the manuscript, together with PD. Dr. rer. nat. Chotima Böttcher, Marlijn van der Poel, Julia K. H. Leman, Porf. Dr. Inge Huitinga, Dr. rer. nat. Jörg Hamman and Prof. Dr. med. Josef Priller.

Publication 3: Böttcher, C.*, Fernández-zapata, C.*, Snijders, G. J. L., Schlickeiser, S., Sneeboer, M. A. M., Kunkel, D., Witte, L. D. De & Priller, J. Single-cell mass cytometry of microglia in major depressive disorder reveals a non-inflammatory phenotype with increased homeostatic marker expression. *Transl. Psychiatry* 1–11 (2020).

Contribution in detail: I, together with PD. Dr. rer. nat. Chotima Böttcher performed all

CyTOF experiments. I further performed all data analyses in all figures and took part in the interpretation of the results, together with PD. Dr. rer. nat. Chotima Böttcher. I took part in the preparation of figures and manuscript, together with PD. Dr. rer. nat. Chotima Böttcher. and Prof. Dr. med. Josef Priller.

_____
Signature, date and stamp of first supervising university professor / lecturer

_____
Signature of doctoral candidate

Extract from the Journal Summary List for Publication 1

Journal Data Filtered By: **Selected JCR Year: 2017** Selected Editions: SCIE,SSCI
Selected Categories: **"MULTIDISCIPLINARY SCIENCES"** Selected Category
Scheme: WoS
Gesamtanzahl: 64 Journale

Rank	Full Journal Title	Total Cites	Journal Impact Factor	Eigenfactor Score
1	NATURE	710,766	41.577	1.355810
2	SCIENCE	645,132	41.058	1.127160
3	Nature Communications	178,348	12.353	0.926560
4	Science Advances	10,194	11.511	0.057080
5	PROCEEDINGS OF THE NATIONAL ACADEMY OF SCIENCES OF THE UNITED STATES OF AMERICA	637,268	9.504	1.108220
6	National Science Review	952	9.408	0.004340
7	GigaScience	1,694	7.267	0.011030
8	Scientific Data	1,567	5.305	0.008550
9	Journal of Advanced Research	1,843	4.327	0.003820
10	Annals of the New York Academy of Sciences	46,160	4.277	0.033270
11	Science Bulletin	1,952	4.136	0.005900
12	Scientific Reports	192,841	4.122	0.718960
13	Journal of the Royal Society Interface	11,357	3.355	0.030960
14	Research Synthesis Methods	1,374	3.218	0.006030
15	PLoS One	582,877	2.766	1.862350
16	PHILOSOPHICAL TRANSACTIONS OF THE ROYAL SOCIETY A-MATHEMATICAL PHYSICAL AND ENGINEERING SCIENCES	17,807	2.746	0.028220
17	Royal Society Open Science	2,145	2.504	0.009260
18	PROCEEDINGS OF THE ROYAL SOCIETY A-MATHEMATICAL PHYSICAL AND ENGINEERING SCIENCES	17,157	2.410	0.018270
19	PeerJ	7,377	2.118	0.031600
20	NPJ Microgravity	94	2.000	0.000350
21	SCIENCE AND ENGINEERING ETHICS	1,496	1.859	0.002520
22	COMPLEXITY	1,369	1.829	0.002380
23	Science of Nature	324	1.789	0.001260

Selected publication 1

Böttcher C*, Fernández-Zapata C*, Schlickeiser S*, Kunkel D, Schulz AR, Mei HE, Weidinger C, Gieß RM, Asseyer S, Siegmund B, Paul F, Ruprecht K, Priller J. Multi-parameter immune profiling of peripheral blood mononuclear cells by multiplexed single-cell mass cytometry in patients with early multiple sclerosis. Sci Rep. 2019 Dec 19;9(1):19471.

OPEN

Multi-parameter immune profiling of peripheral blood mononuclear cells by multiplexed single-cell mass cytometry in patients with early multiple sclerosis

Chotima Böttcher [1,2,11*], Camila Fernández-Zapata [1,2,11], Stephan Schlickeiser [1,3,11], Desiree Kunkel [1,8], Axel R. Schulz [4], Henrik E. Mei[4], Carl Weidinger [1,5], René M. Gieß[1,6,7], Susanna Asseyer[1,7], Britta Siegmund [1,5], Friedemann Paul[1,6,7,8,9], Klemens Ruprecht[1,6,11] & Josef Priller[1,2,8,10,11*]

Multiple sclerosis (MS) is an inflammatory demyelinating and neurodegenerative disease of the central nervous system (CNS). Studies in rodent models demonstrated an association of CNS-infiltrating monocyte-derived macrophages with disease severity. However, little is known about humans. Here, we performed an exploratory analysis of peripheral blood mononuclear cells (PBMCs) isolated from healthy controls and drug-naïve patients with early MS using multiplexed single-cell mass cytometry and algorithm-based data analysis. Two antibody panels comprising a total of 64 antibodies were designed to comprehensively analyse diverse immune cell populations, with particular emphasis on monocytes. PBMC composition and marker expression were overall similar between the groups. However, an increased abundance of CCR7$^+$ and IL-6$^+$ T cells was detected in early MS-PBMCs, whereas NFAT1^{hi}T-bet^{hi}CD4$^+$ T cells were decreased. Similarly, we detected changes in the subset composition of the CCR7$^+$ and MIPβ^{hi} HLA-DR$^+$ lymphocyte compartment. Only mild alterations were detected in monocytes/myeloid cells of patients with early MS, namely a decreased abundance of CD141^{hi}IRF8^{hi}CXCR3$^+$CD68$^-$ dendritic cells. Unlike in Crohn's disease, no significant differences were found in the monocyte fraction of patients with early MS compared to healthy controls. This study provides a valuable resource for future studies designed to characterise and target diverse PBMC subsets in MS.

Multiple sclerosis (MS) is a frequent chronic inflammatory demyelinating and neurodegenerative disease of the human central nervous system (CNS) with a highly variable disease course[1]. Although its precise aetiology remains to be identified, peripheral immune cells have been proposed as one of the main players in MS. Indeed, immunotherapies targeting lymphocytes or subsets thereof (for example natalizumab, rituximab/ocrelizumab, alemtuzumab or fingolimod) have a beneficial effect on relapse rates and neuroimaging outcomes in patients with relapsing-remitting MS, while the effects of these drugs during the progressive phase of the disease are less

[1]Charité – Universitätsmedizin Berlin, corporate member of Freie Universität Berlin, Humboldt-Universität zu Berlin, and Berlin Institute of Health, Berlin, Germany. [2]Department of Neuropsychiatry and Laboratory of Molecular Psychiatry, Berlin, Germany. [3]BIH Center for Regenerative Therapies (BCRT), Berlin, Germany. [4]German Rheumatism Research Center (DRFZ), Berlin, Germany. [5]Division of Gastroenterology, Infectiology and Rheumatology, Medical Department for Gastroenterology, Berlin, Germany. [6]Department of Neurology and Clinical and Experimental Multiple Sclerosis Research Center, Berlin, Germany. [7]NeuroCure Clinical Research Center (NCRC), Berlin, Germany. [8]Berlin Institute of Health, Berlin, 10178, Germany. [9]Experimental and Clinical Research Center (ECRC), Max Delbrueck Center for Molecular Medicine, Berlin, Germany. [10]DZNE, Berlin Germany, University of Edinburgh and UK Dementia Research Institute, Edinburgh, UK. [11]The authors contributed equally: Chotima Böttcher, Camila Fernández-Zapata, Stephan Schlickeiser, Klemens Ruprecht and Josef Priller. *email: chotima.boettcher@charite.de; josef.priller@charite.de

58

pronounced[2–4]. Besides the adaptive immune system, the innate arm including monocytes has also been claimed to be involved in MS pathogenesis and/or disease severity. In mouse models of inflammatory demyelination (namely experimental autoimmune encephalomyelitis, EAE), $CCR2^+Ly6-C^{hi}$ blood monocytes were shown to exert a crucial role in the effector phase of the disease. Inhibition of their recruitment to the CNS strongly reduced EAE severity[5,6]. In humans, genome-wide association studies (GWAS) unravelled causal variants for MS in multiple cell types including different subsets of T and B cells, monocytes and macrophages, suggesting contributions of both adaptive and innate arms of the immune system[7]. Yet, the roles of monocytes/myeloid cells as well and their phenotypic changes in human MS remain elusive.

In humans, peripheral blood monocytes can be classified into three main subsets: classical ($CD14^{++}CD16^-$), intermediate ($CD14^+CD16^+$) and nonclassical ($CD14^{dim/-}CD16^+$) monocytes[8]. Results obtained from whole-genome expression arrays revealed that both $CD14^+$ subsets (namely classical and intermediate monocytes) resemble $CCR2^+Ly6C^{hi}$ "inflammatory" monocytes in mice, whereas the nonclassical subset was more alike to mouse $CX3CR1^{hi}Ly6C^{lo}$ "patrolling" monocytes[8]. However, functional characteristics of human $CD14^{++}CD16^-$ and $CD14^+CD16^+$ monocytes revealed significant differences[8,9]. $CD14^{++}CD16^-$ classical monocytes strongly produce reactive oxygen species (ROS), IL-6, IL-8, CCL2 and CCL3, whereas the $CD14^+CD16^+$ intermediate subset predominantly produces TNF-α and IL-1β[8]. Phenotypic analysis by flow cytometry identified elevated expression of CD40, CD86 and CCR2 in nonclassical and intermediate monocytes from MS patients, while only slight differences were observed in the classical $CD14^+$ subset[10,11]. However, another flow cytometry study found a reduction of CD40, CD163 and CCR2 expression in monocytes from MS patients[12]. These controversies may result from different strategies of the subset identification based on up to 8 markers, as well as the experimental *in vitro* conditions. In particular, the limited number of markers applied for immune profiling using flow cytometry renders it virtually impossible to simultaneously investigate the MS-associated responses of monocytes in comparison to other immune cell subsets such as T and B cells, which are known key players in MS. Massive immune cell profiling using multiplexed single-cell mass cytometry (CyTOF) allows for comprehensive investigation of various immune cell subsets. Commonly, up to 40 markers can be simultaneously investigated at the single-cell level, and this provides an important advantage over the classical flow cytometric analysis. Furthermore, the identification of immune cell subsets using an unbiased algorithm-based approach allows for the investigation of rare cell populations, which may otherwise remain unidentified on the basis of a hierarchical two-dimensional gating strategy.

In this study, we employed multiplexed CyTOF and algorithm-based data processing and analysis for high-dimensional immune cell profiling of PBMCs in early MS, with a particular emphasis on monocytes. We herein report the results of simultaneous analysis of monocyte/myeloid subsets and other immune cell populations in PBMCs (excluding granulocytes) from drug-naïve patients with early MS in comparison to healthy controls. Our findings provide a valuable resource for immune cell identification and profiling in future preclinical and clinical studies in early MS.

Results

The demographic and clinical data of the patients with early MS and healthy controls included in this study are summarized in Supplementary Table 1. Gender and age did not differ between patients with early MS and healthy controls [*sex (% female)*: CON = 90.9, early MS = 72.7, p = 0.5865; *age (years ± SD)*: CON = 36 ± 12, early MS = 35 ± 9, $t_{(df = 20)}$ = 0.0599, p = 0.9529].

Comprehensive phenotyping by multiplexed single-cell mass cytometry. The experimental design of this study is summarized in Fig. 1. In order to minimize the run-to-run variation and to facilitate the comparison of cellular profiles from different cell subsets and individuals, we simultaneously profiled PBMCs of all samples from both early MS patients and healthy controls (CON) in the same run. Isolated PBMCs from patients with early MS and healthy controls were thawed and live (mass-tag) barcoded using pre-conjugated CD45 antibody conjugates[13,14]. Samples were subsequently pooled, split equally and stained with two different antibody panels (35 antibodies/panel) (Supplementary Tables 2 and 3). *Panel A* was designed to detect the major circulating immune cell subsets (i.e. T & B cells, monocytes, natural killer (NK) cells), chemokine receptors and inflammatory mediators, including IRF4, IRF8, CD45, CD3, CD14, CD16, CD62L, CD19, HLA-DR, CD56, CD44, CD33 (Siglec-3), NFAT1, ADRP, CCR2, CCR7, IL-10, CCL2, IFN-γ, and TNF-α. *Panel B* was designed to investigate functional and activity changes in immune cell subsets using 35 antibodies including CD116, IKZF1, CD38, MIPβ, CD172a, PD-L1, Arginase-1, GATA6, GM-CSF, IRF8, GLUT1, IL-4, IL-8. In both antibody panels, anti-HLA-DR, anti-CD8a and anti-CD33 antibodies were included, which allowed tracking and correlation of immune phenotypes (revealed from both panels) of the myeloid cell populations between panels. Finally, multiplexed and stained samples were simultaneously acquired on a CyTOF instrument.

First, we captured and visualized all cell subpopulations in a single two-dimensional (2D) map using unsupervised high-dimensional data analysis, the t-distributed stochastic linear embedding (t-SNE) algorithm[15,16] on the commercially available analysis platform Cytobank (www.cytobank.org) (Figs. 2a and 3a). Subsequently, we performed a comprehensive analysis on R/Bioconductor by high resolution testing for differential abundance at the t-SNE embedding[17] as well as by clustering-based methodologies[18]. Using antibody *Panel A*, in which HLA-DR, CD19, CD44, CD4, CD11c, CD16, CD3, CD56, CD14, CD8a, T-bet, CD33, CCR2 and CD11b were used for meta-clustering, we detected nine distinct clusters and a dispersed cluster containing only very few cells (less than 50 cells), which showed unclear phenotypic profiles (named as unidentified cells). These cells were excluded from the further data analysis (Fig. 2b,c). The immune cell composition of PBMCs was overall similar between the patients with early MS and healthy controls (Fig. 2d). To obtain enough resolution for further analysis, we manually merged some clusters, which resulted in a final of six clusters representing B cells, CD4/CD8-single positive and double-negative T cells, NK cells, and myeloid cells (Fig. 2e). These subsets served
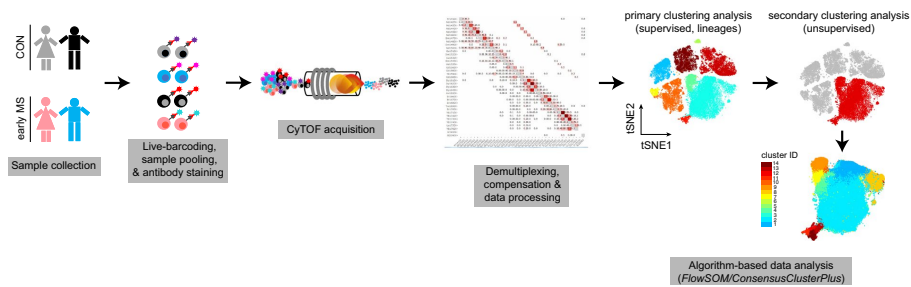
Figure 1. Schematic representation of CyTOF measurement. Peripheral blood mononuclear cells (PBMCs) were collected from healthy controls (CON, n = 11) and patients with early multiple sclerosis (MS) (early MS, n = 11). PBMCs were CD45-barcoded and pooled. Mixed samples were equally divided and stained with two panels (*Panel A and B*, Supplementary Tables 2 and 3) of metal-conjugated antibodies and acquired on the CyTOF instrument. Prior to algorithm-based data analysis, the data were demultiplexed and compensated. Two steps of clustering analysis were performs; the primary supervised clustering analysis to identify the known lineage cell subsets, and the secondary unsupervised clustering analysis to discover small phenotypic differences within each identified lineage cell subset.

as input for further meta-clustering analysis. Using antibody *Panel B*, in which only HLA-DR, CD38, CD64, CD68, CD8a, CD33 and CD64 were used to estimate the frequency of the main circulating cell subsets, four cell subsets were defined. Using this antibody panel, we aimed to particularly analyse the myeloid cell population (HLA-DR$^+$CD33$^+$). Myeloid cells can be clustered from other cell populations (Fig. 3b), whereas CD4$^+$ T cells could not be clearly clustered from NK cells, and some HLA-DR$^+$ T lymphocytes (red dots) were detected in the cluster of B cells (HLA-DR$^+$CD33$^-$, light blue cluster). Similar to *Panel A*, one very rare cell subset (unidentified cells) was excluded from the analysis (Fig. 3b). In both *Panels A and B*, overall mean expressions of all markers used in *Panels A and B* were not different between the two groups (Figs. 2f and 3c).

Phenotypic alterations in the lymphoid compartment in patients with early MS. In order to examine phenotypic differences of PBMCs between patients with early MS and healthy controls, we next performed high-resolution probability binning on the t-SNE map of the entire data set, an approach that has been shown to be an effective exploring strategy to reveal differences between the studied groups[17]. This analysis revealed that the CD4$^+$ T cell composition was different between healthy controls and patients with early MS (Fig. 4a). The differences were detected in the CD4$^+$ T cell sub-populations that expressed CCR7, IL-7R and CD62L (Fig. 4b). Further cluster analysis of CD4$^+$ T cells indicated abundant differences in two out of fourteen subsets (Fig. 4c,d). Cluster 1, defined as NFAT1^{hi}T-bet^{hi}CD4$^+$ T cells was present at a lower frequency in patients with early MS compared to healthy controls (Fig. 4d,e), whereas the abundance of CCR7$^+$T-bet$^-$CD4$^+$ T cells (cluster 13) was higher in patients with early MS (Fig. 4d,e). Similar to the CD4$^+$ lymphocytes, an increased frequency of the CCR7$^+$T-bet$^-$NFAT1^{lo} cell subset (cluster 5) was also found among the CD8$^+$ T cell population (Fig. 4f–h). Within the CD3$^+$CD4$^-$CD8$^-$T-bet$^+$ (double-negative) T cells, we detected differential abundance in two subsets 2 and 3, which differed from the other clusters on the basis of expression levels of ADRP, CCR2 and T-bet (Fig. 5a–c). Notably, in the early MS group, increased cell frequencies were detected in the clusters that were ADRP^{lo}CCR2$^+$T-bet^{lo} (cluster 2), while ADRP$^+$CCR2$^+$T-bet$^+$ cells (cluster 3) were less abundant compared with healthy controls (Fig. 5a–c).

Although we could not detect differential marker expression and abundance in the total B cell population, high-dimensional clustering analysis revealed differences in cell frequencies of two out of seventeen B cell subsets (Fig. 5d–f). These subsets were identified as CCR7$^+$CCR2$^-$TGFβ1$^-$ B cells, which were positive (cluster 2) and negative (cluster 3) for CD62L (L-selectin) expression (Fig. 5d–f). Interestingly, we detected an increased abundance of CD62L-expressing B cells, whereas the frequency of the CD62L-negative cells was reduced (Fig. 5e,f).

Similar to the results obtained for antibody *Panel B*, multi-parameter immune profiling using the antibody *Panel B* revealed differential abundances of lymphoid cell subsets (Fig. 6). In the mixed cluster of CD4$^+$ T cells and NK cells, we detected differences in the frequencies of two cell subsets, namely clusters 3 and 6 in Fig. 6a,b. A unique CD47^{hi}IL-6$^+$ T cell subset (cluster 6) was found to be increased in early MS patients compared to the healthy controls (Fig. 6a–c). This subset could be further defined as CD274^{lo}CD54^{lo}CXCR3$^+$ (Fig. 6a). Finally, the frequency of cells expressing high level of MIPβ (CCL4) and IRF8 (cluster 7) was significantly lower in the mixed cluster of HLA-DR$^+$ T cells and B cells from patients with early MS than in healthy controls (Fig. 6d–f). In sum, harnessing the full power of multi-dimensional mass cytometry we unravelled phenotypic alterations of lymphoid cell subsets in patients with early MS compared to healthy controls. The changes in immune profiles detected herein were found mainly in the B and T cell populations.

Phenotypic alterations of the monocyte/myeloid cell compartment in patients with early MS. Next, we explored the abundance and/or phenotypic changes in the myeloid cell compartment of patients with early MS compared with the control group (Fig. 7). In contrast to previous reports[10–12], we did
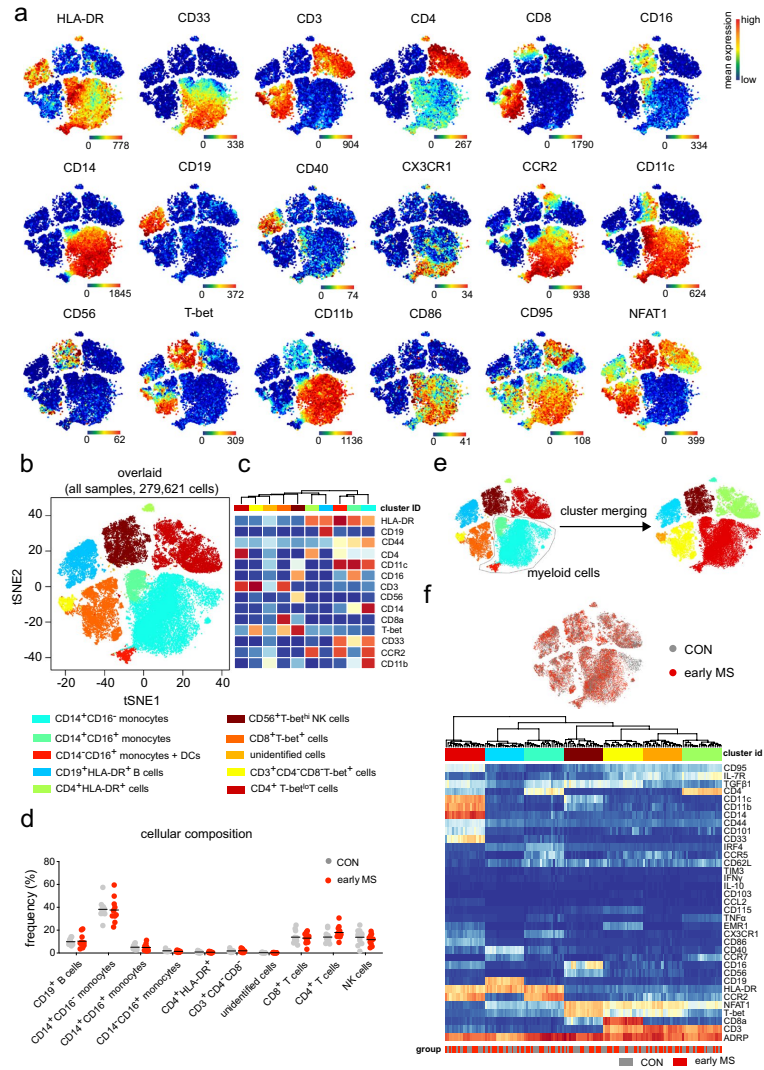
Figure 2. Immune phenotyping of peripheral blood mononuclear cells (PBMCs) – *Panel A*. (**a**) Representative reduced-dimensional single-cell t-SNE maps (of a healthy control) from biologically independent samples of patients with early MS (n = 11) and healthy controls (n = 11). Each dot represents one cell. The 2D t-SNE maps were generated based on expression levels of all markers of *Panel A* (Supplementary Table 2). The colour spectrum represents individual marker-expression levels (red, high expression; dark blue, no expression). (**b**) The t-SNE plot of concatenated FCS files from all 22 samples. The colouring indicates ten defined clusters representing major PBMC-lineages. (**c**) Heat map cluster demonstrates the expression levels of 14 markers used for the cluster analysis. (**d**) Quantified frequencies (%) of each defined cell subset showing comparable cellular composition in PBMCs from the two studied groups (black lines show mean values of the datasets). (**e**) Myeloid clusters including CD14⁺CD16⁻, CD14⁺CD16⁺, CD14⁻CD16⁺ monocytes and dendritic cells were manually merged prior to further data analysis. (**f**) Overlaid t-SNE plot shows cellular distribution of control (grey dots) and early MS (red dots) samples (top image). Heat map and cluster analysis of all samples on the basis of the mean expression of 36 markers. Samples are indicated by dendrograms. Heat colours show overall expression levels (red, high expression; dark blue, no expression).

Figure 3. Immune phenotyping of peripheral blood mononuclear cells – *Panel B*. (**a**) Representative single-cell t-SNE plots (of a healthy control). Each dot represents one cell. The 2D t-SNE maps were generated based on expression levels of all markers of *Panel B* (Supplementary Table 3). The colour spectrum represents expression levels (red, high expression; dark blue, no expression). (**b**) The t-SNE map of concatenated FCS files from all 22 samples. The colouring indicates five defined clusters of myeloid and lymphoid origin. The lower panel shows cluster heat map cluster demonstrating the expression levels of 7 markers used as the embedding parameters. (**c**) Overlaid t-SNE plot shows cellular distribution of control (grey dots) and early MS (red dots) samples (top image). Heat map and cluster analysis of all samples on the basis of the mean expression of 36 markers. Samples are indicated by dendrograms. Heat colours show overall marker expression levels (red, high expression; dark blue, no expression).

not observe major differences in the monocyte/myeloid cell composition between the two groups using antibody *Panel A* (Supplementary Fig. 1). However, results obtained from the profiling using antibody *Panel B* revealed a significant reduction of the frequency of CD141-expressing dendritic cells (DCs, cluster 13) in patients with early MS compared to healthy controls (Fig. 7a–c). This cell subset could be further characterized as CD64−CD68−CXCR3+IRF8+ADRP+CD38+ (Fig. 7a,c). To estimate the degree of phenotypic changes of monocytes in patients with early MS, we compared immune profiles of monocytes from patients with early MS with those from patients with Crohn's disease (CD) and healthy controls. It is known that monocytes are involved in the immunopathology of inflammatory bowel diseases like CD[19–21]. We detected strong differences in the myeloid cell compartment between patients with CD and early MS or healthy controls using antibody *Panels A*

62
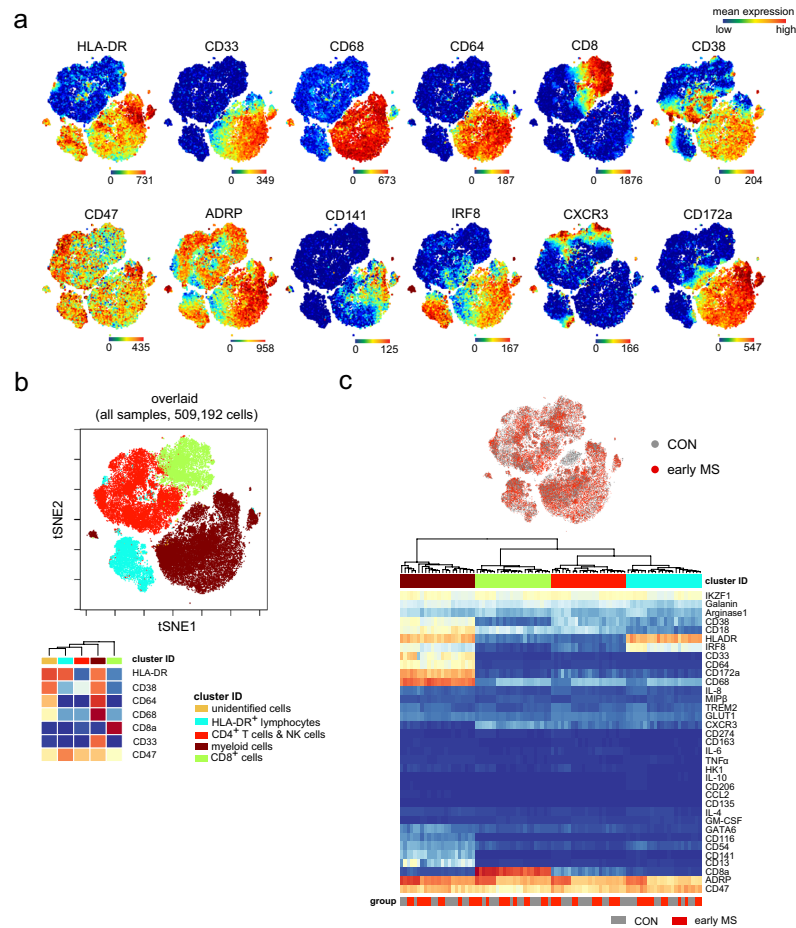
Figure 3. Immune phenotyping of peripheral blood mononuclear cells – *Panel B*. (**a**) Representative single-cell t-SNE plots (of a healthy control). Each dot represents one cell. The 2D t-SNE maps were generated based on expression levels of all markers of *Panel B* (Supplementary Table 3). The colour spectrum represents expression levels (red, high expression; dark blue, no expression). (**b**) The t-SNE map of concatenated FCS files from all 22 samples. The colouring indicates five defined clusters of myeloid and lymphoid origin. The lower panel shows cluster heat map cluster demonstrating the expression levels of 7 markers used as the embedding parameters. (**c**) Overlaid t-SNE plot shows cellular distribution of control (grey dots) and early MS (red dots) samples (top image). Heat map and cluster analysis of all samples on the basis of the mean expression of 36 markers. Samples are indicated by dendrograms. Heat colours show overall marker expression levels (red, high expression; dark blue, no expression).
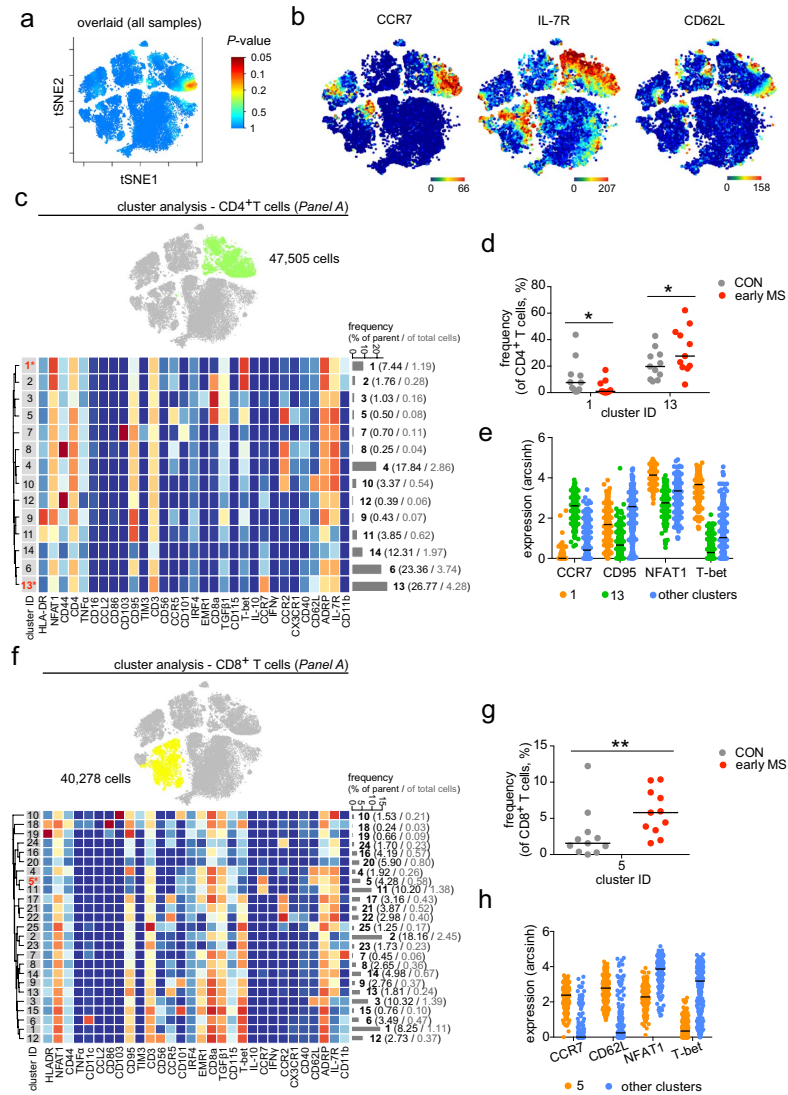
not observe major differences in the monocyte/myeloid cell composition between the two groups using antibody *Panel A* (Supplementary Fig. 1). However, results obtained from the profiling using antibody *Panel B* revealed a significant reduction of the frequency of CD141-expressing dendritic cells (DCs, cluster 13) in patients with early MS compared to healthy controls (Fig. 7a–c). This cell subset could be further characterized as $CD64^{-}CD68^{-}CXCR3^{+}IRF8^{+}ADRP^{+}CD38^{+}$ (Fig. 7a,c). To estimate the degree of phenotypic changes of monocytes in patients with early MS, we compared immune profiles of monocytes from patients with early MS with those from patients with Crohn's disease (CD) and healthy controls. It is known that monocytes are involved in the immunopathology of inflammatory bowel diseases like CD[19–21]. We detected strong differences in the myeloid cell compartment between patients with CD and early MS or healthy controls using antibody *Panels A*

63

Figure 4. Phenotypic analysis of the lymphoid lineage. (**a**) Statistical t-SNE map obtained from bin-wise testing for differential abundance between the two studied groups (CON, n = 11; early MS, n = 11) using *edgeR* statistical framework (with negative binomial GLM) and 10% FDR adjustment. The colour spectrum corresponds to FDR-adjusted P values, ranging from 1 (blue) to ≤ 0.05 (red), detecting significant differences between the group in the CD4+ T cell subset. (**b**) Representative single-cell t-SNE map indicates the expression of CCR7, IL-7R and CD62L. The colour spectrum represents an expression level (red, high expression; dark blue, no expression). (**c**) t-SNE map highlights CD4+ T cell subset (green dots). Heat map and cluster analysis within the CD4+ T cell cluster from all samples on the basis of the mean expression of analysed markers. Identified clusters are indicated by dendrograms. Heat colours show overall marker expression levels. The bar graph shows mean cluster frequencies as % of parent (black number) and % of total cells (grey number). Cluster 1 and 13 (* in red) are quantified as differentially abundant subsets between the groups. (**d**) The graph shows differences in frequency (%) of cluster 1 and 13 between the two studied groups. (**e**) Median expression levels

64

as shown in dot plot representation for randomly selected cells (n = 256/cluster) in the cluster 1 (orange), 13 (green) and all other clusters (blue). The selected markers are identified as defining markers for cluster 1 and 13. (**f**) The t-SNE map, heat map and cluster analysis of CD8$^+$ T cells from all samples on the basis of the mean expression of analysed markers. Cluster 5 (* in red) is quantified as differentially abundant subsets between the groups. (**g**) The graph shows differences in frequency (%) of cluster 5 between the two studied groups. (**h**) Median expression levels as shown in dot plot representation for randomly selected cells (n = 256/cluster) in the cluster 5 (orange) and all other clusters (blue). A P value < 0.05 at 10% FDR was considered statistically significant, determined using GLMM (*P < 0.05; **P < 0.01, unadjusted).

and *B* (Fig. 7d–i). On the basis of the expression levels of markers used in antibody *Panel A*, we identified seven cell subsets in the myeloid compartment that showed differential abundances between the investigated groups (Fig. 7d,e). Furthermore, we defined ADRP, CD101, CD11b, CD14, CD16, CCR2, CD33, CD86, CD95, CX3CR1, HLA-DR, IRF4, NFAT1 and TGFβ1 as markers that were required for the discrimination of these differential cell subsets from the remaining cell subsets (Fig. 7f). Interestingly, all seven differential cell subsets were found to be diminished in the patients with CD (Fig. 7e). Using antibody *Panel B*, we quantified differences in cell frequencies of seven cell subsets (out of 10 defined clusters) in the myeloid compartment of CD patients compared to patients with early MS and healthy controls (Fig. 7g,h). The markers discriminating these differential cell subsets were ADRP, Arginase 1, CD13, CD141, CD172a, CD18, CD33, CD38, CD54, CD64, CD68, CXCR3, GLUT1, HLA-DR, IKFZ1, IRF8 and MIPβ (Fig. 7i). Similar to the significant difference in DCs detected in patients with early MS in comparison to the healthy controls (cluster 13, Fig. 7a), we also found a decreased frequency of CD141$^+$CD64$^-$CD68$^-$CXCR3$^+$IRF8$^+$ADRP$^+$CD38$^+$ DCs (cluster 3) in patients with CD. Nevertheless, changes in the immune phenotypes of the myeloid compartment in patients with early MS were minute in comparison to those observed in CD.

Discussion

MS is an immune-mediated demyelinating and neurodegenerative disease of the CNS with a highly variable disease course. During early MS, immunomodulatory drugs targeting in particular T and B cells are the most effective therapies suggesting strong impacts of these cell populations on the disease. However, it remains unclear whether the aberrant activity of the adaptive arm of the immune system directly contributes to demyelination and/or inflammation of the CNS, or whether a cross-talk between the innate and adaptive arms drives MS pathogenesis[22]. Therefore, comprehensive information about the responses of both adaptive and innate immune cells during early MS will help to better understand the communication between both arms of the immune system, and to potentially manipulate them. In this study, we demonstrate the feasibility of extensive immune profiling by multiplexed single-cell mass cytometry to simultaneously determine phenotypic alterations of innate and adaptive immune cell populations in PBMC samples of patients with early MS compared to healthy controls. We suggest two antibody panels comprising of a total of 64 markers that allow for cell subset identification, as well as determination of phenotypic changes in PBMC samples. Although we did not observe overall differences in PBMC composition and marker expression, high-dimensional cluster analysis revealed changes in the cellular composition of T and B cell subsets, as well as in DCs, suggesting responses of various circulating lymphocyte and myeloid cell subpopulations during early MS.

In the lymphoid cell compartment of patients with early MS, using antibody *Panel A*, we detected increased frequencies of CD4$^+$ and CD8$^+$ cells that highly expressed CCR7 and were negative for CD95 (Fas). These subsets expressed low levels of NFAT1 and T-bet. In contrast, we observed a decreased abundance of the CCR7^{lo}NFAT1^{hi}T-bet^{hi} subset of CD4$^+$ T cells. These findings underscore the importance of T cell-responses in MS, which is in line with results obtained from EAE model in rodents, which suggested that CCR7 plays a crucial role in T cell homing during the priming of autoinflammation CD4$^+$ T cells but not in the CNS[23]. In fact, specific constitutive deletion of CCR7 on CD4$^+$ T cells induced immune tolerance to EAE[23]. T-box transcription factor (T-bet) is expressed in T lymphocytes and committed to T cell development[24]. This transcription factor is recognized as a key regulator for Th1 cell differentiation and is considered to be critical for T cell pathogenicity in EAE since mice deficient in T-bet are resistant to the development of EAE[25]. Also, the nuclear factor of activated T cell (NFAT) transcription factor is involved in the regulation of T-cell development, activation and differentiation[26]. Moreover, our results are in line with observations in patients with relapsing-remitting MS that suggest an increase of circulating CD95$^{-/lo}$CD4$^+$ and CD8$^+$ T cells compared to healthy controls[27,28]. We also identified increased abundance of IL-6-expressing CD8a$^-$CD47^{hi}IKZF1^{hi} T cells in the peripheral blood of patients with early MS. This finding is in line with the previous observation of increased CD3$^+$CD8$^-$ cells producing the Th17-related cytokine IL-6 in inflammatory niches[29]. Moreover, we found reduced frequencies of IRF8$^+$HLA-DR$^+$ lymphocytes that highly expressing MIPβ. Although B cell markers such as CD19 or CD20 were missing in the antibody *Panel B*, this IRF8$^+$HLA-DR$^+$MIPβ$^+$ cell cluster may be identified as a member of the B cell population. Of note, it has been demonstrated that B cells increased MIPβ (or CCL4) expression upon activation, and that MIPβ plays a crucial role in the recruitment of regulatory T cells. Failure of CCL4-mediated T cell recruitment leads to autoimmune activation[30]. Further, an increased abundance of the B cell subset that was CCR7$^+$CD62L$^{low/-}$ was also detected, whereas the proportion of CCR7$^+$CD62L$^+$ B cells was increased in early MS. Shedding expression of CD62L on B cells, for example after infection, could affect B cell receptor signalling and B cell migration[31].

In contrast to lymphocytes, massive immune profiling using both antibody panels revealed no phenotypic differences of monocytes in patients with early MS compared to healthy controls. In contrast, patients with Crohn's disease (CD) showed a strong inflammatory phenotype in monocytes, suggesting that monocyte responses in
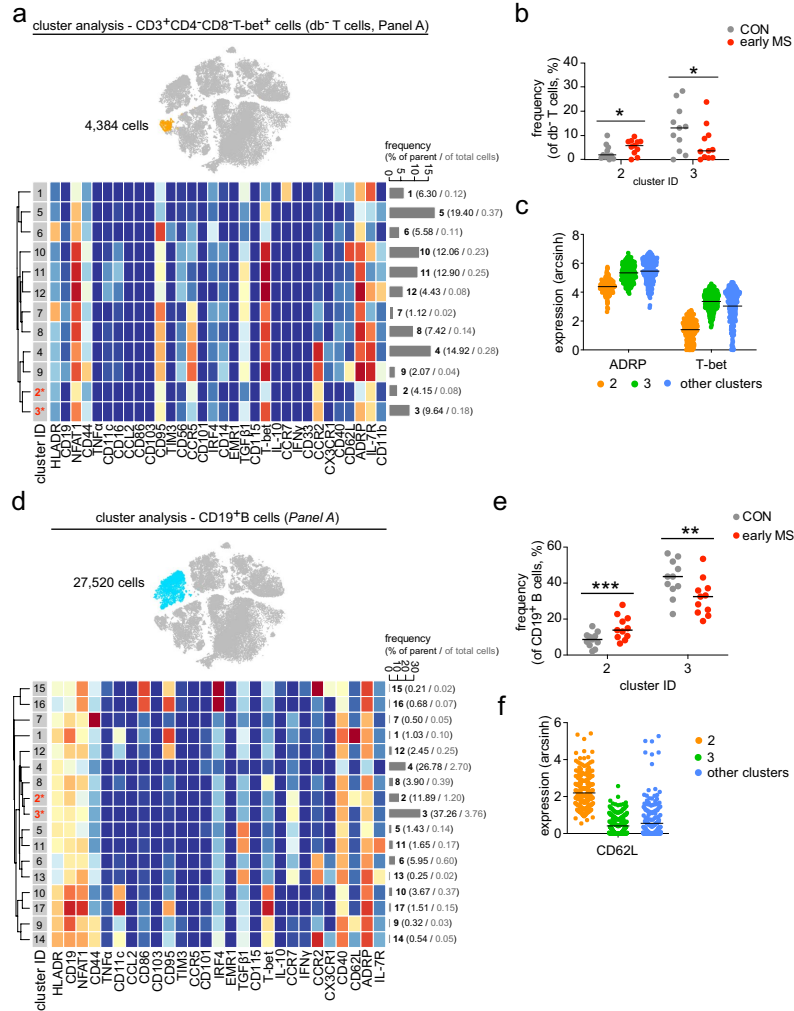
Figure 5. Cluster analysis of CD3+CD4−CD8−Tbet+ T cells and B cells from early MS patients (early MS) compared to the healthy controls (CON). (**a**) t-SNE map highlights CD3+CD4−CD8−Tbet+ T cell subset (orange dots). Heat map and cluster analysis of CD3+CD4−CD8−Tbet+ T cells from all samples on the basis of the mean expression of analysed markers. Identified clusters are indicated by dendrograms. Heat colours show overall marker expression levels (red, high expression; dark blue, no expression). The bar graph shows mean cluster frequencies as % of parent (black number) and % of total cells (grey number). Cluster 2 and 3 (* in red) are quantified as differentially abundant subsets between the healthy controls and the early MS patients. (**b**) The graph shows differences in frequency (%) of the three subsets between the two studied groups (CON, grey; early MS, red). (**c**) Median expression levels as shown in dot plot representation for randomly selected cells (n = 256/cluster) in the cluster 2 (orange), 3 (green), and all other clusters (blue). ADRP and T-bet are identified as defining markers for cluster 2 and 3. (**d**) t-SNE map highlights CD19+ B cell subset (blue dots). Heat map and cluster analysis of CD19+ B cells from all samples on the basis of the mean expression of analysed markers. Identified clusters are indicated by dendrograms. Heat colours show overall marker expression levels (red, high expression; dark blue, no expression). Cluster 2 and 3 (* in red) are quantified as differentially abundant subsets between healthy controls and patients with early MS. (**e**) The graph shows differences in frequency (%) of cluster 2 and 3 between the two studied groups (CON, grey; early MS, red). (**f**) Median expression levels as shown in

dot plot representation for randomly selected cells (n = 256/cluster) in the cluster 2 (orange), 3 (green) and all other clusters (blue). CD62L was statistically detected as a main marker defining the differentially abundant cluster 2 and 3. A P value < 0.05 at 10% FDR was considered statistically significant, determined using GLMM (*P < 0.05; **P < 0.01; ***P < 0.001, unadjusted).

patients with early MS might be related to the more compartmentalized inflammation in the CNS. Nevertheless, since it has been unequivocally shown in EAE that monocytes critically contribute to the pathophysiology of EAE[32,33], the contradictory findings reported herein might be explained by a limitation of markers which were analysed in this study. In contrast to single-cell RNA-sequencing (scRNA-Seq) analysis, CyTOF assesses single-cell phenotypes using an antibody-based approach, which is not a completely unbiased method. Further investigations include the extension to novel markers (possibly identified by RNA-sequencing). Notably, we observed decreased abundance of CD141$^+$CD68^{lo} myeloid DCs in patients with early MS compared to healthy controls. Interestingly, myeloid DCs have been suggested as critical regulators of regulatory T cell development in MS[34].

In sum, we performed comprehensive immune profiling of PBMCs at the single-cell level, which allowed us to unambiguously characterise immune phenotypes and functions of diverse cell populations in the peripheral blood of patients with early MS. Our results extend the findings of previous, in particular transcriptomic, studies that suggested multiple cell types, including different subsets of lymphocytes and myeloid DCs, orchestrate the complex immune responses during early MS[5,35–39] and EAE[40]. These findings underscore the importance of comprehensive immune profiling in diseases with multifaceted aspects of inflammation like MS. The power of high-dimensional single-cell techniques like CyTOF and scRNA-Seq will in the future help to provide a better understanding of the heterogeneity of immune responses in MS.

Methods

Subjects. The study was registered and approved by the Ethics Committee of Charité – Universitätsmedizin Berlin. All participants provided written informed consent before any study-related procedures were undertaken. The study has been performed according to the Declaration of Helsinki and to the relevant ethical guidelines for research in humans. Heparinized blood samples were obtained by peripheral venipuncture from 11 patients with early MS and 11 healthy controls, as well as from 8 patients with Crohn's disease (Supplementary Table 1). All patients with early MS included in this work participated in an ongoing prospective observational study of patients with early MS (Berlin CIS Cohort; NCT01371071), which started recruitment in January 2011. Inclusion criteria were: age > 18 years, a first clinical event suggestive of inflammatory demyelination (clinically isolated syndrome (CIS) or early MS) not meeting the McDonald 2010 criteria for relapsing-remitting MS (RRMS)[41] within six months before inclusion into the study or a diagnosis of RRMS according to the McDonald 2010 criteria within 24 months before inclusion into the study. Exclusion criteria were: a history of alcohol or drug abuse, any conditions precluding magnetic resonance imaging examinations and any ocular diseases precluding optical coherence tomography. Patients investigated in the present analysis were drug naïve at the time of the blood draw. Patients underwent a thorough neurological examination, including determination of the expanded disability status scale (EDSS) score.

PBMC isolation. PBMCs were isolated from heparinized blood (27 ml) within 4.5 hours of the blood draw through Biocoll (Biochrom GmbH, Berlin, Germany) density centrifugation at 760 × g for 20 minutes at room temperature as described before[42]. The blood mononuclear cell fraction was recovered and washed in phosphate-buffered saline (PBS; Biochrom GmbH) at 560 × g for 20 minutes and at 400 × g for 15 minutes. Cell pellets were stored in liquid nitrogen for further analysis at a concentration of 5×10^6 cells/ml in RPMI-1640 (Gibco) containing 10% dimethyl sulfoxide (Sigma Aldrich Chemie GmbH), 20% fetal bovine serum (Biochrom GmbH) and 1% Hepes (Gibco).

Live cell barcoding. Individual PBMC samples (~5×10^6 cells) were stained with premade combinations of preconjugated ^{89}Y-CD45 (HI30, Fluidigm) and in house-conjugated ^{113}In, ^{115}In, ^{195}Pt, ^{196}Pt or ^{198}Pt-CD45 (HI30, Biolegend)[13,14] for 30 minutes at 4 °C. Cells were then washed twice and pooled. The multiplexed samples were then stained for surface and intracellular markers and subsequently measured by mass cytometry.

Antibodies. Anti-human antibodies (Supplementary Table 2 for *Panel A* & Supplementary Table 3 for *Panel B*) were purchased either preconjugated to metal isotopes (Fluidigm) or from commercial suppliers in purified form and conjugated in house using the MaxPar X8 kit (Fluidigm) according to the manufacturer's protocol. Each antibody was titrated and validated as into the working panels prior to use to ensure that the resulted signals were informative.

Cell-surface and intracellular staining. After cell barcoding, washing and pelleting, the combined samples were stained and processed as described previously[17]. Briefly, cells were re-suspended in 100 μl of antibody cocktail directed against cell surface markers (Supplementary Tables 2 and 3) and incubated for 30 minutes at 4 °C. Then, cells were washed twice with cell staining buffer (PBS containing 0.5% bovine serum albumin and 2 mM EDTA). For intracellular staining, the stained (non-stimulated) cells were then incubated in fixation/permeabilization buffer (Fix/Perm Buffer, eBioscience) for 60 minutes at 4 °C. Cells were then wash twice with permeabilization buffer (eBioscience). The samples were then stained with antibody cocktails directed against intracellular molecules (Supplementary Tables 2 and 3) in permeabilization buffer for 1 hour at 4 °C. Cells were subsequently washed twice with permeabilization buffer and incubated overnight in 4% methanol-free formaldehyde solution.
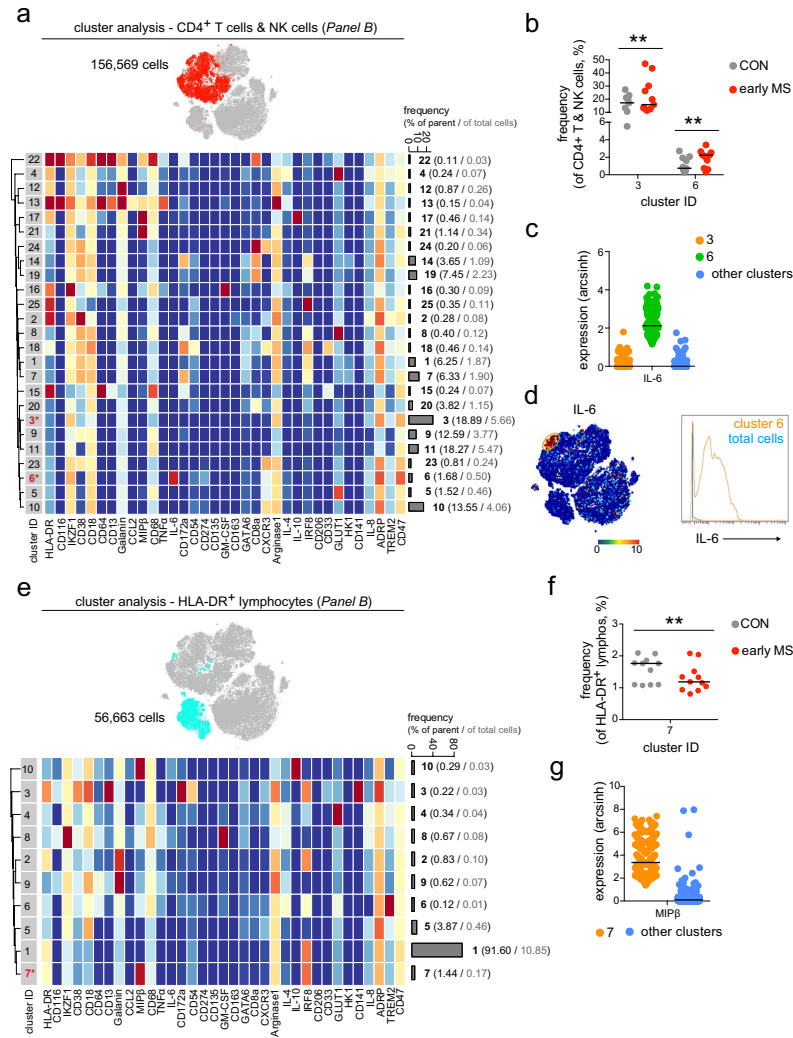
Figure 6. Differential abundances of lymphoid cell subsets in patients with early MS. (**a**) t-SNE map highlights mixed T and NK cell population (red dots). Heat map and cluster analysis of the mixed CD4^{+} T cell and NK cell population from all samples on the basis of the mean marker expressions (*Panel B*). Clusters are indicated by dendrograms. Heat colours show marker expression levels (red, high expression; dark blue, no expression). The bar graph shows mean cluster frequencies as % of parent (black number) and % of total cells (grey number). Cluster 3 and 6 (* in red) show differential abundances between healthy controls and patients with early MS. (**b**) The graph shows differences in frequency (%) of cluster 3 and 6 between the two studied groups (CON, grey; early MS, red). (**c**) Median expression levels as shown in the dot plot representation for randomly selected cells (n = 256/cluster) in the cluster 3 (orange), 6 (green) and all other clusters (blue). IL-6 was defined as a marker discriminating the differentially abundant cluster 6. (**d**) The representative t-SNE plot shows IL-6 expression levels and indicates the IL-6-expressing cell subset (orange circle, left image). The right image shows expression levels of IL-6 expressing cluster 6 (orange line), compared to the total cells (blue line). (**e**) t-SNE map highlights HLA-DR[+] lymphocyte population (light blue dots). Heat map and cluster analysis of B cells from all samples on the basis of the mean marker expressions (*Panel B*). Cluster 7 (* in red) show differential abundances between the studied groups. (**f**) The graph shows differences in frequency (%) of cluster 7 between the two

studied groups (CON, grey; early MS, red). (**g**) Median expression levels as shown in the dot plot representation for randomly selected cells (n = 256/cluster) in the cluster 7 (orange) and all other clusters (blue). MIPβ was identified as a marker discriminating the differentially abundant cluster 7. A P value < 0.05 at 10% FDR was considered statistically significant, determined using GLMM (**P < 0.01, unadjusted).

The fixed cells were then washed and re-suspended in 1 ml iridium intercalator solution (Fluidigm) for 1 hour at room temperature, followed by two washes with cell staining buffer and two washes with ddH$_2$O (Fluidigm). Finally, cells were pelleted and kept at 4 °C until CyTOF measurement.

Bead staining. For the bead-based compensation of the signal spillover, AbC total antibody compensation beads (Thermo Fisher Scientific) were single stained with each of the antibodies used in *Panel A* and *B* according to manufacturer's instructions.

CyTOF measurement. Cells were analysed using a CyTOF2 upgraded to Helios specifications, with software version 6.7.1014[17]. The instrument was tuned according to the manufacturer's instructions with tuning solution (Fluidigm) and measurement of EQ four element calibration beads (Fluidigm) containing 140/142Ce, 151/153Eu, 165Ho, and 175/176Lu served as a quality control for sensitivity and recovery.

Directly prior to analysis cells were re-suspended in ddH$_2$O, filtered through a 20 µm cell strainer (Celltrix, Sysmex), counted and adjusted to 3–5 × 10^5 cells/ml. EQ four element calibration beads were added at a final concentration of 1:10 v/v of the sample volume to be able to normalize the data to compensate for signal drift and day-to-day changes in instrument sensitivity.

Samples were acquired with a flow rate of 300–400 events/second. The lower convolution threshold was set to 400, with noise reduction mode turned on and cell definition parameters set at event duration of 10–150 pushes (push = 13 µs). The resulting flow cytometry standard (FCS) files were normalized and randomized using the CyTOF software's internal FCS-Processing module on the non-randomized ('original') data. The default settings in the software were used with time interval normalization (100 seconds/minimum of 50 beads) and passport version 2. Intervals with less than 50 beads per 100 seconds were excluded from the resulting FCS-file.

Mass cytometry data processing and analysis. As described previously[17], Cytobank (www.cytobank.org) was used for initial manual gating on live single cells and boolean gating for de-barcoding. Nucleated single intact cells were manually gated according to DNA intercalators ^{191}Ir/^{193}Ir signals and event length. For de-barcoding, Boolean gating was used to deconvolute individual sample according to the barcode combination. All de-barcoded samples were then exported as individual FCS files for further analysis. No significant difference in number cell count was detected between the studied groups (cell count per sample (mean ± sd; rang): *Panel A* = 14,246 ± 17,800; 2,800–59,686 (early MS) and 11,174 ± 12,350; 2,370–43,960 (control), and *Panel B* = 25,497 ± 29,518; 2,383–98,367 (early MS) and 20,793 ± 23,592; 3,048–82,960 (control)). Each FCS file was compensated for signal spillover using R package CATALYST[43] and transformed with arcsinh transformation (scale factor 5) prior to data analysis. Immune phenotypes of PBMCs were visualized using reduced-dimensional (2D) t-SNE maps generated according to the expression level of all markers used in the panel (both *Panel A* and *B*). For embedding, we set hyperparameters to perplexity of 30, theta of 0.5, and iterations of 1000 per 100,000 analysed cells. FCS files containing the t-SNE coordination as additional two parameters were exported from Cytobank for downstream exploratory and statistical analyses using R, as previously described[17,18]. For population identification, *FlowSOM/ConsensusClusterPlus*[18,43,44] (used all defaults with maxK = 25) clustering was used with 100 initial SOM-grid points and maxim of 25 meta-clusters. At first, we identified clusters of the main PBMC-lineages on the basis of expression levels of HLA-DR, CD19, CD44, CD4, CD11c, CD16, CD3, CD56, CD14, CD8a, T-bet, CD33, CCR2 and CD11b in the *Panel A*; and HLA-DR, CD38, CD64, CD68, CD8a, CD33 and CD64 in the *Panel B*. Subsequently, to obtain high enough resolution for further analysis and calculate frequencies within individual lineages, clusters were manually merged according to consensual marker-expression patterns into subsets representing B cells, CD4/CD8-single positive and double-negative T cells, NK cells, and myeloid cells, respectively. Each individual lineage cluster contained on average at least 200 events. These subsets served as input for second-level *FlowSOM/ConsensusClusterPlus* meta-clustering. Based on visual inspection of t-SNE plots and heat maps generated at each merging step, for each parent subset a final number of meta-clusters was chosen that merged clusters into populations with consistent phenotypes (with a minimal mean frequency of 0.1% of parent). Of note, we followed the concept of over-clustering for second-level meta-clustering, in order to study more specific subpopulations at higher detail in each main subsets (especially in myeloid cells)[18]. The number of defined clusters may not solely represent biologically functional subsets in PBMCs, but it should rather be interpreted as an exploratory tool for discovery of the differential abundance of small cell populations between the two studied groups. Based on visual inspection of t-SNE plots and heat maps generated at each merging step for each parent subset, a final number of meta-clusters was decided to display the merged clusters into populations with consistent phenotypes.

Statistical analysis. No randomization and blinding strategies were applied in this study. However, data processing and analysis, as well as statistical testing were carried out in an unsupervised manner. Dichotomous variables of the sample cohort were analysed with Fisher's exact test (GraphPad Prism). Quantitative data are shown as independent data points with median or Box-Whisker-Plot. Analyses of statistical significance were performed by computational analysis using generalized linear mixed-effects model (GLMM) available through R package *diffcyt* (used all defaults with analysis_type = "DA", method_DA = "diffcyt-DA-GLMM", min-cells = 3)

69
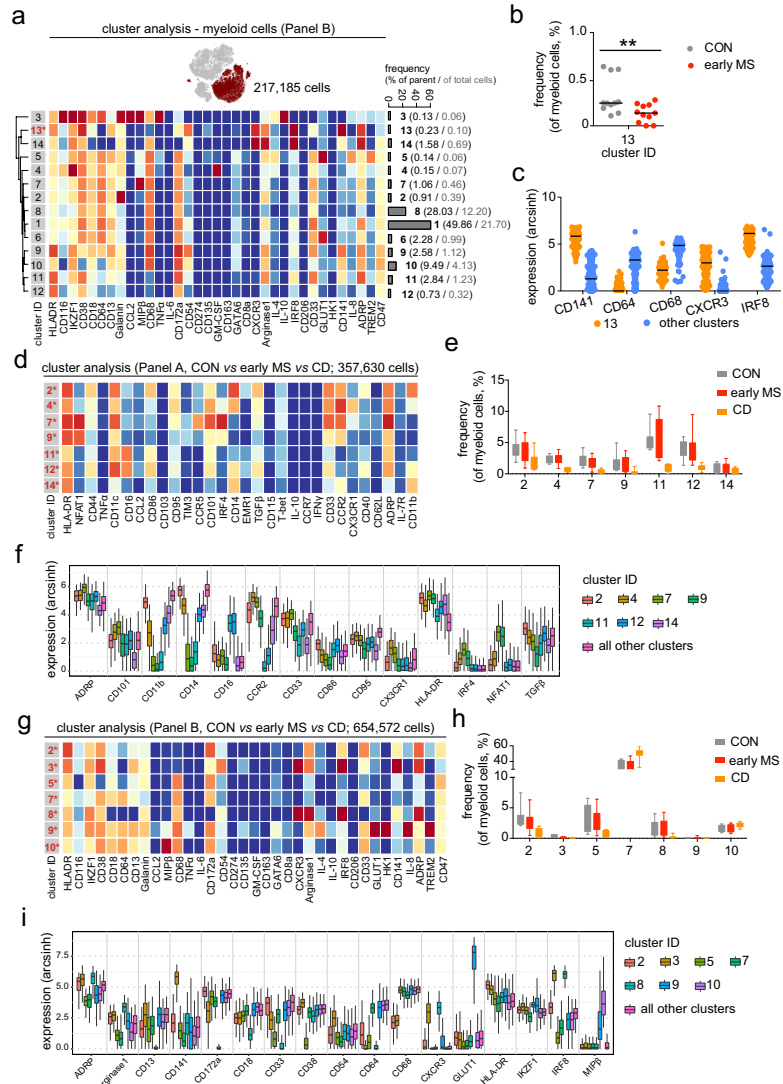
Figure 7. Phenotypic changes in myeloid cell populations from patients with early MS. (**a**) t-SNE map highlights myeloid population (merlot dots). Heat map and cluster analysis of myeloid cells from all samples on the basis of the mean marker expressions (*Panel B*). The bar graph shows mean cluster frequencies as % of parent (black number) and % of total cells (grey number). Cluster 13 (* in red) shows differential abundances between the controls (CON) and patients (early MS). (**b**) The graph shows differences in frequency (%) of cluster 13 between the two studied groups. (**c**) Median expression levels as shown in the dot plot representation for randomly selected cells (n = 256/cluster) in the cluster 13 (orange) and all other clusters (blue). (**d**) Heat map and cluster analysis of differentially abundant subsets of myeloid cells between healthy controls (CON, n = 11), patients with early MS (early MS, n = 11) and Crohn's disease (CD, n = 8) on the basis of the mean expression of analysed markers using the antibody *Panel A*. (**e**) The graph shows differences in the frequency (%) of all seven differential clusters compared between the three studied groups. (**f**) The Boxplot shows median expression levels of the discriminating markers defining the differentially abundant subsets. The plot was a

representation for randomly selected cells (256 cells per cluster) in the seven differential clusters. (**g**) Heat map and cluster analysis of differentially abundant subsets of myeloid cells between the three studied groups on the basis of the mean expression of analysed markers using the antibody *Panel B*. (**h**) The graph shows differences in frequency (%) of all seven differential clusters compared between the three studied groups (CON = grey; early MS = red; CD = orange). (**i**) The Box plot shows median expression levels of the discriminating markers defining the differentially abundant subsets. The plot was a representation for randomly selected cells (256 cells per cluster) in the seven differential clusters. A P value < 0.05 was considered statistically significant at 10% FDR, determined using GLMM (**$P < 0.01$, unadjusted).

and false discovery rate (FDR) adjustment (at 10% using Benjamini-Hochberg procedure) for multiple hypothesis testing. A P value < 0.05 (unadjusted) at 10% FDR was considered statistically significant. In addition, a cluster was defined as differentially abundant if it presented in at least 80% of the samples (of each or either (in the case of a disease/control-specific cluster) studied group).

Ethics approval and consent to participate. The study was registered and approved by the Ethics Committee of Charité – Universitätsmedizin Berlin, Berlin, Germany.

Data availability
The datasets used and/or analysed during the current study are available from the corresponding author on reasonable request that does not include confidential patient information.

References
1. Krieger, S. C., Cook, K., De Nino, S. & Fletcher, M. The topographical model of multiple sclerosis: A dynamic visualization of disease course. *Neurol. Neuroimmunol. Neuroinflamm.* **3**, e279, https://doi.org/10.1212/NXI.0000000000000279 (2016).
2. Dörr, J. & Paul, F. The transition from first-line to second-line therapy in multiple sclerosis. *Curr. Treat. Options Neurol.* **17**, 354, https://doi.org/10.1007/s11940-015-0354-5 (2015).
3. Hemmer, B., Kerschensteiner, M. & Korn, T. Role of the innate and adaptive immune responses in the course of multiple sclerosis. *Lancet Neurol.* **14**, 406–419 (2015).
4. Buck, D. & Hemmer, B. Treatment of multiple sclerosis: current concepts and future perspectives. *J. Neurol.* **258**, 1747–1762 (2011).
5. Ajami, B., Bennett, J. L., Krieger, C., McNagny, K. M. & Rossi, F. M. V. Infiltrating monocytes trigger EAE progression, but do not contribute to the resident microglial pool. *Nat. Neurosci.* **14**, 1142–1149 (2011).
6. Mildner, A. *et al.* CCR2+Ly-6C^{hi} monocytes are crucial for the effector phase of autoimmunity in the central nervous system. *Brain.* **132**, 2487–2500 (2009).
7. Farh, K. K. *et al.* Genetic and epigenetic fine mapping of causal autoimmune disease variants. *Nature.* **518**, 337–343 (2015).
8. Cros, J. *et al.* Human CD14^{dim} monocytes patrol and sense nucleic acids and viruses via TLR7 and TLR8 receptors. *Immunity.* **33**, 375–386 (2010).
9. Zhao, C. *et al.* The CD14(+/low)CD16(+) monocyte subset is more susceptible to spontaneous and oxidant-induced apoptosis than the CD14(+)CD16(−) subset. *Cell Death Dis.* **1**, e95, https://doi.org/10.1038/cddis.2010.69 (2010).
10. Chuluundorj, D., Harding, S. A., Abernethy, D. & La Flamme, A. C. Expansion and preferential activation of the CD14(+)CD16(+) monocyte subset during multiple sclerosis. *Immunol. Cell Biol.* **92**, 509–517 (2014).
11. Chuluundorj, D., Harding, S. A., Abernethy, D. & La Flamme, A. C. Glatiramer acetate treatment normalized the monocyte activation profile in MS patients to that of healthy controls. *Immunol. Cell Biol.* **95**, 297–305 (2017).
12. Gjelstrup, M. C. *et al.* Subsets of activated monocytes and markers of inflammation in incipient and progressed multiple sclerosis. *Immunol. Cell Biol.* **96**, 160–174 (2018).
13. Mei, H. E., Leipold, M. D., Schulz, A. R., Chester, C. & Maecker, H. T. Barcoding of live human peripheral blood mononuclear cells for multiplexed mass cytometry. *J. Immunol.* **194**, 2022–2031 (2015).
14. Mei, H. E., Leipold, M. D. & Maecker, H. T. Platinum-conjugated antibodies for application in mass cytometry. *Cytometry A.* **89**, 292–300 (2016).
15. Amir, el-A. D. *et al.* viSNE enables visualization of high dimensional single-cell data and reveals phenotypic heterogeneity of leukemia. *Nat. Biotechnol.* **31**, 545–552 (2013).
16. Van der Maaten, L. & Hinton, G. Visualizing high-dimensional data using tSNE. *J. Mach. Learn. Res.* **9**, 2579–2605 (2008).
17. Böttcher, C. *et al.* Human microglia regional heterogeneity and phenotypes determined by multiplexed single-cell mass cytometry. *Nat. Neurosci.* **22**, 78–90 (2019).
18. Nowicka, M. *et al.* CyTOF workflow: differential discovery in high-throughput high-dimensional cytometry datasets. *Version 3. F1000Res.* **6**, 748, https://doi.org/10.12688/f1000research.11622.3 (2017).
19. Gren, S. T. & Grip, O. Role of monocytes and intestinal macrophages in Crohn's disease and ulcerative colitis. *Inflamm. Bowel Dis.* **22**, 1992–1998 (2016).
20. Nieto, J. C. *et al.* CSF-1 regulates the function of monocytes in Crohn's disease patients in remission. *Sci. Rep.* **7**, 92, https://doi.org/10.1038/s41598-017-00145-4 (2017).
21. Xavier, R. J. & Podolsky, D. K. Unravelling the pathogenesis of inflammatory bowel disease. *Nature.* **448**, 427–434 (2007).
22. Thomas, K. *et al.* Fingolimod additionally acts as immunomodulator focused on the innate immune system beyond its prominent effects on lymphocyte recirculation. *J. Neuroinflamm.* **14**, 41, https://doi.org/10.1186/s12974-017-0817-6 (2017).
23. Belikan, P. *et al.* CCR7 on CD4+ T cells plays a crucial role in the induction of experimental autoimmune encephalomyelitis. *J. Immunol.* **200**, 2554–2562 (2018).
24. Racke, M. K., Yang, Y. & Lovett-Racke, A. E. Is T-bet a potential therapeutic target in multiple sclerosis. *J. Interferon Cytokine Res.* **34**, 623–632 (2014).
25. Hermann-Kleiter, N. & Baier, G. NFAT pulls the strings during CD4+ T helper cell effector function. *Blood.* **115**, 2989–2997 (2010).
26. Julià, E. *et al.* Deficient Fas expression by CD4+ CCR5+ T cells in multiple sclerosis. *J. Neuroimmunol.* **180**, 147–158 (2006).
27. Bettelli, E. *et al.* Loss of T-bet, but not STAT1, prevents the development of experimental autoimmune encephalomyelitis. *J. Exp. Med.* **200**, 79–87 (2004).
28. Petelin, Z. *et al.* CD95/Fas expression on peripheral blood T lymphocytes in patients with multiple sclerosis: effect of high-dose methylprednisolone therapy. *Clin. Neurol. Neurosurg.* **106**, 259–262 (2004).

71

29. De Simone, V. *et al*. Th17-type cytokines, IL-6 and TNF-α synergistically activate STAT3 and NF-kB to promote colorectal cancer cell growth. *Oncogene.* **34**, 3493–3503 (2015).
30. Bystry, R. S., Aluvihare, V., Welch, K. A., Kallikourdis, M. & Betz, A. G. B cells and professional APCs recruit regulatory T cells via CCL4. *Nat. Immunol.* **2**, 1126–1132 (2001).
31. Morrison, V. L., Barr, T. A., Brown, S. & Gray, D. TLR-mediated loss of CD62L focuses B cell traffic to the spleen during Salmonella typhimurium infection. *J. Immunol.* **185**, 2737–2746 (2010).
32. Mildner, A. *et al*. CCR2+Ly-6Chi monocytes are crucial for the effector phase of autoimmunity in the central nervous system. *Brain.* **132**, 2487–500 (2009).
33. Ajami, B., Bennett, J. L., Krieger, C., McNagny, K. M. & Rossi, F. M. Infiltrating monocytes trigger EAE progression, but do not contribute to the resident microglia pool. *Nat. Neurosci.* **14**, 1142–1149 (2011).
34. Haas, J., Schwarz, A., Korporal-Kuhnke, M., Jarius, S. & Wildemann, B. Myeloid dendritic cells exhibit defects in activation and function in patients with multiple sclerosis. *J. Neuroinflamm.* **301**, 53–60 (2016).
35. Ruiz-Alcaraz, A. J. *et al*. Characterization of human peritoneal monocyte/macrophage subsets in homeostasis: Phenotype, GATA6, phagocytic/oxidative activities and cytokines expression. *Sci. Rep.* **8**, 12794, https://doi.org/10.1038/s41598-018-30787-x (2018).
36. Raj, T. *et al*. Polarization of the effects of autoimmune and neurodegenerative risk alleles in leukocytes. *Science.* **344**, 519–523 (2014).
37. International Multiple Sclerosis Genetics Consortium. *et al*. Risk alleles for multiple sclerosis identified by a genome wide study. *N. Engl. J. Med.* **357**, 851–862 (2007).
38. Maltby, V. E. *et al*. Genome-wide DNA methylation changes in CD19+ B cells from relapsing-remitting multiple sclerosis patients. *Sci. Rep.* **8**, 17418, https://doi.org/10.1038/s41598-018-35603-0 (2018).
39. Cotsapas, C. & Hafler, D. A. Immune-mediated disease genetics: the shared basis of pathogenesis. *Trends Immunol.* **34**, 22–26 (2013).
40. Jordão, M. J. C. *et al*. Single-cell profiling identifies myeloid cell subsets with distinct fates during neuroinflammation. *Science.* **363**, eaat7554, https://doi.org/10.1126/science.aat7554 (2019).
41. Polman, C. H. *et al*. Diagnostic criteria for multiple sclerosis: 2010 revisions to the McDonald criteria. *Ann. Neurol.* **69**, 292–302 (2011).
42. Rasche, L. *et al*. Analysis of lymphocytic DNA damage in early multiple sclerosis by automated gamma-H2AX and 53BP1 foci detection: a case control study. *PLoS One.* **11**, e0147968, https://doi.org/10.1371/journal.pone.0147968 (2016).
43. Chevrier, S. *et al*. Compensation of signal spillover in suspension and imaging mass cytometry. *Cell Syst.* **6**, 612–620 (2018).
44. Van Gassen, S. *et al*. FlowSOM: Using self-organizing maps for visualization and interpretation of cytometry data. *Cytometry A.* **87**, 636–645 (2015).

Author contributions

C.B., K.R. and J.P. conceived and designed the project. C.B., S.S. and D.K. designed the antibody panel for mass cytometry. A.R.S. and H.E.M. provided custom barcoding reagents, discussed results and edited the manuscript. C.W. and B.S. recruited and diagnosed patients with Crohn's disease. K.R., R.M.G., S.A. and F.P. recruited and diagnosed early MS patients. C.B., C.F. and D.K. performed the experiments and acquired data. C.B., C.F. and S.S. analysed the data. C.B., S.S., B.S., K.R. and J.P. wrote the manuscript.

Competing interests

K.R. received research support from Novartis, Merck Serono and German Ministry of Education and Research as well as speaking fees and travel grants from Bayer Healthcare, Biogen Idec, Merck Serono, sanofi-aventis/ Genzyme, Teva Pharmaceuticals, Roche, Novartis, and Guthy Jackson Charitable Foundation.

Additional information

Supplementary information is available for this paper at https://doi.org/10.1038/s41598-019-55852-x.

Correspondence and requests for materials should be addressed to C.B. or J.P.

Reprints and permissions information is available at www.nature.com/reprints.

Publisher's note Springer Nature remains neutral with regard to jurisdictional claims in published maps and institutional affiliations.

72

Extract from the Journal Summary List for Publication 2

Journal Data Filtered By: **Selected JCR Year: 2018 Selected Editions: SCIE,SSCI**
Selected Categories: "NEUROSCIENCES" Selected Category Scheme: WoS
Gesamtanzahl: 267 Journale

Rank	Full Journal Title	Total Cites	Journal Impact Factor	Eigenfactor Score
1	NATURE REVIEWS NEUROSCIENCE	43,107	33.162	0.068480
2	NATURE NEUROSCIENCE	63,390	21.126	0.164700
3	ACTA NEUROPATHOLOGICA	20,206	18.174	0.041660
4	BEHAVIORAL AND BRAIN SCIENCES	9,377	17.194	0.010240
5	TRENDS IN COGNITIVE SCIENCES	27,095	16.173	0.040040
6	JOURNAL OF PINEAL RESEARCH	10,695	15.221	0.010560
7	NEURON	95,348	14.403	0.218680
8	TRENDS IN NEUROSCIENCES	20,163	12.314	0.024480
9	Annual Review of Neuroscience	14,042	12.043	0.015020
10	MOLECULAR PSYCHIATRY	20,353	11.973	0.049290
11	BRAIN	52,970	11.814	0.074030
12	BIOLOGICAL PSYCHIATRY	43,122	11.501	0.053320
13	PROGRESS IN NEUROBIOLOGY	12,929	10.658	0.013230
14	Nature Human Behaviour	1,230	10.575	0.006550
15	SLEEP MEDICINE REVIEWS	6,920	10.517	0.010920
16	ANNALS OF NEUROLOGY	37,336	9.496	0.048630
17	Molecular Neurodegeneration	4,248	8.274	0.011350
18	NEUROSCIENCE AND BIOBEHAVIORAL REVIEWS	26,724	8.002	0.051580
19	FRONTIERS IN NEUROENDOCRINOLOGY	4,196	7.852	0.005490
20	Neurology-Neuroimmunology & Neuroinflammation	1,996	7.353	0.008220
21	NEUROPSYCHOPHARMACOLOGY	25,672	7.160	0.039090

Selected JCR Year: 2018; Selected Categories: "NEUROSCIENCES"

Rank	Full Journal Title	Total Cites	Journal Impact Factor	Eigenfactor Score
22	Brain Stimulation	5,457	6.919	0.014470
23	NEUROPATHOLOGY AND APPLIED NEUROBIOLOGY	3,876	6.878	0.006420
24	NEUROENDOCRINOLOGY	5,046	6.804	0.005690
25	NEUROSCIENTIST	4,986	6.791	0.008520
26	BRAIN BEHAVIOR AND IMMUNITY	14,533	6.170	0.025700
27	BRAIN PATHOLOGY	5,263	6.155	0.007880
28	Alzheimers Research & Therapy	3,160	6.142	0.010700
29	JOURNAL OF NEUROSCIENCE	175,046	6.074	0.233460
30	JOURNAL OF CEREBRAL BLOOD FLOW AND METABOLISM	19,766	6.040	0.028050
31	PAIN	38,312	6.029	0.039070
32	CURRENT OPINION IN NEUROBIOLOGY	15,090	6.014	0.033650
33	Acta Neuropathologica Communications	3,063	5.883	0.014190
34	Translational Stroke Research	1,955	5.847	0.004330
35	GLIA	14,003	5.829	0.018760
36	NEUROIMAGE	99,720	5.812	0.132720
37	NEURAL NETWORKS	13,063	5.785	0.016060
38	NEUROPSYCHOLOGY REVIEW	2,971	5.739	0.003940
39	Molecular Autism	2,107	5.712	0.008000
40	Journal of Neuroinflammation	11,767	5.700	0.023240
41	Multiple Sclerosis Journal	11,501	5.649	0.022750
42	Annual Review of Vision Science	458	5.622	0.003300
43	Neurotherapeutics	4,475	5.552	0.009060
44	Translational Neurodegeneration	810	5.534	0.002420

Selected JCR Year: 2018; Selected Categories: "NEUROSCIENCES"

Selected publication 2

Böttcher C*, van der Poel M*, Fernández-Zapata C*, Schlickeiser S, Leman JKH, Hsiao CC, Mizee MR, Adelia, Vincenten MCJ, Kunkel D, Huitinga I, Hamann J, Priller J. Single-cell mass cytometry reveals complex myeloid cell composition in active lesions of progressive multiple sclerosis. Acta Neuropathol Commun. 2020 Aug 18;8(1):136.

Single-cell mass cytometry reveals complex myeloid cell composition in active lesions of progressive multiple sclerosis

Chotima Böttcher[1*†], Marlijn van der Poel[2†], Camila Fernández-Zapata[1†], Stephan Schlickeiser[3],
Julia K. H. Leman[1], Cheng-Chih Hsiao[2,4], Mark R. Mizee[2], Adelia[5], Maria C. J. Vincenten[2], Desiree Kunkel[6],
Inge Huitinga[2,7†], Jörg Hamann[2,4†] and Josef Priller[1,8,9*†]

Abstract

Myeloid cells contribute to inflammation and demyelination in the early stages of multiple sclerosis (MS), but it is still unclear to what extent these cells are involved in active lesion formation in progressive MS (PMS). Here, we have harnessed the power of single-cell mass cytometry (CyTOF) to compare myeloid cell phenotypes in active lesions of PMS donors with those in normal-appearing white matter from the same donors and control white matter from non-MS donors. CyTOF measurements of a total of 74 targeted proteins revealed a decreased abundance of homeostatic and TNF^{hi} microglia, and an increase in highly phagocytic and activated microglia states in active lesions of PMS donors. Interestingly, in contrast to results obtained from studies of the inflammatory early disease stages of MS, infiltrating monocyte-derived macrophages were scarce in active lesions of PMS, suggesting fundamental differences of myeloid cell composition in advanced stages of PMS.

Keywords: Progressive multiple sclerosis, Mass cytometry, Microglia, Myeloid cells, Active lesion

Introduction

Multiple sclerosis (MS) is a chronic inflammatory disease of the central nervous system (CNS) which leads to demyelinating lesions and diffuse neurodegeneration spreading throughout the white and grey matter of the brain and the spinal cord [1, 2]. In most cases (85–90% of patients with MS), the disease starts with a relapsing-remitting course (RRMS), which may develop into a progressive course (secondary progressive MS, SPMS) with ongoing neuroinflammation [3, 4]. For some MS patients (10–15% of patients), neurological disability increases progressively over time without relapse or remission (primary progressive MS, PPMS). From a

neuropathological perspective, MS lesions are characterized as active, mixed active/inactive, inactive remyelinated (shadow plaques), or inactive lesions, based on demyelination and the presence of HLA-DR$^+$ myeloid cells [1, 5]. Both active and mixed active/inactive lesions are characterized by the loss of myelin and the presence of activated foamy microglia/macrophages containing myelin, indicating that microglia/macrophages play a pathogenic role in MS [1, 5]. Active lesions are thought to be the earliest stage in MS lesion formation [5, 6]. As the disease progresses, axonal damage and neurodegeneration become more pronounced. A higher proportion of mixed active/inactive lesions and a less prominent peripheral immune cell infiltrate are observed in progressive MS (PMS) as compared to relapsing disease [5, 7]. Unlike RRMS, immunomodulatory treatments are not effective in patients with PMS [8, 9], suggesting that different pathological processes besides classical neuroinflammation may occur in the progressive form of the disease. As well as

* Correspondence: chotima.boettcher@charite.de; josef.priller@charite.de
†Chotima Böttcher, Marlijn van der Poel, Camila Fernández-Zapata, Inge
Huitinga, Jörg Hamann and Josef Priller contributed equally to this work.
[1]Department of Neuropsychiatry and Laboratory of Molecular Psychiatry,
Charité – Universitätsmedizin Berlin, Berlin, Germany
Full list of author information is available at the end of the article

B cell-targeted therapies and sphingosine-1-phosphate antagonists, promotion of remyelination and targeting of myeloid cells are promising strategies for treating PMS [10].

Activation of microglia/macrophages is considered a key mechanism which contributes to inflammation, demyelination and neurodegeneration in MS. Using bulk transcriptomic analysis, we have recently demonstrated subtle changes in expression of microglial genes involved in lipid storage and metabolism in normal-appearing white matter (NAWM) in late-stage PMS [11]. These altered microglial signatures are early signs of MS pathology as a similar transcriptional microglial profile was found in chronic active lesions [11]. We have also demonstrated overall preservation of microglial homeostatic functions in NAWM PMS tissue [11]. However, the phenotypic heterogeneity of microglia regarding their homeostatic and inflammatory state in PMS active lesions remains unknown. A landmark study using single-cell RNA-sequencing (scRNA-Seq) showed unique transcriptomic profiles of microglia in active lesion biopsies from patients in the early disease stages of MS, compared with microglia isolated from control tissue of non-MS donors [12]. Further, in the early disease stages of MS and in a mouse model of demyelination, homeostatic microglial genes such as *P2RY12*, *TMEM119* and *CX3CR1* were downregulated in active lesions, whereas genes associated with microglia states *SPP1*, *CD74* and *CTSD* and the cytokine *CCL4* were upregulated [12, 13]. However, it is yet to be investigated whether these changes can also be detected in active lesions of PMS at the single-cell protein level. Furthermore, whereas approximately 10% of Iba1$^+$ cells in brain sections of patients with early MS are infiltrating monocytes [12], it is not yet known whether a similar contribution of monocyte-derived cells to MS lesion initiation and/or maturation can be detected in active lesions of PMS. Together, microglia show context-dependent signatures in lesions of early MS, but the differential functions of microglia and the involvement of infiltrating monocyte-derived macrophages in PMS are not clear.

In this study, we have used single-cell mass cytometry by time of flight (CyTOF) to comprehensively characterize the phenotypes of myeloid cells in active lesions and in NAWM from ten PMS donors. Subsequently, we compared these cells to those isolated from control WM of eight non-MS donors. The results obtained from this study suggest that active lesions of PMS contain diverse clusters of highly phagocytic and activated WM myeloid cells with little infiltration of monocyte-derived macrophages.

Materials and methods
Human post-mortem tissue
Post-mortem tissue of brain donors was provided by the Netherlands Brain Bank (NBB, Amsterdam, The Netherlands, www.brainbank.nl). All brain donors gave informed consent to perform autopsies and to use tissue, clinical and neuropathological information for research purposes, approved by the Ethics Committee of VU medical center (Amsterdam, The Netherlands).

Subcortical white matter (WM) tissue was collected from non-MS WM control donors ($n = 8$), and from MS donors we collected subcortical NAWM ($n = 10$) and subcortical WM lesions (n = 10). NAWM MS tissue was dissected on post-mortem magnetic resonance imaging (MRI) guidance during autopsy [14]. In addition, macroscopically visible MS lesions were dissected by a neuropathologist.

Neurological diagnoses were confirmed by a neuropathologist. Information on MS diagnosis and disease duration was obtained from clinical data, showing that all donors were diagnosed with progressive MS, 3 donors with primary progressive MS and 7 donors with secondary progressive MS. Donor characteristics and post-mortem variables are displayed in Additional file 1, Supplementary Table 1-3 and 6.

MS lesion characterization
From post-mortem tissue that was taken out for microglia isolation, a small part was snap-frozen in liquid nitrogen and stored in − 80 °C until further use. Frozen tissue sections (20 μm) of control WM, NAWM and MS lesions were cut and dried overnight. For immunohistochemistry, these sections were fixed for 15 min with 4% paraformaldehyde in phosphate buffered saline (PBS) pH 7.6, followed by endogenous peroxidase blocking in 1% H_2O_2 in PBS for 20 min. Sections were incubated with primary antibodies HLA-DR/DQ/DP (1:1000, M0775; Dako, Glostrup, Denmark) or PLP (1:3000, MCA839G; Serotec, Oxford, UK) in incubation buffer (0.5% Triton X-100 and 1% bovine serum albumin (BSA) in PBS) overnight at 4 °C. Secondary antibodies were incubated for 1 h at room temperature (RT); for HLA-DR biotinylated anti-mouse (1:400, BA-2001; Vector Laboratories, Burlingame, CA, USA) was diluted in incubation buffer, for PLP the HRP-labeled mouse antibody (K5007, Dako Real EnVision detection system; Dako) was used. Next, sections for HLA-DR staining were incubated for 45 min in avidin-biotin complex (1:800, PK-6100; Vector Laboratories) at RT, followed by 3, 3′-diaminobenzidine (DAB) incubation (1:100, K5007; Dako) for 10 min at RT, for both HLA-DR and PLP stainings. Immunoreactivity was examined using an Axioskop980 microscope (Zeiss, Oberkochen, Germany) and Photomacroscope M420 (Wild Heerbrugg, Zwitserland) to characterize lesions based on HLA-DR presence and morphology of HLA-DR$^+$ cells together with myelin intactness based on PLP staining [5].

B cell-targeted therapies and sphingosine-1-phosphate antagonists, promotion of remyelination and targeting of myeloid cells are promising strategies for treating PMS [10].

Activation of microglia/macrophages is considered a key mechanism which contributes to inflammation, demyelination and neurodegeneration in MS. Using bulk transcriptomic analysis, we have recently demonstrated subtle changes in expression of microglial genes involved in lipid storage and metabolism in normal-appearing white matter (NAWM) in late-stage PMS [11]. These altered microglial signatures are early signs of MS pathology as a similar transcriptional microglial profile was found in chronic active lesions [11]. We have also demonstrated overall preservation of microglial homeostatic functions in NAWM PMS tissue [11]. However, the phenotypic heterogeneity of microglia regarding their homeostatic and inflammatory state in PMS active lesions remains unknown. A landmark study using single-cell RNA-sequencing (scRNA-Seq) showed unique transcriptomic profiles of microglia in active lesion biopsies from patients in the early disease stages of MS, compared with microglia isolated from control tissue of non-MS donors [12]. Further, in the early disease stages of MS and in a mouse model of demyelination, homeostatic microglial genes such as *P2RY12*, *TMEM119* and *CX3CR1* were downregulated in active lesions, whereas genes associated with microglia states *SPP1*, *CD74* and *CTSD* and the cytokine *CCL4* were upregulated [12, 13]. However, it is yet to be investigated whether these changes can also be detected in active lesions of PMS at the single-cell protein level. Furthermore, whereas approximately 10% of Iba1^{+} cells in brain sections of patients with early MS are infiltrating monocytes [12], it is not yet known whether a similar contribution of monocyte-derived cells to MS lesion initiation and/or maturation can be detected in active lesions of PMS. Together, microglia show context-dependent signatures in lesions of early MS, but the differential functions of microglia and the involvement of infiltrating monocyte-derived macrophages in PMS are not clear.

In this study, we have used single-cell mass cytometry by time of flight (CyTOF) to comprehensively characterize the phenotypes of myeloid cells in active lesions and in NAWM from ten PMS donors. Subsequently, we compared these cells to those isolated from control WM of eight non-MS donors. The results obtained from this study suggest that active lesions of PMS contain diverse clusters of highly phagocytic and activated WM myeloid cells with little infiltration of monocyte-derived macrophages.

Materials and methods
Human post-mortem tissue
Post-mortem tissue of brain donors was provided by the Netherlands Brain Bank (NBB, Amsterdam, The Netherlands, www.brainbank.nl). All brain donors gave informed consent to perform autopsies and to use tissue, clinical and neuropathological information for research purposes, approved by the Ethics Committee of VU medical center (Amsterdam, The Netherlands).

Subcortical white matter (WM) tissue was collected from non-MS WM control donors ($n = 8$), and from MS donors we collected subcortical NAWM ($n = 10$) and subcortical WM lesions (n = 10). NAWM MS tissue was dissected on post-mortem magnetic resonance imaging (MRI) guidance during autopsy [14]. In addition, macroscopically visible MS lesions were dissected by a neuropathologist.

Neurological diagnoses were confirmed by a neuropathologist. Information on MS diagnosis and disease duration was obtained from clinical data, showing that all donors were diagnosed with progressive MS, 3 donors with primary progressive MS and 7 donors with secondary progressive MS. Donor characteristics and post-mortem variables are displayed in Additional file 1, Supplementary Table 1-3 and 6.

MS lesion characterization
From post-mortem tissue that was taken out for microglia isolation, a small part was snap-frozen in liquid nitrogen and stored in − 80 °C until further use. Frozen tissue sections (20 μm) of control WM, NAWM and MS lesions were cut and dried overnight. For immunohistochemistry, these sections were fixed for 15 min with 4% paraformaldehyde in phosphate buffered saline (PBS) pH 7.6, followed by endogenous peroxidase blocking in 1% H_2O_2 in PBS for 20 min. Sections were incubated with primary antibodies HLA-DR/DQ/DP (1:1000, M0775; Dako, Glostrup, Denmark) or PLP (1:3000, MCA839G; Serotec, Oxford, UK) in incubation buffer (0.5% Triton X-100 and 1% bovine serum albumin (BSA) in PBS) overnight at 4 °C. Secondary antibodies were incubated for 1 h at room temperature (RT); for HLA-DR biotinylated anti-mouse (1:400, BA-2001; Vector Laboratories, Burlingame, CA, USA) was diluted in incubation buffer, for PLP the HRP-labeled mouse antibody (K5007, Dako Real EnVision detection system; Dako) was used. Next, sections for HLA-DR staining were incubated for 45 min in avidin-biotin complex (1:800, PK-6100; Vector Laboratories) at RT, followed by 3, 3′-diaminobenzidine (DAB) incubation (1:100, K5007; Dako) for 10 min at RT, for both HLA-DR and PLP stainings. Immunoreactivity was examined using an Axioskop980 microscope (Zeiss, Oberkochen, Germany) and Photomacroscope M420 (Wild Heerbrugg, Zwitserland) to characterize lesions based on HLA-DR presence and morphology of HLA-DR^{+} cells together with myelin intactness based on PLP staining [5].

Microglia isolation

Microglia were isolated from post-mortem WM tissue, as described previously [11, 15]. Briefly, post-mortem tissue that was collected during autopsy was stored in Hibernate-A medium (Invitrogen, Carlsbad, CA, USA) at 4 °C until further processing. Within 24 h, the tissue was homogenized for 5 min in Hibernate-A medium supplemented with DNAseI (10 mg/ml; Roche, Basel, Switzerland), using a tissue homogenizer (VWR, Radnor, PA, USA). Next, undiluted Percoll (density of 1.13 g/ml; GE Healthcare, Little Chalfont, UK) was added to form a single gradient for density centrifugation and the interlayer was collected for magnetic activated cell sorting (MACS; Miltenyi, Bergisch Gladbach, Germany) using CD11b magnetic beads (catalogue number #130–049-601, Miltenyi Biotech). Viable cells were counted using a hemocytometer (Optic Labor, Friedrichshof, Germany) or eFluor™ 506. Cells were then collected in beads buffer (0.5% BSA + 2 mM EDTA in PBS, pH 7.6) for flow cytometry analysis. Using this protocol, about 95% of viable cells were identified as myeloid cells (Supplementary Fig. 1). For CyTOF analysis, CD11b$^+$ cells were incubated for 11 min in fixation/stabilization buffer (Smart Tube Inc., San Carlos, CA, USA) and stored in − 80 °C.

IRF8$^+$ nuclei isolation and sorting

IRF8$^+$ nuclei were isolated and sorted as described previously [11]. Briefly, frozen tissue from MS donors, NAWM tissue ($n = 7$) and tissue containing MS lesions ($n = 5$), matched for age, was provided by the NBB. For each tissue block, the first and last section were double stained for HLA-DR/PLP to determine microglia activation and myelin integrity. MS lesions were characterized as previously described by Luchetti and colleagues [5].

From each tissue block, 10–12 sections of 50 μm thickness were cut and homogenized in 1 ml homogenization buffer (1 μm DTT (Thermo Fischer Scientific), 1x protease inhibitor (Roche), 80 U/ml RNAseIN (Promega, Madison, WI, USA) and 1% Triton X-100) with nuclei isolation medium #1 (NIM #1; 250 mM sucrose, 25 mM KCL, 5 mM MgCl$_2$, 10 mM Tris buffer pH 8 diluted in nuclease free water) filtered through a 30-μm cell strainer. The amount of nuclei was counted using a hemocytometer (Optic Labor) and nuclei were incubated with Hoechst (#H3570, 1:1000; Invitrogen) and IRF8 antibody (#566373, PE-labeled, 1:50, clone U31–644; BD Biosciences, San Diego, CA, USA) in staining buffer (0.5% RNAse free BSA, 1% normal human serum and 0.2 U/μl RNAseIn in RNAse-free PBS, pH 7.4) for 1 h at 4 °C. Isotype control antibody IgG-PE (#12–4714-42, clone P3.6.8.1, 1:25; Invitrogen) was used to determine background staining.

Stained nuclei were sorted using a Sony SH800S cell sorter (Sony Biotechnology, San Jose, CA, USA). The Hoechst and IRF8 double positive nuclei fractions was collected and lysed in RNA lysis buffer (RNeasy Isolation mini kit; Qiagen, Hilden, Germany).

RNA isolation

RNA from sorted IRF8$^+$ nuclei was isolated using the RNeasy Mini kit (Qiagen), according to the manufacturer's protocol. Lysed samples were mixed with 70% ethanol and transferred to a mini spin column. After washing steps, elution was collected in 20 μl deionized water.

DNA synthesis and quantitative real-time PCR

The Quantitect Reverse Transcription Kit (Qiagen) was used for cDNA synthesis. According to manufacturer's protocol, isolated RNA (25 ng) from sorted IRF8$^+$ nuclei was mixed with gDNA wipeout buffer, incubated for 2 min at 42 °C and put on ice. Next, Quantiscript RT buffer, RT primer mix and Quantiscript Reverse Transcriptase were mixed and incubated with RNA sample at 42 °C for 30 min, followed by 3 min incubation at 95 °C.

For RT-qPCR, 0.6 ng cDNA was mixed with 17 μl SYBR Green PCR master mix (Applied Biosystems, Foster City, CA, USA) and 2 μl primer pairs. Samples were measured and analyzed using 7300 RT-PCR machine and software (Applied Biosystems).

Primer pairs were designed at the Integrated DNA Technologies website (eu.ifdna.com), using the PrimerQuest tool. For primer design the following criteria were used: same Tm, 50% GC content, amplicon size between 80 and 140 base pairs and exclude primers that span introns, to detect unspliced nuclear DNA. Primer pairs were checked for specificity using cDNA derived from pooled MS and control donor brain tissue. Optimal primers (Additional file 1: Supplementary Table 4) were selected based on dissociation curve, and 8% sodium dodecyl sulfate polyacrylamide gel electrophoresis gel was used to detect PCR product and exclude primer pairs that can form dimers. Gene expression was normalized to the mean of 2 housekeeping genes, glyceraldehyde 3-phosphate dehydrogenase (*GAPDH*) and elongation factor-1 alpha (*EEF1A1*). Target gene expression values were calculated using the 2- ΔΔCT method.

Flow cytometric analysis

Isolated microglia from MS donors ($n = 7$) were incubated for 15 min in FcR-blocking buffer (1:5; Miltenyi Biotec), to block unspecific binding of antibodies to Fc-receptors. Next, microglia were incubated with conjugated primary antibodies (Additional file 1: Supplementary Table 5) diluted in beads buffer (0.5% BSA and 2 mM EDTA in PBS, pH 7.6) for 30 min at 4 °C. To

79

determine viability, cells were incubated with viability dye efluor506 (Additional file 1: Supplementary Table 5).

To assess minimal phenotyping of isolated microglia, CD45 and CD11b expression was determined. In addition, expression of homeostatic microglia receptors, $P2Y_{12}$, CX3CR1 and GPR56 was measured. To exclude infiltrating leukocytes in the samples collected from MS lesion tissue, CD3, CD19, CD56 and CD66b were included.

Surface protein expression was detected on a 3-laser BD FACSCanto II machine (BD Biosciences) with software BD DIVA version 8.1. FlowJo software version 10.1 (Ashland, OR, USA) was used to determine median fluorescence intensity.

Immunohistochemical quantification

Paraffin tissue blocks from age-matched control ($n = 5$) and MS ($n = 11$) donors (Additional file 1: Supplementary Tables 1 and 6) were cut into 8 μm-thick sections. Tissue sections were deparaffinized with xylene and rehydrated in ethanol series, followed by antigen retrieval with citrate buffer pH 6 for 20 min in a steamer. Sections were blocked in 10% normal horse serum/normal donkey serum for 30 min and incubated with $P2Y_{12}$ antibody and either CD68 (DAKO, # M0814) or HLA-DR (DAKO, #M0775) antibodies diluted in incubation buffer (0.5% Triton-X100 and 0.25% gelatin in tris-buffered saline (TBS, pH 7.6) and incubated overnight at 4 °C. After overnight incubation with primary antibody, samples were incubated for 2 h at RT with Alexa Fluor 568 and Alexa Fluor 488-conjugated secondary antibody. Nuclei were stained with DAPI. All images were acquired in a Leica TCS SP5 microscope (Leica microsystems). $P2Y_{12}^{+}DAPI^{+}$ and $P2Y_{12}^{+}CD68^{+}DAPI^{+}$ or $P2Y_{12}^{+}HLA-DR^{+}DAPI^{+}$ cells were counted using IMARIS software. All image processing for visualization was performed with ImageJ software.

Intracellular barcoding for mass cytometry

Percoll-isolated myeloid cells were fixed with fixation/stabilization buffer (SmartTube) [16] and frozen at −80 °C until analysis by mass cytometry. Cell were thawed and subsequently stained with premade combinations of six different palladium isotopes: ^{102}Pd, ^{104}Pd, ^{105}Pd, ^{106}Pd, ^{108}Pd and ^{110}Pd (Cell-ID 20-plex Pd Barcoding Kit, Fluidigm). This multiplexing kit applies a 6-choose-3 barcoding scheme that results in 20 different combinations of three Pd isotopes. After 30 min staining (at room temperature), individual samples were washed twice with cell staining buffer (0.5% bovine serum albumin in PBS, containing 2 mM EDTA). All samples were pooled together, washed and further stained with antibodies.

Antibodies

Anti-human antibodies (Additional file 1: Supplementary Tables 7 and 8) were purchased either pre-conjugated to metal isotopes (Fluidigm) or from commercial suppliers in purified form and conjugated in house using the Max-Par X8 kit (Fluidigm) according to the manufacturer's protocol. Using different cell types from different body compartments, each antibody was titrated and validated as into the working panels prior to use to ensure that the resulted signals were informative [16, 17].

Cell-surface and intracellular staining

After cell barcoding, washing and pelleting, the combined samples were stained and processed as described previously [16, 17]. Briefly, cells were re-suspended in 100 μl of antibody cocktail directed against cell surface markers (Additional file 1: Supplementary Tables 7 and 8) and incubated for 30 min at 4 °C. Then, cells were washed twice with cell staining buffer (PBS containing 0.5% BSA and 2 mM EDTA). For intracellular staining, the stained (non-stimulated) cells were then incubated in fixation/permeabilization buffer (Fix/Perm Buffer, eBioscience) for 60 min at 4 °C. Cells were then wash twice with permeabilization buffer (eBioscience). The samples were then stained with antibody cocktails directed against intracellular molecules (Additional file 1: Supplementary Tables 7 and 8) in permeabilization buffer for 1 h at 4 °C. Cells were subsequently washed twice with permeabilization buffer and incubated overnight in 4% methanol-free formaldehyde solution. The fixed cells were then washed and re-suspended in 1 ml iridium intercalator solution (Fluidigm) for 1 h at RT, followed by two washes with cell staining buffer and two washes with ddH₂O (Fluidigm). Finally, cells were pelleted and kept at 4 °C until CyTOF measurement.

Bead staining

For the bead-based compensation of the signal spillover, AbC total antibody compensation beads (Thermo Fisher Scientific) were single stained with each of the antibodies used in all three antibody panels according to manufacturer's instructions. Stained beads were then measured with CyTOF and the compensation matrix was then generated [17, 18].

CyTOF measurement

Cells were analysed using a CyTOF2 upgraded to Helios specifications, with software version 6.7.1014 [16, 17], using a narrow bore injector. The instrument was tuned according to the manufacturer's instructions with tuning solution (Fluidigm) and measurement of EQ four element calibration beads (Fluidigm) containing $^{140/142}Ce$, $^{151/153}Eu$, ^{165}Ho and $^{175/176}Lu$ served as a quality control for sensitivity and recovery.

80

Directly prior to analysis cells were re-suspended in ddH$_2$O, filtered through a 20-µm cell strainer (Celltrics, Sysmex), counted and adjusted to 5–8 × 10^5 cells/ml. EQ four element calibration beads were added at a final concentration of 1:10 v/v of the sample volume to be able to normalize the data to compensate for signal drift and day-to-day changes in instrument sensitivity.

Samples were acquired with a flow rate of 300–400 events/s. The lower convolution threshold was set to 400, with noise reduction mode turned on and cell definition parameters set at event duration of 10–150 pushes (push = 13 µs). The resulting flow cytometry standard (FCS) files were normalized and randomized using the CyTOF software's internal FCS-Processing module on the non-randomized ('original') data. The default settings in the software were used with time interval normalization (100 s/minimum of 50 beads) and passport version 2. Intervals with less than 50 beads per 100 s were excluded from the resulting FCS file.

Mass cytometry data processing and analysis

Following the workflow from our previous study [16, 17], Cytobank (www.cytobank.org) was used for initial manual gating on live single cells and Boolean gating for de-barcoding. Nucleated single intact cells were manually gated according to DNA intercalators [191]Ir/[193]Ir signals and event length. For de-barcoding, Boolean gating was used to deconvolute individual sample according to the barcode combination. Prior to data analysis, each FCS file was compensated for signal spillover using R package *CATALYST* [18]. For dimensionality reduction, visualization and further exploration, (2D) tSNE maps were generated according to the expression levels of all markers in each panel. For embedding, we set hyperparameters to perplexity of 30, theta of 0.5, and iterations of 1000 per 100,000 analysed cells. To visualize marker expression arcsinh transformation was applied to the data. All FCS files were then loaded into R and further data analysis was performed with an in-house written script based on the workflow proposed by M. Nowicka and colleagues [19]. Briefly, for unsupervised cell population identification we performed cell clustering with the *FlowSOM* [20] and *ConsensusClusterPlus* [21] packages using all markers (*Exp-I*) or TYPE markers (*Exp-II* and *-III*). We then performed visual inspection of cluster-coloured tSNE plots and phenotypic heatmaps for a more detailed profile of each cluster and determined the number of meta-clusters on the basis of delta area under cumulative distribution function (CDF) curve and k value of the clustering analysis and the consistency of phenotypes for statistical test. For detection of differential abundance of clusters between conditions we used generalized linear mixed models (GLMM) performed with the *diffcyt* package [17], with a false discovery rate

(FDR) adjustment (Benjamini-Hochberg (BH) procedure) for multiple hypothesis testing. A *P* value < 0.05 (unadjusted) and < 0.05 (FDR-BH adjusted) was considered statistically significant.

Imaging mass cytometry

Paraffin tissue microarray (TMA) blocks containing samples from control, NAWM and lesion were cut into 5 µm-thick sections. Sections were deparaffinized with xylene and rehydrated in ethanol series, followed by heat-induced antigen retrieval in Tris-EDTA buffer (pH = 9.0) for 20 min at 95 °C in a steamer. The sections were then blocked with 3% purified BSA in 0.1% Triton-X PBS for 1 h at RT. Sections were incubated overnight at 4 °C with anti-P2Y$_{12}$ conjugated with biotin. After washing, all sections were incubated with metal-conjugated antibodies (Additional file 1: Supplementary Table 9) overnight at 4 °C. Nuclei were detected using an Ir-Intercalator (1:500). Samples were then dried and stored at RT until measurement.

Imaging mass cytometry acquisition and data analysis

Imaging mass cytometry was performed on a CyTOF2/upgraded to Helios specifications coupled to a Hyperion Tissue Imager (Fluidigm), using CyTOF software version 6.7.1014. Prior to ablation the instrument was tuned according to the manufactures instructions, using the 3-Element Full Coverage Tuning Slide (Fluidigm). The dried slide was loaded into the imaging module and regions of interest were selected for each sample of the TMA on a preview (panorama). Optimal laser power was determined for each sample to obtain complete ablation of the tissue. Laser ablation was performed at a resolution of 1 µm and a frequency of 200 Hz. Data were stored as MCD files as well as txt files. Original files were opened with MCD viewer and single 16-bit images were extracted as. TIFF files. For visualization only, images were transferred to ImageJ and the different channels were merged. A Gaussian blur (kernel width, 0.70 pixels) was used for noise reduction.

For single-cell analysis, we first processed images from each sample using *Ilastik* [22], an open-source program that uses interactive machine learning to separate single cells from background. The program was trained to identify DNA iridium-intercalator as nuclei and P2Y$_{12}$-[Ho]165 as cell membrane, and the pixel classificator was then applied to all images. As a result, a binary mask delimiting each single-cell was obtained and transferred on to *CellProfiler* [23]. We applied a set of modules to create single-cell masks, the modules included filters for cell size, negative selection for cells on the border of the image or exclusion of cytoplasm signal with no nuclei, thus generating 16-bit *.tiff* single-cell masks with only full cells for each image. Each of the *.tiff*

files and single-cell masks were then transferred to *histo-CAT* [24] for further analysis. In *histoCAT*, we ran a dimensionality reduction tSNE algorithm to visualize single cell data from all samples. We then ran a Phenograph analysis in which cells were clustered according to their marker expression (for markers CD11c, CD44, CD45, CD68, HLA-DR, $P2Y_{12}$ and TNF, using k = 50 nearest neighbours). The mean expression and cell frequencies per sample/cluster where then extracted using R.

Statistical analysis

No randomization and blinding strategies were applied in this study. However, data processing and analysis, as well as statistical testing were carried out in an unsupervised manner. No priori statistical methods were used to predetermine sample sizes due to sample accessibility and insufficient previous data to enable this. However, sample sizes were chosen based on estimates of anticipated variability through previous studies on scRNA-Seq analysis of microglia in acute lesion MS [12]. Dichotomous variables of the sample cohort were analysed with Fisher's exact test (GraphPad Prism). Quantitative data are shown as independent data points with median or Box-Whisker. Unless otherwise stated, analyses of statistical significance were performed by computational analysis using generalized linear mixed-effects model (GLMM) available through R package *diffcyt* and false discovery rate (FDR) adjustment (using Benjamini-Hochberg procedure) for multiple hypothesis testing. A p-value < 0.05 (FDR-adjusted) was considered statistically significant.

Results

Characterization of MS lesions

This study used post-mortem WM brain from ten MS donors. All donors were diagnosed with PMS and had a mean disease duration of 24.7 years (sd = 11 years), and an average disease severity (defined as years until the patients reached an expanded disability status scale (EDSS) score of 6.0) of 13.1 years (sd = 7.8) (Additional file 1: Supplementary Tables 1 and 2).

For each MS donor, the NAWM tissue was dissected using magnetic resonance imaging (MRI) guidance [14] and MS lesions were dissected by a neuropathologist based on macroscopic appearance. Active MS lesions were characterized as previously described [5, 25]. For each MS donor, myeloid cells were isolated from a block of NAWM tissue and a block of active lesion tissue surrounded by NAWM, using an optimized protocol involving density gradient separation and CD11b-magnetic bead sorting (MACS) [15]. To confirm the active status of MS lesions, immunohistochemical analysis was retrospectively performed on tissue blocks. Myelin

proteolipid protein (PLP) and human leukocyte antigen (HLA)-DR were used to define myelin integrity and microglia/macrophage activation and morphology, respectively (Additional file 2: Supplementary Fig. 2a). PLP staining of NAWM tissue sections showed intact myelin (Additional file 2: Supplementary Fig. 2a). In contrast, loss of PLP expression, which indicates demyelination, was used to identify active lesions (Additional file 2: Supplementary Fig. 2a). HLA-DR positive cells were present throughout the entire lesion and the majority of microglia/macrophages in active lesions had amoeboid or foamy morphology (Additional file 2: Supplementary Fig. 2a). However, using bulk quantitative polymerase chain reaction (qPCR) analysis of isolated $IRF8^+$ nuclei (comprising microglia and macrophages) from frozen tissue sections [11] (Supplementary Table 3), we could not detect significant alterations of heteronuclear RNA expression of homeostatic genes *CX3CR1*, *TMEM119*, *P2RY12* and *ADGRG1* in active lesions of PMS, compared to NAWM (Additional file 1: Supplementary Table 4; Additional file 2: Supplementary Fig. 2b). Low-dimensional flow cytometric analysis also revealed no significant differences in the expression levels of the microglial homeostatic proteins CX3CR1, $P2Y_{12}$ and GPR56 (*ADGRG1*) in active MS lesions compared to NAWM (Additional file 1: Supplementary Table 5; Additional file 2: Supplementary Fig. 2c). However, immunohistochemical analysis of the tissue revealed a reduction of $P2Y_{12}$-expressing cells in active lesions of PMS as compared to NAWM from MS donors and control WM tissues from non-MS donors (Additional file 1: Supplementary Table 1 and 6; Additional file 2: Supplementary Fig. 2d). No significant difference in the number of $P2Y_{12}$-expressing cells was found between NAWM and non-MS white matter. Increased expression of HLA-DR was found in $P2Y_{12}^+$ cells in active lesions, compared to those in NAWM (Supplementary Fig. 3). Slightly enhanced expression of CD68 was also detected in $P2Y_{12}^+$ cells in active lesions but was not statistically significant (Supplementary Fig. 3).

Majority of active lesion microglia in PMS preserve homeostatic signatures

To prove an assumption that subtle changes of microglia (which may have been obscured in bulk analysis and/or in low-dimensional phenotypic profiling) characterize active lesions of PMS, we next investigated microglia/macrophage phenotypes in PMS at single-cell resolution. Three multiplexed single-cell CyTOF analyses were performed on MACS-sorted CD11b-expressing cells from active lesions and NAWM (from ten PMS donors), using three different antibody panels (*Exp-I*, *–II* and *-III*; Additional file 1: Supplementary Table 8). With this experimental design, we aimed to demonstrate the
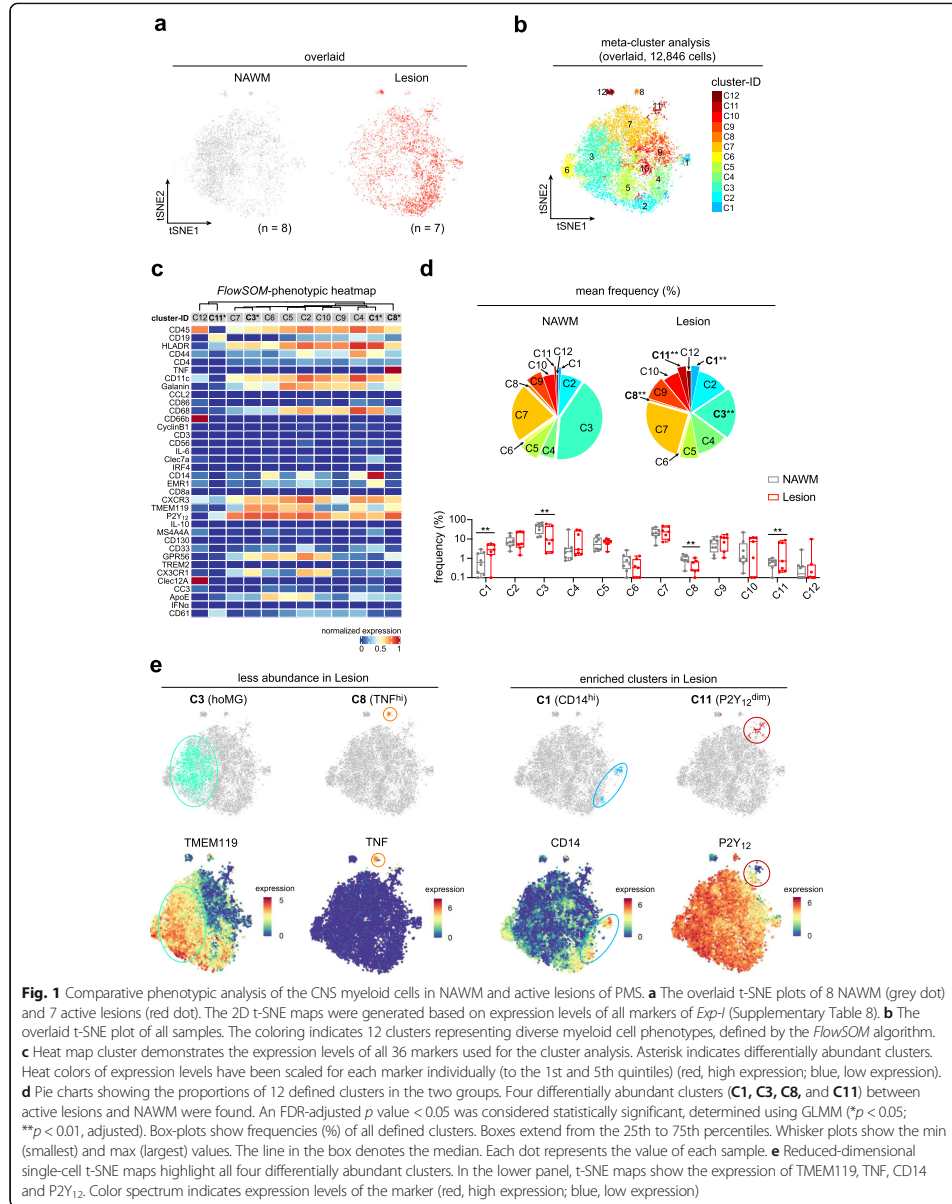
reproducibility of the obtained results, along with in-depth phenotypic profiling using a total of 74 antibodies.
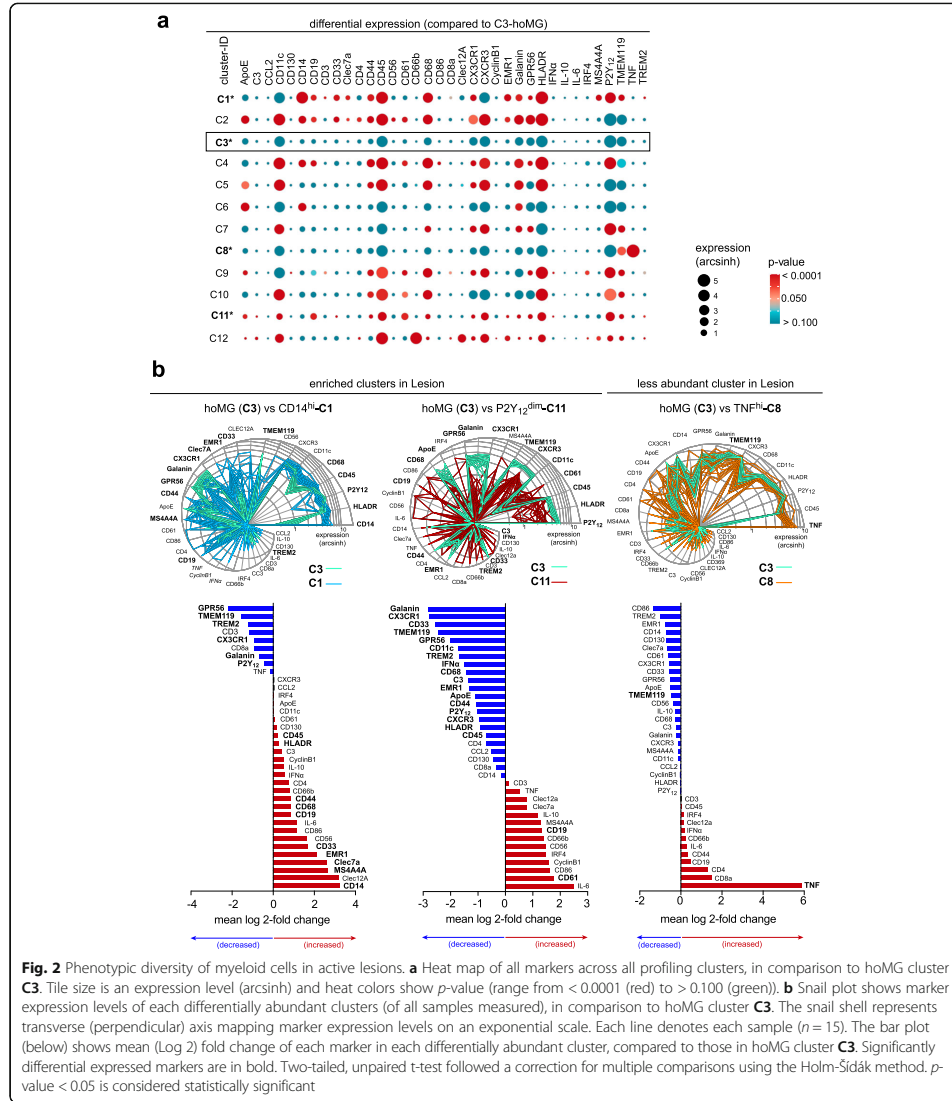
In *Exp-I*, the antibody panel (Additional file 1: Supplementary Table 8) was designed to characterize microglia as well as to detect the major circulating immune cell subsets including myeloid cells, T, B and natural killer (NK) cells using 36 antibodies recognizing CX3CR1, P2Y$_{12}$, TMEM119, GPR56, TREM2, EMR1, ApoE, Clec7A, MS4A4A, CC3, CD45, CD44, CD19, CD3, CD4, CD8a, CD56, CD66b, CD14, IRF4, Clec12A, HLA-DR, CD11c, CD130, CD86, CD33, CXCR3, Galanin, CD61, CD68, IL-10, IL-6, CCL2, IFN-α, TNF and cyclinB1. First, we embedded all cells from NAWM ($n = 8$) and active lesion WM tissue ($n = 7$) on a reduced dimension t-SNE map (Fig. 1a; Additional file 2: Supplementary Fig. 4). To identify differentially abundant rare cell populations or different cell states between conditions, we performed an exploratory meta-clustering using the FlowSOM algorithm (*FlowSOM/Consensus-ClusterPlus*) [18–21]. Importantly, the number of clusters defined may not necessarily represent functionally distinct subsets of myeloid cells, as it could also include transient cell states. Meta-clustering is proven to be useful to exploratory study cell subsets/states within a cell population in more detail [16, 17, 19]. Meta-clustering analysis revealed 12 clusters with consistently distinct phenotypes (Fig. 1b-d). Overall, 10 of 12 defined clusters (**C1-C10**) were positive for both P2Y$_{12}$ and TMEM119, indicating microglial populations (Fig. 1b, c). The other two clusters were a cluster of P2Y$_{12}$^{dim}TMEM119$^{lo/−}$CD19-^{dim}HLA-DR$^+$CXCR3$^+$CD61$^+$ myeloid cells, which was enriched in active lesion compared to NAWM (**C11**, Fig. 1b-e), and one P2Y$_{12}$$^-$TMEM119$^-$ cluster of mixed CD45^{hi}CD66b$^+$Clec12A$^+$ infiltrating immune cells, which was present at a comparable frequency in NAWM and active lesions (**C12**, Fig. 1c, d). The homeostatic microglial cluster (hoMG, **C3**), which was characterized as P2Y$_{12}$$^+$TMEM119$^+$CD14^{lo}CD68^{dim}HLA-DR^{dim}CD11c^{dim}, was less abundant in active lesions compared to NAWM tissue (Fig. 1c-e). Similarly, we also detected a lower abundance of a unique cluster of P2Y$_{12}$$^+$TMEM119^{dim}TNF^{hi} microglia (**C8**) in active lesions (Fig. 1c-e). Furthermore, a cluster of P2Y$_{12}$$^+$TMEM119^{dim}Clec7A^{dim}CD14^{hi} activated microglia (**C1**) was detected at higher abundance in active lesions of PMS (Fig. 1c-e). Of note, in each defined cluster, small phenotypic differences were found between myeloid cells in active lesions and NAWM (Supplementary Fig. 6).

Comparing the phenotypes of the three differentially abundant clusters to the homeostatic microglia cluster (hoMG, **C3**) revealed significantly lower expression of microglial markers P2Y$_{12}$, TMEM119, CX3CR1 and GPR56 in both lesion-enriched clusters **C1** and **C11** (Fig. 2a, b). Significantly higher expression of CD45, HLA-DR, CD44, CD68, CD19, CD33, EMR1, Clec7a,

MS4A4A and CD14 was detected in the activated microglial cluster **C1** (Fig. 2a, b), whereas only CD19 and CD61 were higher in another P2Y$_{12}$^{dim} myeloid cell cluster **C11** (Fig. 2a, b). Of note, TREM2 expression was found to be lower in these clusters, compared to the hoMG cluster (Fig. 2a, b; Additional file 2: Supplementary Fig. 5). In the less abundant TNF^{hi} microglial cluster **C8**, only TMEM119 and TNF expression was found to be different from the hoMG cluster (Fig. 2a, b). Interestingly, both of the lesion-enriched clusters **C1** and **C11** showed lower expression of microglial homeostatic markers and increased expression of CD19, a B cell marker which has been previously reported in rare cases of human post-mortem microglia sample, compared to the homeostatic cluster [16]. Similar to our previous finding [16], these cells were characterized as CD19$^+$CD45^{dim}P2Y$_{12}$^{dim}HLA-DR^{dim}, and thus were phenotypically different from peripheral B cells.

Of note, in contrast to the scRNA-Seq study of small biopsies of MS lesions from patients with early MS [12], this study performed a single-cell protein array of larger brain autopsy tissue containing an active lesion surrounded by NAWM in PMS. To validate whether differentially abundant clusters were indeed located in active lesions, we performed imaging CyTOF (IMC) on formalin-fixed paraffin-embedded (FFPE) tissue blocks from the same donors (Additional file 1: Supplementary Table 1) that were used for CyTOF. IMC simultaneously measures up to 37 proteins at subcellular resolution. This approach allows delineation and quantification of cell heterogeneity in a large area of interest (e.g. 1 mm^2) [26]. However, due to limitation of commercially available antibodies for IMC and restricted antigen retrieval protocol, we performed the analysis using a panel of 13 antibodies, including those that were analyzed in *Exp-I* (Additional file 1: Supplementary Table 9; Additional file 2: Supplementary Fig. 7a). Tissue microarrays of brain sections (1.5-mm diameter) of all samples (1–3 sections per sample) were generated and stained. A 1-mm^2 image of each section was taken and analyzed (Additional file 2: Supplementary Fig. 7a). We observed higher abundance of TNF$^+$P2Y$_{12}$$^+$ microglia in NAWM (Fig. 3a). To further quantify the abundance of this cell subset, P2Y$_{12}$ (a marker defining area of cell cytoplasm) and DNA ($^{191/193}$Ir, a marker defining cell nucleus) signals were used to segment individual cells in each image. The segmented cells (DNA$^+$P2Y$_{12}$$^+$ and DNA$^+$P2Y$_{12}$$^-$) were used to perform unsupervised PhenoGraph analysis [27], which partitioned all segmented cells into 17 clusters with distinct phenotypes (Fig. 3b, c; Additional file 2: Supplementary Fig. 7b). Among these clusters, we found five differentially abundant clusters in active lesions, compared to NAWM tissue (Fig. 3c). We could confirm a lower abundance of a

Fig. 1 Comparative phenotypic analysis of the CNS myeloid cells in NAWM and active lesions of PMS. **a** The overlaid t-SNE plots of 8 NAWM (grey dot) and 7 active lesions (red dot). The 2D t-SNE maps were generated based on expression levels of all markers of *Exp-I* (Supplementary Table 8). **b** The overlaid t-SNE plot of all samples. The coloring indicates 12 clusters representing diverse myeloid cell phenotypes, defined by the *FlowSOM* algorithm. **c** Heat map cluster demonstrates the expression levels of all 36 markers used for the cluster analysis. Asterisk indicates differentially abundant clusters. Heat colors of expression levels have been scaled for each marker individually (to the 1st and 5th quintiles) (red, high expression; blue, low expression). **d** Pie charts showing the proportions of 12 defined clusters in the two groups. Four differentially abundant clusters (**C1, C3, C8,** and **C11**) between active lesions and NAWM were found. An FDR-adjusted p value < 0.05 was considered statistically significant, determined using GLMM (*$p < 0.05$; **$p < 0.01$, adjusted). Box-plots show frequencies (%) of all defined clusters. Boxes extend from the 25th to 75th percentiles. Whisker plots show the min (smallest) and max (largest) values. The line in the box denotes the median. Each dot represents the value of each sample. **e** Reduced-dimensional single-cell t-SNE maps highlight all four differentially abundant clusters. In the lower panel, t-SNE maps show the expression of TMEM119, TNF, CD14 and P2Y$_{12}$. Color spectrum indicates expression levels of the marker (red, high expression; blue, low expression)

Böttcher *et al. Acta Neuropathologica Communications*   (2020) 8:136

Page 9 of 18

Fig. 2 Phenotypic diversity of myeloid cells in active lesions. **a** Heat map of all markers across all profiling clusters, in comparison to hoMG cluster **C3**. Tile size is an expression level (arcsinh) and heat colors show *p*-value (range from < 0.0001 (red) to > 0.100 (green)). **b** Snail plot shows marker expression levels of each differentially abundant clusters (of all samples measured), in comparison to hoMG cluster **C3**. The snail shell represents transverse (perpendicular) axis mapping marker expression levels on an exponential scale. Each line denotes each sample ($n = 15$). The bar plot (below) shows mean (Log 2) fold change of each marker in each differentially abundant cluster, compared to those in hoMG cluster **C3**. Significantly differential expressed markers are in bold. Two-tailed, unpaired t-test followed a correction for multiple comparisons using the Holm-Šídák method. *p*-value < 0.05 is considered statistically significant

cluster of $P2Y_{12}{}^{+}TNF^{+/hi}$ cells (similar to **C8** identified by CyTOF (Fig. 2b)) in lesions compared to NAWM (Fig. 3c-e). We also noted a higher abundance of $CD45^{+/hi}CD68^{+/hi}$ clusters in active lesions (Fig. 3c-e), which had a similar phenotype to **C1** identified by CyTOF (Fig. 2b). Nevertheless, these lesion-enriched

clusters expressed low levels of CD44, CD11c, HLA-DR and CD14 (Additional file 2: Supplementary Fig. 7b), which is similar to the phenotype of **C11** identified by CyTOF (Fig. 2b), indicating that these clusters may contain mixed cells that have similar phenotypes to both **C1** and **C11** identified by CyTOF (Fig. 2b).

Fig. 3 Differentially abundant clusters in active lesions, determined by imaging CyTOF. **a** Representative mass cytometry images of NAWM (*n* = 5 biological replication) and lesion white matter (n = 5 biological replication) (scale bar = 100 μm). Microglia/macrophage are stained with P2Y$_{12}$, CD68, CD45, CD163, CD14 and TNF, and nuclei/DNA are counterstained with Iridium (grey). Arrow head indicates P2Y$_{12}^{+}$ microglia, which are positive or negative for TNF. **b** The overlaid t-SNE plot of all segmented cells from all samples. The coloring indicates NAWM (grey dots), Lesion (red dots) or 17 clusters representing diverse myeloid cell phenotypes on the analyzed brain tissues, defined by the PhenoGraph algorithm using an input of k-nearest neighbors of 60. **c** The Box plots shows frequency (%) of all defined clusters. Five differentially abundant clusters (**C3**, **C5**, **C10**, **C11** and **C17**) in lesions, compared to NAWM samples, were labelled with asterisk. Boxes extend from the 25th to 75th percentiles. Whisker plots show the min (smallest) and max (largest) values. The line in the box denotes the median. Each dot represents the value of each sample. Two-tailed, unpaired t-test. *p*-value < 0.05 (*) is considered statistically significant. **d** Reduced-dimensional single-cell t-SNE maps show the expression of TNF, P2Y$_{12}$, CD68 and CD45. Color spectrum indicates expression levels of the marker (red, high expression; blue, low expression). Dot plot shows the correlation between TNF- and P2Y$_{12}$-signal intensity of **C5** (lower abundance in lesions), **C10** and **C17** (lesion-enriched clusters) of all samples measured, and the correlation between CD68- and CD45-signal intensity of **C5** (lower abundance in lesions), **C3** and **C11** (lesion-enriched clusters) of all samples measured. **e** Representative IMC images of five differentially abundant clusters detected in lesion WM (scale bar = 50 μm)

86

Increased phagocytic phenotypes in lesion-enriched myeloid cells

Microglial activation and phagocytic activity have long been considered key events in MS pathology [28–31]. In *Exp-I*, we found increased expression of markers involved in the clearance of apoptotic cells/bodies including CD61 [32], along with the increased expression of HLA-DR (major histocompatibility (MHC)-II) and phagocytosis-associated markers, such as CD44 and CD68, in the lesion-enriched microglial clusters (Fig. 2a, b), compared to the hoMG cluster. In contrast to results obtained from a mouse model of experimental autoimmune encephalomyelitis (EAE) and from brain biopsies of patients with early MS [12, 13], we did not detect a significant increase in myeloid cell infiltration or strong inflammatory phenotype of microglia in the active lesions of PMS (**C12**, Fig. 1c, d). However, limitations in the antibody panel used in *Exp-I* (Figs. 1 and 2) may have caused the discrepancy with findings from EAE or early MS studies using scRNA-Seq with much higher dimensionality [12, 13]. Furthermore, in *Exp-I* we have also observed a highly phagocytic microglia cluster **C4** (Fig. 2), which was enriched in active lesions but did not reach significant difference compared to NAWM (FDR-adjusted P value = 0.0838). This may due to lacking of markers identifying phagocytic and activated states. Therefore, to further investigate the phagocytic and inflammatory phenotypes of myeloid cells, including infiltrating cells, in active lesions of PMS, we used two additional antibody panels (*Exp-II* and *Exp-III*; Additional file 1: Supplementary Table 8). The antibody panels used in *Exp-II* and *Exp-III* had some overlap in phenotypic-defining markers (designated as *TYPE* markers: HLA-DR, CD11c, CCR2, CD172a (SIRPα), CD196, CD91, CD95 (Fas), CD56, CD54 (ICAM-1), CD116, CD74, CD47, IRF7, CD274, CD35). These *TYPE* markers identified different cell subsets/clusters of WM myeloid cells, and allowed us to compare the cell populations between experiments (*Exp-II* and *-III*). In addition, we further phenotypically profiled the defined clusters using *STATE* markers (Additional file 1: Supplementary Table 8), a set of markers characterizing microglia/myeloid cells with particular emphasis on inflammation- and phagocytosis-associated markers, including MIP-1β (CCL4), TNF, GM-CSF, CD206, Clec7a, AXL, CD36, CD163, CD14, CD64 (FcγRI), CD32 (FcγRII), TGF-β, IL-1β, IFNγ, IFNα and osteopontin (OPN; *SPP1*).

As in *Exp-I* (Fig. 1), we first embedded all analyzed cells on t-SNE maps using the *TYPE* markers. Meta-clustering resulted in 12 clusters with consistent phenotypes (Fig. 4a-d; Additional file 2: Supplementary Fig. 8–10). As shown in *Exp-I* (Fig. 1c, d), more than 98% of CD11b-MACS-sorted cells were P2Y$_{12}$$^{+/dim}$TMEM119$^{+/dim}$ microglia. In *Exp-I*, the
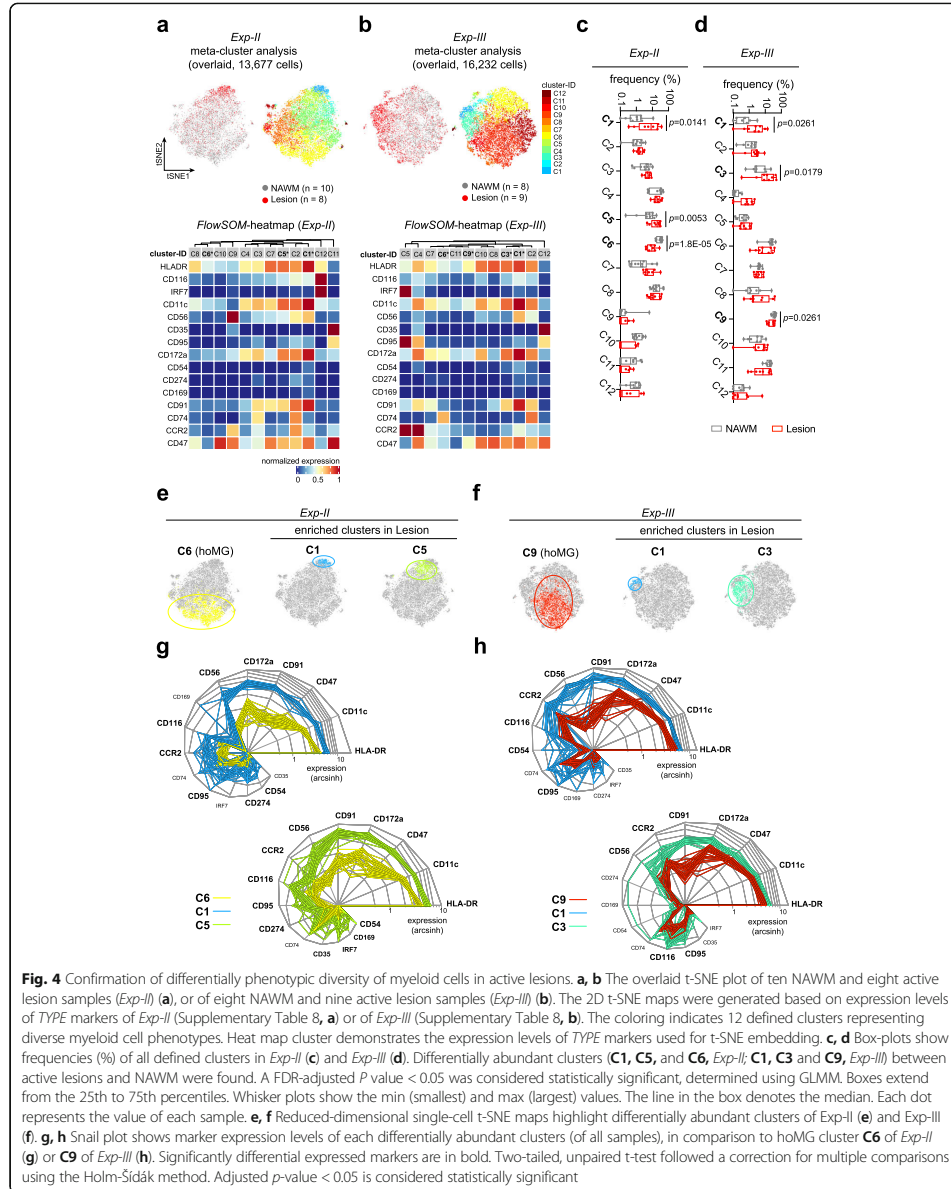
hoMG cluster was characterized as P2Y$_{12}$$^{+}$TMEM119^{+}HLA-DR^{dim}CD11c^{dim}CD68^{dim}. In *Exp-II* and *-III* (in which P2Y$_{12}$ and TMEM119 were not measured, due to limitation of metal channels available), we therefore identified the HLA-DR^{dim}CD11c^{dim}CCR2$^{lo/-}$ cluster as the hoMG cluster (**C6** in *Exp-II* and **C9** in *Exp-III*). A lower abundance of HLA-DR^{dim}CD11c^{dim}CCR2$^{lo/-}$ hoMG in active lesions was detected in both *Exp-II* and *-III*, which was similar to results obtained from *Exp-I* (Fig. 4a-f). Increased abundance of two activated microglial clusters was consistently detected in active lesions in both experiments (**C1** and **C5** in *Exp-II*; **C1** and **C3** in *Exp-III*, Fig. 4a-f). These clusters were similarly characterized by higher expression of HLA-DR, CD11c, CD47, CD172a, CD91, CD56, CCR2, CD116 and CD95, compared to the hoMG cluster (Fig. 4g, h). The two activated microglial clusters (**C1** and **C5** in *Exp-II*; **C1** and **C3** in *Exp-III*) displayed similar phenotypes with varying degrees of activation regarding, in particular, the different expression level of HLA-DR, CD11c, CD172a, CD91 and CD47 (Fig. 4g, h). In-depth phenotypic profiling using *STATE* markers revealed significantly increased expression of inflammation- and phagocytosis-associated markers, including NFAT1, MIP-1β (CCL4), CD36, CD44, CD14, CD64 (FcγRI), CD32 (FcγRII), IFNα, AXL, ABCA7, CD115, Toll-like receptors (TLRs), Galanin and GLUT5 in highly activated microglial clusters in active lesions (**C1** in *Exp-II* and **C1** in *Exp-III*, Fig. 5a, b). The clusters with a less activated phenotypes (**C5** in *Exp-II* and **C3** in *Exp-III*, Fig. 5c, b) displayed fewer phenotypic differences in active lesions. We did not detect increased infiltration of CCR2$^{hi/+}$ myeloid cells in active lesions of PMS (Fig. 4a-f; **C2** and **C9** in *Exp-II*; **C4** and **C5** in *Exp-III*), which was in line with the result from *Exp-I* showing no different abundance of Clec12A^{+} myeloid cells in active lesions of PMS (**C12**; Fig. 1c, d).

Similar to results obtained from *Exp-I*, comparing the phenotypes of myeloid cells in active lesions to those in NAWM within the same defined cluster of both *Exp-II* (Supplementary Fig. 11) and *Exp-III* (Supplementary Fig. 12) resulted in small phenotypic differences, with one exception in the case of **C12** (*Exp-II*). In this cluster, strongly reduced expressions of CD116, NFAT1, CD44 and GM-CSF was found in active lesions (Supplementary Fig. 11).
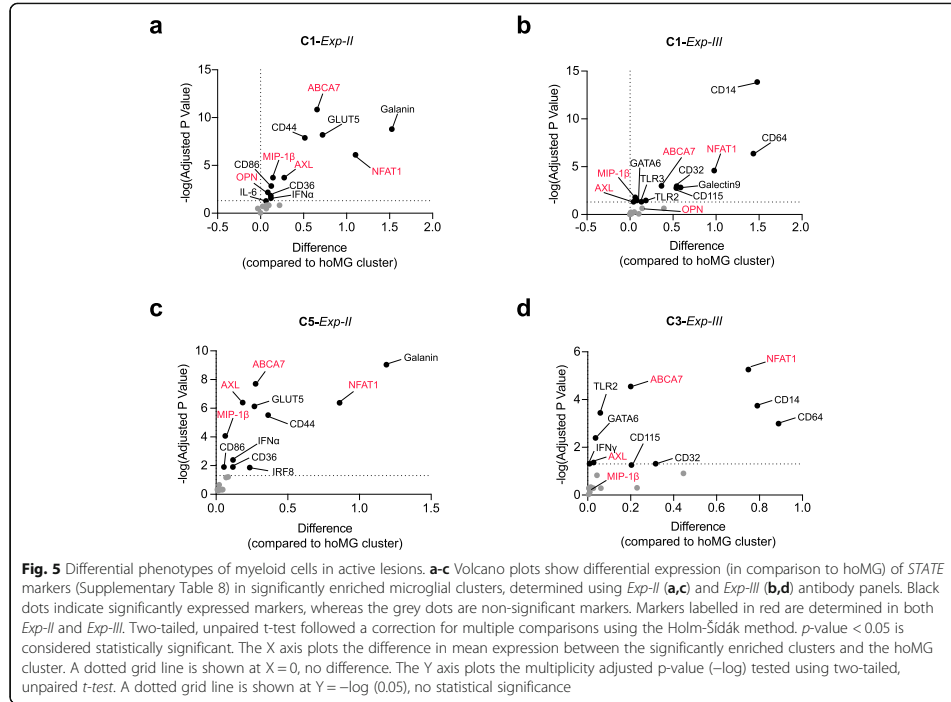
NAWM microglial phenotypes are comparable to the control aged microglia

Disease onset of primary progressive MS (PPMS) and secondary progressive MS (SPMS) is generally around 10 years later than RRMS [33]. In addition, the incidence of irreversible disability in PPMS and SPMS follows a similar pattern [33], which suggests that aging could be an important risk factor for MS progression. During normal aging, microglia undergo phenotypic and functional changes, resulting in reduced ability to repair CNS

Fig. 4 Confirmation of differentially phenotypic diversity of myeloid cells in active lesions. **a, b** The overlaid t-SNE plot of ten NAWM and eight active lesion samples (*Exp-II*) (**a**), or of eight NAWM and nine active lesion samples (*Exp-III*) (**b**). The 2D t-SNE maps were generated based on expression levels of *TYPE* markers of *Exp-II* (Supplementary Table 8, **a**) or of *Exp-III* (Supplementary Table 8, **b**). The coloring indicates 12 defined clusters representing diverse myeloid cell phenotypes. Heat map cluster demonstrates the expression levels of *TYPE* markers used for t-SNE embedding. **c, d** Box-plots show frequencies (%) of all defined clusters in *Exp-II* (**c**) and *Exp-III* (**d**). Differentially abundant clusters (**C1, C5,** and **C6,** *Exp-II*; **C1, C3** and **C9,** *Exp-III*) between active lesions and NAWM were found. A FDR-adjusted *P* value < 0.05 was considered statistically significant, determined using GLMM. Boxes extend from the 25th to 75th percentiles. Whisker plots show the min (smallest) and max (largest) values. The line in the box denotes the median. Each dot represents the value of each sample. **e, f** Reduced-dimensional single-cell t-SNE maps highlight differentially abundant clusters of Exp-II (**e**) and Exp-III (**f**). **g, h** Snail plot shows marker expression levels of each differentially abundant clusters (of all samples), in comparison to hoMG cluster **C6** of *Exp-II* (**g**) or **C9** of *Exp-III* (**h**). Significantly differential expressed markers are in bold. Two-tailed, unpaired t-test followed a correction for multiple comparisons using the Holm-Šídák method. Adjusted *p*-value < 0.05 is considered statistically significant
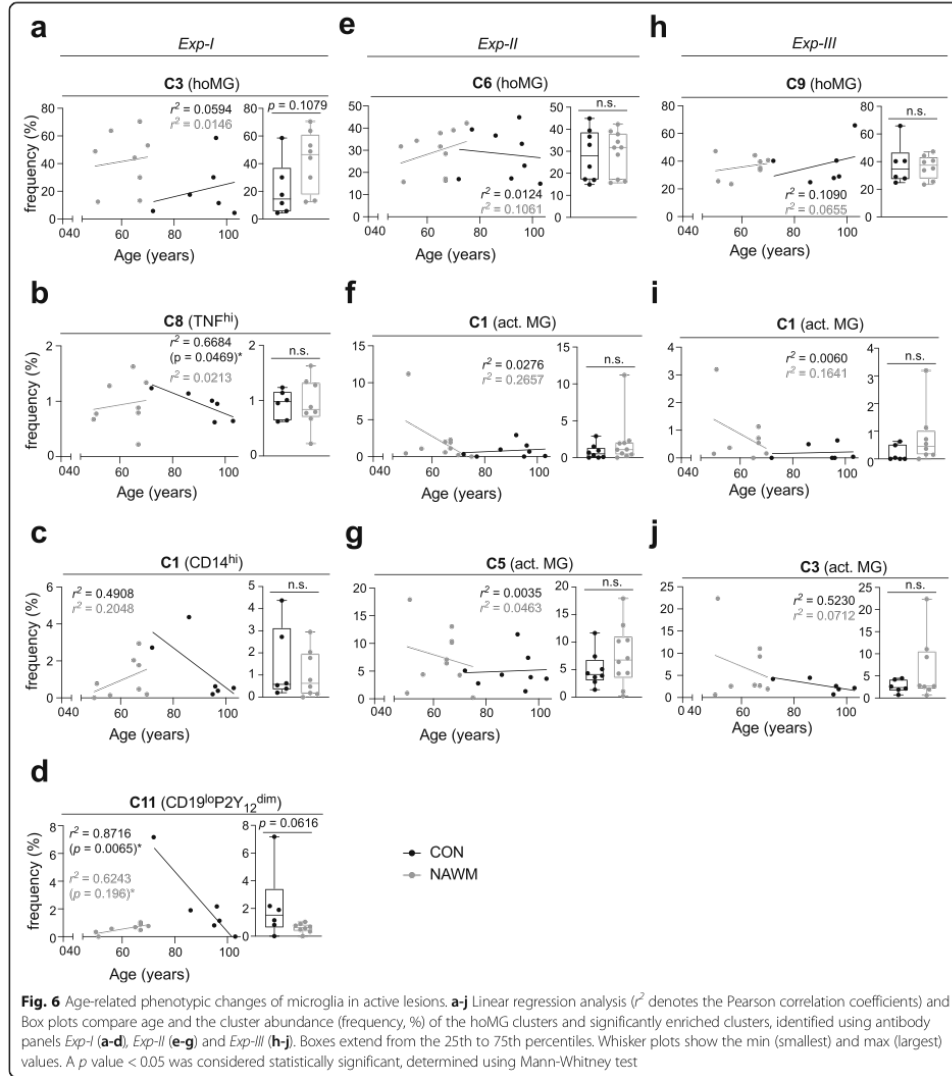
Fig. 5 Differential phenotypes of myeloid cells in active lesions. **a-c** Volcano plots show differential expression (in comparison to hoMG) of *STATE* markers (Supplementary Table 8) in significantly enriched microglial clusters, determined using *Exp-II* (**a,c**) and *Exp-III* (**b,d**) antibody panels. Black dots indicate significantly expressed markers, whereas the grey dots are non-significant markers. Markers labelled in red are determined in both *Exp-II* and *Exp-III*. Two-tailed, unpaired t-test followed a correction for multiple comparisons using the Holm-Šidák method. *p*-value < 0.05 is considered statistically significant. The X axis plots the difference in mean expression between the significantly enriched clusters and the hoMG cluster. A dotted grid line is shown at X = 0, no difference. The Y axis plots the multiplicity adjusted p-value (−log) tested using two-tailed, unpaired *t-test*. A dotted grid line is shown at Y = −log (0.05), no statistical significance

damage, which may result in more vulnerable axons and neurons [34]. Furthermore, aged microglia have been observed to display an activated phenotype characterized by increased expression of MHC class II, CD68 and pro-inflammatory cytokines such as IL-1, IL-6 and TNF [16, 35]. This activation is associated with increased expression of TLRs and other pattern recognition receptors, as well as decreased expression of immune-suppressive factors, such as CD200-CD200R and fractalkine-CX3CR1 interactions [35]. Consequently, the active lesion-associated phenotypic changes described above (Figs. 1, 2, 3, 4 and 5) could resemble those observed with aging. In addition, our previous study using bulk transcriptomic analysis revealed subtle changes of the microglial signature in NAWM of PMS donors compared to age-matched non-MS control donors [11], so it is interesting to test whether the phenotypic alterations identified in active lesions (in a comparison to NAWM) can also be detected in non-MS aged WM microglia. Myeloid cells were isolated and MACS-sorted from control white matter as described above, and were characterized using the antibody panels from *Exp-I*, *−II* and *-III*. In comparison to NAWM, we did not detect differentially abundant

clusters in control aged microglia (CON) in either experiment (Fig. 6a-j), which was similar to our results obtained from our previous study comparing microglia isolated from NAWM and age-matched control WM [11]. Furthermore, the lesion-enriched clusters, which were identified in *Exp-I*, *−II* and *-III* (Fig. 4), were not correlated with age in all three studied groups, except TNF^{hi} **C8** (*Exp-I*, Fig. 6b) and CD19^{lo}P2Y$_{12}$^{dim} **C11** clusters (*Exp-I*, Fig. 6d).

Discussion

In this study, we characterized and compared WM myeloid cells isolated from active lesions and NAWM of ten PMS donors, using single-cell mass cytometry to analyse three different antibody panels (a total of 74 markers). Depending on a set of markers analyzed, we consistently detected a lower abundance of a cluster of P2Y$_{12}$$^+$TMEM119$^+$ and/or HLA-DR^{dim}CD11c^{dim} hoMG in active lesions and significantly enriched clusters of highly phagocytic and activated microglia. These clusters were mainly characterized by lower expression of homeostatic markers CX3CR1, P2Y$_{12}$, TMEM119, GPR56, and/or increased expression of proteins involved in phagocytic activity and microglial activation

Fig. 6 Age-related phenotypic changes of microglia in active lesions. **a-j** Linear regression analysis (r^2 denotes the Pearson correlation coefficients) and Box plots compare age and the cluster abundance (frequency, %) of the hoMG clusters and significantly enriched clusters, identified using antibody panels *Exp-I* (**a-d**), *Exp-II* (**e-g**) and *Exp-III* (**h-j**). Boxes extend from the 25th to 75th percentiles. Whisker plots show the min (smallest) and max (largest) values. A *p* value < 0.05 was considered statistically significant, determined using Mann-Whitney test

including CD45, HLA-DR, CD44, CD14, CD11c, CD68, Clec7a, MS4A4A, CCR2, CD64, CD32, CD47, CD91, CD95, NFAT1, AXL, ABCA7 and/or cytokine MIP-1β (CCL4) and osteopontin (OPN, or *SPP1*). Our findings are greatly complementary to the results of previous transcriptomic studies in EAE and early MS at the level of single-cell proteomics [12, 13]. Importantly, the abundance of infiltrating myeloid cells was not increased in active lesions of PMS in all three experiments.

In contrast to scRNA-Seq, a single-cell protein array using CyTOF is often limited to a maximum of 40 markers per measurement, and thus it is challenging to comprehensively characterize a targeted cell population with only one antibody panel. We applied three

90

different antibody panels to increase the capacity for in-depth phenotypic profiling. We demonstrated the use of *TYPE* markers to compare differentially abundant clusters between measurements. Moreover, this study underscored the feasibility of performing single-cell phenotypic screening of small microglia/macrophage samples (3 measurements of 10^5 cells), as we have demonstrated previously [16]. To identify differentially abundant clusters between conditions, we applied meta-clustering analysis (the FlowSOM algorithm: *FlowSOM/Consensus-ClusterPlus*) [19–21], a powerful tool to explore cellular heterogeneity. However, the identified clusters are descriptive and could be interpreted as distinct cell subsets and/or transient cell states. Further functional analysis of each identified cluster remains to-date exceedingly challenging but essential. In addition to CyTOF, we performed imaging CyTOF (IMC) to validate the results obtained from single-cell suspension samples. To date, IMC has been applied to identify multiple myeloid phenotypes on highly inflamed active lesions from one [36] or two [37] patients with RRMS. In this study, using IMC we could confirm phenotypic changes of myeloid cells characterized by CyTOF in active lesions compared with NAWM (from a total of seven PMS donors, Fig. 3; Additional file 1: Supplementary Table 1). However, a direct comparison between the two CyTOF technologies remains technically challenging, due to for example a big difference in the area of analysis (tissue weight of ~ 1 g (CyTOF) vs 1-mm^2 image (IMC)), differences in cell types analyzed, tissue/cell quality (MACS-pre-isolated single-cell from enzymatically digested fresh postmortem tissue (CyTOF) vs formalin-fixed, paraffin-embedded tissues (IMC)) or the number of antibodies compatible in one staining protocol that includes antigen-retrieval process, which would limit the dimensionality of the IMC data.

Myeloid cells including microglia are emerging as key players in neuroinflammatory diseases like MS [38–40]. Numerous findings in rodent models such as EAE highlight the importance of myeloid cells including microglia, monocyte-derived macrophages and dendritic cells in neuroinflammation [39, 41]. However, these models only partially replicate the complexity of human MS and thus, our understanding of how myeloid cells either respond or contribute to MS pathogenesis is still limited. This is particularly true for the advanced stages of MS where progressive neurodegeneration predominates [42]. The present study nicely complements the single-nuclei RNA-sequencing study from WM in SPMS [43] and other studies using bulk and single-cell/nuclei transcriptomic analysis in early and PMS as well as the EAE model [12, 13, 41, 44–47], in which microglia show an increased

gene expression of MHC class II-related molecules such as *HLA-DR, Cd74* and molecules involved in phagocytosis and/or myelin uptake including *GPNMB, SPP1* and *Cd68* in MS. Using CyTOF, we detected decreased abundance of the homeostatic microglial cluster in lesion-enriched microglia populations, which consistently coincided with increased expression of the antigen-processing and phagocytosis-related markers HLA-DR, CD11c, AXL, CD45, CD68, ATP-binding cassette (ABC) transporter A7 (ABCA7) [48] and CD44 (a receptor of GPNMB) [49], as well as the molecules involved in the inflammatory process in microglia such as CD14 and Clec7a (dectin-1) and its co-activator MS4A4A [50]. Expanding the analyzed markers with *Exp-II* and *-III* revealed active lesion-enriched clusters of cells with higher expression of phagocytosis-related and inflammatory molecules such as inflammatory cytokines MIP-1β (CCL4) and OPN, the receptor tyrosine kinase AXL, the myeloid inhibitory immunoreceptor SIRPα (CD172a) and its co-activator CD47 [51], ABCA7, CD91 (LRP1 or ApoE receptor) and Fcγ receptors (CD64 and CD32). Furthermore, the expression of molecules involved in apoptosis-regulation CD95 (Fas) and immune regulatory function NFAT1 (a transcription factor regulating T-cell function) and galanin [52, 53] were also found to be increased in lesion-enriched clusters. Even though our study lacks functional investigation, it is tempting to speculate that, at this late disease stage of PMS, microglia are multi-functional. On the one hand, microglia attempt to maintain brain homeostasis by up-regulating expression of molecules involved in clearance of apoptotic cells and myelin debris such as AXL [54], phospholipid transporter ABCA7 [48], HLA-DR, CD45 and CD68, as well as the neuropeptide galanin, which provides neuroprotective effect in EAE mouse model [53]. On the other hand, some microglia become activated and up-regulate the expression of inflammatory mediators MIP-1β and OPN. An expansion of MIP-1β (*Ccl4*)-expressing microglia subset has been detected in EAE [13] and MS active lesions [12], and was proposed to be a neurotoxic population. Similarly, OPN (*SPP1*) is involved in microglia activation pathway and has been found up-regulated in EAE [13] and WM active lesions of MS patients [12], as well as in an Alzheimer's disease model [55]. It has also been demonstrated in a mouse model of demyelination that OPN exacerbated disease progression, promoted worsening paralysis and induced neurological deficits [56]. Furthermore, the increased expression of the immune regulator NFAT1 in microglia in active lesions may be linked to chronic activation and neuroinflammation of these cells [52, 57].

91

It has been challenging to distinguish microglia from infiltrating macrophages in human brain and thus recognize their contribution to MS lesion formation and pathology. In this study, to distinguish microglia from infiltrating macrophages in active MS lesions, we used either microglia signature markers $P2Y_{12}$, TMEM119 and GRP56, together with Clec12A, a marker for hematogenic macrophage (*Exp-I*) or CD14 and CCR2 for monocytes and/or monocyte-derived macrophages (*Exp-II* and *-III*) [58]. Interestingly, the cluster with high Clec12A expression and low $P2Y_{12}$, TMEM119 and GPR56 expression was not significantly enriched in active MS lesions. Similarly, the abundance of $CCR2^{hi/+}$ cells was comparable between NAWM and active lesions. Our findings are similar to a previous study performed in a mouse model of demyelination, in which microglia became activated in response to lysophosphatidylcholine (LPC)-induced demyelination, and dominated the CNS lesion by limiting the dispersion of CNS-infiltrating macrophages into the lesioned WM [59]. On the contrary, recent studies using scRNA-Seq have demonstrated that monocyte-derived macrophages can enter the CNS during early MS or EAE [12, 41]. This discrepancy in findings may be due to differences in studied models/diseases (e.g. early MS vs PMS; EAE vs LPC-induced demyelination) or an analytical method used (scRNA-Seq vs CyTOF), which may lead to differences in cell identification/clustering. A direct comparison between studied models/diseases using a single analytical method is required to make a meaningful conclusion.

We detected a distinct cluster of $P2Y_{12}^+$ microglia that highly expressed TNF (Fig. 1e). Interestingly, a lower abundance of this TNF^{hi} microglial cluster was found in active lesions of PMS, compared to NAWM. TNF has long been recognized as an immune modulator [60]. During neuroinflammation, TNF is mainly expressed by myeloid cells [61, 62], and provides neuroprotective effects, possibly by limiting the extent and severity of autoimmune pathology [60–63]. TNF deficiency is related to disturbed microglial homeostasis [61], suggesting an important role of TNF in microglia function. This concept is supported by the results obtained from the EAE model, indicating that impairment of TNF signaling is associated with the induction of demyelination and less removal of T lymphocytes from the lesion area [64]. Moreover, monoclonal antibody therapies targeting TNF and its receptors (TNFRs) have been shown to potentially induce demyelinating disorders in human [65]. It has been also demonstrated that lipid uptake in microglia induced non-inflammatory phenotype by downregulating TNF expression [66]. Together, TNF-TNFRs signaling may play an important role in maintaining homeostatic function of microglia. However, it is technically impossible to selectively sort this rare population, thus their precise function in PMS remains to be investigated.

Conclusions
In summary, we demonstrate herein the power of multi-dimensional single-cell phenotyping to unravel the diversity of myeloid cells in PMS post-mortem brain tissue. Our results underscore the heterogeneity and complexity of myeloid cell phenotypes in active lesions of PMS, and suggest potential differences of pathogenesis between early MS and PMS. Active lesions of PMS contain highly phagocytic and activated microglia, pointing towards their role in clearing up myelin/cellular debris without being fully activated by the lesion environment. This may explain why anti-inflammatory therapies that are highly effective in early MS are less effective in PMS. It will be important to consider the heterogeneity of myeloid cell phenotypes when designing novel treatment interventions for PMS.

Availability of data and materials
The datasets used and/or analyzed during the current study are available from the corresponding author on reasonable request that does not include confidential patient information.

Ethics approval and consent to participate
All brain donors gave informed consent to perform autopsies and to use tissue, clinical and neuropathological information for research purposes, approved by the Ethics Committee of VU medical center (Amsterdam, The Netherlands).

Competing interests
The authors declare no competing financial interests.

Author details
[1]Department of Neuropsychiatry and Laboratory of Molecular Psychiatry, Charité – Universitätsmedizin Berlin, Berlin, Germany. [2]Neuroimmunology Research Group, Netherlands Institute for Neuroscience, Amsterdam, The Netherlands. [3]BIH Center for Regenerative Therapies (BCRT), Charité – Universitätsmedizin Berlin, Berlin, Germany. [4]Department of Experimental Immunology, Amsterdam University Medical Centers, University of Amsterdam, Amsterdam, The Netherlands. [5]Netherlands Brain Bank, Netherlands Institute for Neuroscience, Amsterdam, The Netherlands. [6]Flow & Mass Cytometry Core Facility, Charité – Universitätsmedizin Berlin and Berlin Institute of Health (BIH), Berlin, Germany. [7]Swammerdam Institute for Life Sciences, Center for Neuroscience, University of Amsterdam, Amsterdam, The Netherlands. [8]German Center for Neurodegenerative Diseases (DZNE), Berlin, Germany. [9]University of Edinburgh and UK Dementia Research Institute (DRI), Edinburgh, UK.

References
1. Lassmann H (2018) Multiple sclerosis pathology. Cold Spring Harb Perspect Med 8. https://doi.org/10.1101/cshperspect.a028936 PMID: 29358320
2. Lucchinetti C, Brück W, Parisi J, Scheithauer B, Rodriguez M, Lassmann H (2000) Heterogeneity of multiple sclerosis lesions: implications for the pathogenesis of demyelination. Ann Neurol 47:707–717. https://doi.org/10.1002/1531-8249(200006)47:6<707::aid-ana3>3.0.co;2-q PMID: 10852536
3. Ontaneda D, Thompson AJ, Fox RJ, Cohen JA (2017) Progressive multiple sclerosis: prospects for disease therapy, repair, and restoration of function. Lancet 389:1357–1366. https://doi.org/10.1016/S0140-6736(16)31320-4 PMID: 27889191
4. Lassmann H (2017) Targets of therapy in progressive MS. Mult Scler 23: 1593–1599. https://doi.org/10.1177/1352458517729455 PMID: 29041864
5. Luchetti S, Fransen NL, van Eden CG, Ramaglia V, Mason M, Huitinga I (2018) Progressive multiple sclerosis patients show substantial lesion activity that correlates with clinical disease severity and sex: a retrospective autopsy cohort analysis. Acta Neuropathol 135:511–528. https://doi.org/10.1007/s00401-018-1818-y PMID: 29441412
6. Stadelmann C, Wegner C, Brück W (2011) Inflammation, demyelination, and degeneration - recent insights from MS pathology. Biochim Biophys Acta 1812:275–282. https://doi.org/10.1016/j.bbadis.2010.07.007 PMID: 20637864
7. Fransen NL, Hsiao CC, van der Poel M, Engelenburg HJ, Verdaasdonk K, Vincenten MCJ et al (2020) Tissue-resident memory T cells invade the brain parenchyma in multiple sclerosis white matter lesions. Brain:awaa117. https://doi.org/10.1093/brain/awaa117 PMID: 32400866
8. Feinstein A, Freeman J, Lo AC (2015) Treatment of progressive multiple sclerosis: what works, what does not, and what is needed. Lancet Neurol 14: 194–207. https://doi.org/10.1016/S1474-4422(14)70231-5 PMID: 25772898
9. Ontaneda D, Fox RJ, Chataway J (2015) Clinical trials in progressive multiple sclerosis: lessons learned and future perspectives. Lancet Neurol 14:208–223. https://doi.org/10.1016/S1474-4422(14)70264-9 PMID: 25772899
10. Faissner S, Gold R (2019) Progressive multiple sclerosis: latest therapeutic developments and future directions. Ther Adv Neurol Disord 12: 1756286419878323. https://doi.org/10.1177/1756286419878323 PMID: 31598138
11. van der Poel M, Ulas T, Mizee MR, Hsiao CC, Miedema SSM, Adelia et al (2019) Transcriptional profiling of human microglia reveals grey-white matter heterogeneity and multiple sclerosis-associated changes. Nat

Commun 10:1139. https://doi.org/10.1038/s41467-019-08976-7 PMID: 30867424
12. Masuda T, Sankowski R, Staszewski O, Böttcher C, Amann L, Sagar et al (2019) Spatial and temporal heterogeneity of mouse and human microglia at single-cell resolution. Nature 566:388–392. https://doi.org/10.1038/s41586-019-0924-x PMID: 30760929
13. Hammond TR, Dufort C, Dissing-Olesen L, Giera S, Young A, Wysoker A et al (2019) Single-cell RNA sequencing of microglia throughout the mouse lifespan and in the injured brain reveals complex cell-state changes. Immunity 50:253–271. https://doi.org/10.1016/j.immuni.2018.11.004 PMID: 30471926
14. Jonkman LE, Geurts JJG (2018) Postmortem magnetic resonance imaging. Handb Clin Neurol 150:335–354. https://doi.org/10.1016/B978-0-444-63639-3.00023-2 PMID: 29496152
15. Mizee MR, Miedema SS, van der Poel M, Adelia, Schuurman KG, van Strien ME et al (2017) Isolation of primary microglia from the human post-mortem brain: effects of ante- and post-mortem variables. Acta Neuropathol Commun 5:16. https://doi.org/10.1186/s40478-017-0418-8 PMID: 28212663
16. Böttcher C, Schlickeiser S, Sneeboer MAM, Kunkel D, Knop A, Paza E et al (2019) Human microglia regional heterogeneity and phenotypes determined by multiplexed single-cell mass cytometry. Nat Neurosci 22:78–90. https://doi.org/10.1038/s41593-018-0290-2 PMID: 30559476
17. Böttcher C, Fernández-Zapata C, Schlickeiser S, Kunkel D, Schulz AR, Mei HE et al (2019) Multi-parameter immune profiling of peripheral blood mononuclear cells by multiplexed single-cell mass cytometry in patients with early multiple sclerosis. Sci Rep 9:19471. https://doi.org/10.1038/s41598-019-55852-x PMID: 31857644
18. Chevrier S, Crowell HL, Zanotelli VRT, Engler S, Robinson MD, Bodenmiller B (2018) Compensation of signal spillover in suspension and imaging mass cytometry. Cell Syst 6:612–620.e5. https://doi.org/10.1016/j.cels.2018.02.010 PMID: 29605184
19. Nowicka M, Krieg C, Crowell HL, Weber LM, Hartmann FJ, Guglietta S et al (2017) CyTOF workflow: differential discovery in high-throughput high-dimensional cytometry datasets. Version 3. F1000Res 6:748. https://doi.org/10.12688/f1000research.11622.3 PMID: 28663787
20. Van Gassen S, Callebaut B, Van Helden MJ, Lambrecht BN, Demeester P, Dhaene T (2015) FlowSOM: using self-organizing maps for visualization and interpretation of cytometry data. Cytometry A 87:636–645. https://doi.org/10.1002/cyto.a.22625 PMID: 25573116
21. Wilkerson MD, Hayes DN (2010) ConsensusClusterPlus: a class discovery tool with confidence assessments and item tracking. Bioinformatics 26:1572–1573. https://doi.org/10.1093/bioinformatics/btq170 PMID: 20427518
22. Berg S, Kutra D, Kroeger T, Straehle CN, Kausler BX, Haubold C et al (2019) Ilastik: interactive machine learning for (bio) image analysis. Nat Methods 16:1226–1232. https://doi.org/10.1038/s41592-019-0582-9 PMID: 31570887
23. McQuin C, Goodman A, Chernyshev V, Kamentsky L, Cimini BA, Karhohs KW et al (2018) CellProfiler 3.0: next-generation image processing for biology. PLoS Biol 16:e2005970. https://doi.org/10.1371/journal.pbio.2005970 PMID: 29969042
24. Schapiro D, Jackson HW, Raghuraman S, Fischer JR, Zanotelli VRT, Schulz D et al (2017) histoCAT: analysis of cell phenotypes and interactions in multiplex image cytometry data. Nat Methods 14:873–876. https://doi.org/10.1038/nmeth.4391 PMID: 28783155
25. Kuhlmann T, Ludwin S, Prat A, Antel J, Brück W, Lassmann H (2017) An updated histological classification system for multiple sclerosis lesions. Acta Neuropathol 133:13–24. https://doi.org/10.1007/s00401-016-1653-y PMID: 27988845
26. Giesen C, Wang HA, Schapiro D, Zivanovic N, Jacobs A, Hattendorf B et al (2014) Highly multiplexed imaging of tumor tissues with subcellular resolution by mass cytometry. Nat Methods 11:417–422. https://doi.org/10.1038/nmeth.2869 PMID: 24584193
27. Levine JH, Simonds EF, Bendall SC, Davis KL, el AD A, Tadmor MD et al (2015) Data-driven phenotypic dissection of AML reveals progenitor-like cells that correlate with prognosis. Cell 162:184–197. https://doi.org/10.1016/j.cell.2015.05.047 PMID: 26095251
28. Aloisi F, Ria F, Penna G, Adorini L (1998) Microglia are more efficient than astrocytes in antigen processing and in Th1 but not Th2 cell activation. J Immunol 160:4671–4680 PMID: 9590212
29. Benveniste EN (1997) Role of macrophages/microglia in multiple sclerosis and experimental allergic encephalomyelitis. J Mol Med (Berl) 75:165–173. https://doi.org/10.1007/s001090050101 PMID: 9106073

30. Cash E, Zhang Y, Rott O (1993) Microglia present myelin antigens to T cells after phagocytosis of oligodendrocytes. Cell Immunol 147:129–138. https://doi.org/10.1006/cimm.1993.1053 PMID: 7681729
31. Yamasaki R, Lu H, Butovsky O, Ohno N, Rietsch AM, Cialic R et al (2014) Differential roles of microglia and monocytes in the inflamed central nervous system. J Exp Med 211:1533–1549. https://doi.org/10.1084/jem.20132477 PMID: 25002752
32. Canton J, Neculai D, Grinstein S (2013) Scavenger receptors in homeostasis and immunity. Nat Rev Immunol 13:621–634. https://doi.org/10.1038/nri3515 PMID: 23928573
33. Confavreux C, Vukusic S (2006) Natural history of multiple sclerosis: a unifying concept. Brain 129:606–616. https://doi.org/10.1093/brain/awl007 PMID: 16415308
34. Beanrroch EE (2013) Microglia: multiple roles in surveillance, circuit shaping and response to injury. Neurology 81:1079–1088. https://doi.org/10.1212/WNL.0b013e3182a4a577 PMID: 23946308
35. Wong WT (2013) Microglial aging in the healthy CNS: phenotype, drivers and rejuvenation. Front Cell Neurosci 7:22. https://doi.org/10.3389/fncel.2013.00022 PMID: 23493481
36. Ramaglia V, Sheikh-Mohamed S, Legg K, Park C, Rojas OL, Zandee S et al (2019) Multiplexed imaging of immune cells in staged multiple sclerosis lesions by mass cytometry. Elife 8:e48051. https://doi.org/10.7554/eLife.48051 PMID: 31368890
37. Park C, Ponath G, Levine-Ritterman M, Bull E, Swanson EC, De Jager PL et al (2019) The landscape of myeloid and astrocyte phenotypes in acute multiple sclerosis lesions. Acta Neuropathol Commun 7:130. https://doi.org/10.1186/s40478-019-0779-2 PMID: 31405387
38. Priller J, Prinz M (2019) Targeting microglia in brain disorders. Science 365:32–33. https://doi.org/10.1126/science.aau9100 PMID: 31273114
39. Prinz M, Jung S, Priller J (2019) Microglia biology: one century of evolving concepts. Cell 179292–311. https://doi.org/10.1016/j.cell.2019.08.053 PMID: 31585077
40. Prinz M, Priller J (2014) Microglia and brain macrophages in the molecular age: from origin to neuropsychiatric disease. Nat Rev Neurosci 15:300–312. https://doi.org/10.1038/nrn3722 PMID: 24713688
41. Jordão MJC, Sankowski R, Brendecke SM, Sagar, Locatelli G, Tai YH et al (2019) Single-cell profiling identifies myeloid cell subsets with distinct fates during neuroinflammation. Science 363:eaat7554. https://doi.org/10.1126/science.aat7554 PMID: 30679343
42. Dendrou CA, Fugger L, Friese MA (2015) Immunopathology of multiple sclerosis. Nat Rev Immunol 15:545–558. https://doi.org/10.1038/nri3871 PMID: 26250739
43. Jäkel S, Agirre E, Mendanha Falcão A, van Bruggen D, Lee KW, Knuesel I et al (2019) Altered human oligodendrocyte heterogeneity in multiple sclerosis. Nature 566:543–547. https://doi.org/10.1038/s41586-019-0903-2 PMID: 30747918
44. Hendrickx DA, Koning N, Schuurman KG, van Strien ME, van Eden CG, Hamann J et al (2013) Selective upregulation of scavenger receptors in and around demyelinating areas in multiple sclerosis. J Neuropathol Exp Neurol 72:106–118. https://doi.org/10.1097/NEN.0b013e31827fd9e8 PMID: 23334594
45. Mizee MR, Miedema SS, van der Poel M, Adelia, Schuurman KG, van Strien ME et al (2019) Transcriptome analysis of normal-appearing white matter reveals cortisol- and disease-associated gene expression profiles in multiple sclerosis. Acta Neuropathol Commun 7:60. https://doi.org/10.1186/s40478-019-0705-7 PMID: 31023360
46. Krasemann S, Madore C, Cialic R, Baufeld C, Calcagno N, El Fatimy R et al (2017) The TREM2-APOE pathway drives the transcriptional phenotype of dysfunctional microglia in neurodegenerative diseases. Immunity 47:566–581.e9. https://doi.org/10.1016/j.immuni.2017.08.008 PMID: 28930663
47. Hendrickx DAE, van Scheppingen J, van der Poel M, Bossers K, Schuurman KG, van Eden CG et al (2017) Gene expression profiling of multiple sclerosis pathology identifies early patterns of demyelination surrounding chronic active lesions. Front Immunol 8:1810. https://doi.org/10.3389/fimmu.2017.01810 PMID: 29312322
48. Aikawa T, Ren Y, Yamazaki Y, Tachibana M, Johnson MR, Anderson CT et al (2019) ABCA7 haplodeficiency disturbs microglial immune responses in mouse brain. Proc Natl Acad Sci U S A 116:23790–23796. https://doi.org/10.1073/pnas.1908529116 PMID: 31690660
49. Neal ML, Boyle AM, Budge KM, Safadi FF, Richardson JR (2018) The glycoprotein GPNMB attenuates astrocyte inflammatory responses through the CD44 receptor. J Neuroinflammation 15:73. https://doi.org/10.1186/s12974-018-1100-1 PMID: 29519253
50. Mattiola I, Tomay F, De Pizzol M, Silva-Gomes R, Savino B, Gulic T et al (2019) The macrophage tetraspan MS4A4A enhances dectin-1-dependent NK cell-mediated resistance to metastasis. Nat Immunol 20:1012–1022. https://doi.org/10.1038/s41590-019-0417-y PMID: 31263276
51. Barclay AN, Van den Berg TK (2014) The interaction between signal regulatory protein alpha (SIRPα) and CD47: structure, function, and therapeutic target. Annu Rev Immunol 32:25–50. https://doi.org/10.1146/annurev-immunol-032713-120142 PMID: 24215318
52. Nagamoto-Combs K, Combs CK (2010) Microglial phenotype is regulated by activity of the transcription factor, NFAT (nuclear factor of activated T cells). J Neurosci 30:9641–9646. https://doi.org/10.1523/JNEUROSCI.0828-10.2010 PMID: 20631193
53. Wraith DC, Pope R, Butzkueven H, Holder H, Vanderplank P, Lowrey P et al (2009) A role for galanin in human and experimental inflammatory demyelination. Proc Natl Acad Sci U S A 106:15466–15471. https://doi.org/10.1073/pnas.0903360106 PMID: 19717462
54. Weinger JG, Brosnan CF, Loudig O, Goldberg MF, Macian F, Arnett HA et al (2011) Loss of the receptor tyrosine kinase Axl leads to enhanced inflammation in the CNS and delayed removal of myelin debris during experimental autoimmune encephalomyelitis. J Neuroinflammation 8:49. https://doi.org/10.1186/1742-2094-8-49 PMID: 21569627
55. Keren-Shaul H, Spinrad A, Weiner A, Matcovitch-Natan O, Dvir-Szternfeld R, Ulland TK et al (2017) A unique microglia Type associated with restricting development of Alzheimer's disease. Cell 169:1276–1290. https://doi.org/10.1016/j.cell.2017.05.018 PMID: 28602351
56. Hurr EM, Youssef S, Haws ME, Zhang SY, Sobel RA, Steinman L (2006) Osteopontin-induced relapse and progression of autoimmune brain disease through enhanced survival of active T cells. Nat Immunol 8:74–83. https://doi.org/10.1038/ni1415 PMID: 17143274
57. Ma B, Yu J, Xie C, Sun L, Lin S, Ding J et al (2015) Toll-like receptors promote mitochondrial translocation of nuclear transcription factor nuclear factor of activated T cells in prolonged microglial activation. J Neurosci 35:10799–10814. https://doi.org/10.1523/JNEUROSCI.2455-14.2015 PMID: 26224862
58. Bennett FC, Bennett ML, Yaqoob F, Mulinyawe SB, Grant GA, Hayden Gephart M et al (2018) A combination of ontogeny and CNS environment establishes microglial identity. Neuron 98:1170–1183.e8. https://doi.org/10.1016/j.neuron.2018.05.014 PMID: 29861285
59. Plemel JR, Stratton JA, Michaels NJ, Rawji KS, Zhang E, Sinha S et al (2020) Microglia response following acute demyelination is heterogeneous and limits infiltrating macrophage dispersion. Sci Adv 6:eaay6324. https://doi.org/10.1126/sciadv.aay6324 PMID: 31998844
60. McCoy MK, Tansey MG (2008) TNF signaling inhibition in the CNS: implications for normal brain function and neurodegenerative disease. J Neuroinflammation 5:45. https://doi.org/10.1186/1742-2094-5-45 PMID: 18925972
61. Lambertsen KL, Clausen BH, Babcock AA, Gregersen R, Fenger C, Nielsen HH et al (2009) Microglia protect neurons against ischemia by synthesis of tumor necrosis factor. J Neurosci 29:1319–1330. https://doi.org/10.1523/JNEUROSCI.5505-08.2009 PMID: 19193879
62. Morganti-Kossman MC, Lenzlinger PM, Hans V, Stahel P, Csuka E, Ammann E et al (1997) Production of cytokines following brain injury: beneficial and deleterious for the damaged tissue. Mol Psychiatry 2:133–136. https://doi.org/10.1038/sj.mp.4000227 PMID: 9106236
63. Probert L (2015) TNF and its receptors in the CNS: the essential, the desirable and the deleterious effects. Neuroscience 302:2–22. https://doi.org/10.1016/j.neuroscience.2015.06.038 PMID: 26117714
64. Bachmann R, Eugster HP, Frei K, Fontana A, Lassmann H (1999) Impairment of TNF-receptor-1 signaling but not fas signaling diminishes T-cell apoptosis in myelin oligodendrocyte glycoprotein peptide-induced chronic demyelinating autoimmune encephalomyelitis in mice. Am J Pathol 154:1417–1422. https://doi.org/10.1016/S0002-9440(10)65395-3 PMID: 10329594
65. Bosch X, Saiz A, Ramos-Casals M, BIOGEAS Study Group (2011) Monoclonal antibody therapy-associated neurological disorders. Nat Rev Neurol 7:165–172. https://doi.org/10.1038/nrneurol.2011.1 PMID: 21263460
66. Grajchen E, Hendriks JJA, Bogie JFJ (2018) The physiology of foamy phagocytes in multiple sclerosis. Acta Neuropathol Commun 6:124. https://doi.org/10.1186/s40478-018-0628-8 PMID: 30454040

Publisher's Note

Extract from the Journal Summary List for Publication 3

Rank	Full Journal Title	Total Cites	Journal Impact Factor	Eigenfactor Score
1.	World Psychiatry	6,486	40.595	0.017130
2.	JAMA Psychiatry	13,433	17.471	0.056110
3.	Lancet Psychiatry	6,405	16.209	0.028290
4.	PSYCHOTHERAPY AND PSYCHOSOMATICS	4,275	14.864	0.006480
5.	AMERICAN JOURNAL OF PSYCHIATRY	41,967	14.119	0.034380
6.	MOLECULAR PSYCHIATRY	22,227	12.384	0.054730
7.	BIOLOGICAL PSYCHIATRY	44,016	12.095	0.053910
8.	JOURNAL OF NEUROLOGY NEUROSURGERY AND PSYCHIATRY	30,621	8.234	0.028510
9.	SCHIZOPHRENIA BULLETIN	17,703	7.958	0.027070
10.	BRITISH JOURNAL OF PSYCHIATRY	24,380	7.850	0.020520
11.	JOURNAL OF CHILD PSYCHOLOGY AND PSYCHIATRY	19,837	7.035	0.021080
12.	JOURNAL OF CHILD PSYCHOLOGY AND PSYCHIATRY	19,837	7.035	0.021080
13.	JOURNAL OF THE AMERICAN ACADEMY OF CHILD AND ADOLESCENT PSYCHIATRY	19,831	6.936	0.017840
14.	NEUROPSYCHOPHARMACOLOGY	26,281	6.751	0.040680
15.	BRAIN BEHAVIOR AND IMMUNITY	16,285	6.633	0.028560
16.	JOURNAL OF ABNORMAL PSYCHOLOGY	16,003	6.484	0.014170
17.	ADDICTION	19,861	6.343	0.030820
18.	Epidemiology and Psychiatric Sciences	1,584	5.876	0.004770
19.	PSYCHOLOGICAL MEDICINE	26,702	5.813	0.039350
20.	Clinical Psychological Science	2,599	5.415	0.011100

Rank	Full Journal Title	Total Cites	Journal Impact Factor	Eigenfactor Score
21.	BIPOLAR DISORDERS	4,838	5.410	0.006610
22.	ACTA PSYCHIATRICA SCANDINAVICA	13,539	5.362	0.011750
23.	Translational Psychiatry	9,160	5.280	0.029500
24.	Journal of Behavioral Addictions	2,184	5.143	0.005970
25.	CNS DRUGS	4,768	4.786	0.007670
26.	PSYCHONEUROENDOCRINOLOGY	19,287	4.732	0.027100
27.	DEPRESSION AND ANXIETY	9,355	4.702	0.013860
28.	AUSTRALIAN AND NEW ZEALAND JOURNAL OF PSYCHIATRY	7,192	4.657	0.008620
29.	Current Psychiatry Reports	4,785	4.539	0.010670
30.	EUROPEAN PSYCHIATRY	6,054	4.464	0.009470
31.	CURRENT OPINION IN PSYCHIATRY	4,182	4.392	0.006260
32.	JOURNAL OF PSYCHIATRY & NEUROSCIENCE	3,297	4.382	0.004290
33.	PROGRESS IN NEURO-PSYCHOPHARMACOLOGY & BIOLOGICAL PSYCHIATRY	11,179	4.361	0.013670
34.	PHARMACOPSYCHIATRY	1,787	4.340	0.001580
35.	INTERNATIONAL JOURNAL OF NEUROPSYCHOPHARMACOLOGY	6,749	4.333	0.011150
36.	npj Schizophrenia	502	4.304	0.002060
37.	JOURNAL OF CLINICAL PSYCHIATRY	18,652	4.204	0.018530
38.	WORLD JOURNAL OF BIOLOGICAL PSYCHIATRY	2,567	4.164	0.004200
39.	DRUG AND ALCOHOL DEPENDENCE	20,269	3.951	0.040630
40.	EUROPEAN CHILD & ADOLESCENT PSYCHIATRY	5,422	3.941	0.009450
41.	JOURNAL OF AFFECTIVE DISORDERS	32,869	3.892	0.055920
42.	SUICIDE AND LIFE-THREATENING BEHAVIOR	4,512	3.867	0.005980

Selected JCR Year: 2019; Selected Categories: "PSYCHIATRY"

Selected publication 3

Böttcher, C.*, Fernández-Zapata, C.*, Snijders, G. J. L., Schlickeiser, S., Sneeboer, M. A. M., Kunkel, D., Witte, L. D. De & Priller, J. Single-cell mass cytometry of microglia in major depressive disorder reveals a non-inflammatory phenotype with increased homeostatic marker expression. *Transl. Psychiatry* 1–11 (2020).

ARTICLE   **Open Access**

Single-cell mass cytometry of microglia in major depressive disorder reveals a non-inflammatory phenotype with increased homeostatic marker expression

Chotima Böttcher [1], Camila Fernández-Zapata [1], Gijsje J. L. Snijders[2], Stephan Schlickeiser[3], Marjolein A. M. Sneeboer[2,4], Desiree Kunkel[5], Lot D. De Witte[2,4,6] and Josef Priller[1,7,8]

Abstract

Stress-induced disturbances of brain homeostasis and neuroinflammation have been implicated in the pathophysiology of mood disorders. In major depressive disorder (MDD), elevated levels of proinflammatory cytokines and chemokines can be found in peripheral blood, but very little is known about the changes that occur directly in the brain. Microglia are the primary immune effector cells of the central nervous system and exquisitely sensitive to changes in the brain microenvironment. Here, we performed the first single-cell analysis of microglia from four different post-mortem brain regions (frontal lobe, temporal lobe, thalamus, and subventricular zone) of medicated individuals with MDD compared to controls. We found no evidence for the induction of inflammation-associated molecules, such as CD11b, CD45, CCL2, IL-1β, IL-6, TNF, MIP-1β (CCL4), IL-10, and even decreased expression of HLA-DR and CD68 in microglia from MDD cases. In contrast, we detected increased levels of the homeostatic proteins P2Y$_{12}$ receptor, TMEM119 and CCR5 (CD195) in microglia from all brain regions of individuals with MDD. We also identified enrichment of non-inflammatory CD206^{hi} macrophages in the brains of MDD cases. In sum, our results suggest enhanced homeostatic functions of microglia in MDD.

Introduction

Major depressive disorder (MDD) is one of the most common mental disorders across the lifespan and represents a leading cause of disability worldwide[1]. MDD is more prevalent in women than men and it increases the risk of suicide, obesity, and coronary heart disease[2]. Recent genome-wide association studies have associated MDD with variants in genes involved in hypothalamic-pituitary-adrenal (HPA) axis function, neuronal differentiation, synaptic transmission, cytokine production, and immune response[3]. Cell type-specific methylome studies have confirmed the involvement of the innate immune system in MDD[4]. The polygenic risk for MDD is moderated by environmental factors, such as childhood trauma[5]. Strong gene-environment interactions exist between HPA axis genes (*Corticotrophin releasing hormone receptor 1*, *FK506 binding protein 5*) and MDD[6]. Notably, higher *FKBP5* expression promotes nuclear factor (NF)-κB-mediated peripheral inflammation and chemotaxis[7]. Along these lines, chronic stress and low-grade inflammation are believed to contribute to the pathophysiology of MDD[8–10]. In fact, patients with MDD express increased levels of proinflammatory cytokines like interleukin (IL)-1, IL-6 and tumor necrosis factor (TNF)-α

Correspondence: Chotima Böttcher (chotima.boettcher@charite.de) or
Josef Priller (josef.priller@charite.de)
[1]Department of Neuropsychiatry and Laboratory of Molecular Psychiatry, Charité – Universitätsmedizin Berlin, Berlin, Germany
[2]Department of Psychiatry, Brain Center Rudolf Magnus, University Medical Center Utrecht, Utrecht, The Netherlands
Full list of author information is available at the end of the article
These authors contributed equally: Chotima Böttcher, Camila Fernández-Zapata, Lot D. De Witte, Josef Priller

in peripheral blood, which can access the central nervous system (CNS) and activate tissue-resident macrophages like microglia, impair HPA axis function, modulate monoaminergic neurotransmission, and reduce neural plasticity[11–13]. The tryptophan-kynurenine pathway links depression and inflammation, and under stressful and inflammatory conditions, microglial indoleamine 2,3-dioxygenase (IDO) activity reduces serotonin availability and results in the production of excitotoxic metabolites such as quinolinic acid[8,9]. In recent years, peripheral blood cytokines have been proposed as biomarkers of MDD[14], and combinations of pro- and anti-inflammatory cytokines (e.g. IL-10) can help predict the response to antidepressant treatment[15–18].

However, it remains an unresolved question of high therapeutic relevance whether the inflammation in MDD originates primarily in the periphery or in the CNS. Peripheral blood monocytes of MDD patients express higher levels of inflammatory/immune mediators like IL-1β and IL-6, as well as *TNF, TLR2, CEBPA,* and *CCL2* mRNAs[19–24]. In contrast, studies of CNS microglia have resulted in contradictory findings. Microglia are specialized tissue macrophages that originate from the yolk sac during early embryonic life, and play essential roles in brain development and maintenance of CNS homeostasis[25]. Neuropathological examination of post-mortem frontal lobe tissue from MDD cases revealed increased numbers of activated microglia expressing ionized calcium-binding adaptor molecule (Iba)1[26] or quinolinic acid[27]. The number of primed Iba1-positive microglia and CD45-immunoreactive perivascular macrophages was increased in depressed suicides[28]. In contrast, many other studies did not detect significant changes in the density of major histocompatibility complex HLA-DR-immunoreactive microglia in frontal lobe, temporal lobe, thalamus or brain stem of MDD cases[29–32]. Gene expression profiling of post-mortem frontal lobe tissue from psychotropic drug-free persons with a history of MDD revealed increased expression of *IL1A, IL3, IL5, IL8, IL10,* but not *IL6* or *TNF*[33]. Gene expression of *TNF, IFNG,* and *CCL2* was even reduced in the prefrontal cortex of depressed suicides[28]. Strong support for the neuroinflammation hypothesis of MDD comes from positron emission tomography (PET) studies of translocator protein 18 kDa (TSPO) binding in depressed individuals with MDD. TSPO binding was found to be elevated in frontal lobe, temporal lobe and thalamus of depressed patients, and correlated with the severity of depression[34], cognitive dysfunction[35], and the duration of antidepressant treatment[36]. However, no correlation with peripheral inflammatory markers like IL-1β, IL-6, TNF, and C-reactive protein (CRP) was detected[34]. It is also still controversial whether TSPO binding is a good indicator of microglial activation in the human brain[37].

Given that the role of microglia is not yet clear in major depression[38], we decided to use single-cell high-dimensional mass cytometry (CyTOF) to examine microglia from different post-mortem brain regions of medicated individuals with MDD compared to controls. We have recently demonstrated that this technique allows us to detect subtle phenotypic differences of human microglia across different brain regions with good correlation between post-mortem tissue and fresh brain biopsies[39]. In this study, we determined 59 protein markers at the single-cell level that unequivocally distinguish microglia from other brain macrophages and peripherally derived immune cells. The results suggest a non-inflammatory phenotype of microglia with increased homeostatic marker expression in MDD.

Methods
Human post-mortem tissue

Human post-mortem brain tissue was obtained from the Psychiatric Donor Program of the Netherlands Brain Bank (NBB-Psy; www.brainbank.nl). The Netherlands Brain Bank received permission to perform autopsies and to use tissue and medical records from the Ethical Committee of the VU University Medical Center. Tissue was collected post-mortem from donors from whom full consent had been obtained during life to conduct brain autopsy and research. Mediacted MDD cases ($n = 6$) were defined as donors with a diagnosis of MDD according to the DSM-IV or III. Control donors ($n = 5$) were defined as donors without a history of depression, confirmed by retrospective medical chart review. Detailed donor information is provided in Supplementary Tables 1–3.

Microglia isolation

Microglia were isolated from post-mortem brain tissue as described previously[39]. After autopsy, tissue was stored in Hibernate medium (Invitrogen, Carlsbad, CA, USA) at 4 °C until further processing. Microglia isolation started as soon as possible, at the latest after 24 h. A single-cell suspension was generated by mechanical and enzymatic digestion with collagenase (3700 units/mL; Worthington, USA) and DNase (200 μg/mL; Roche, Switzerland) for frontal lobe (GFM), temporal lobe (GTS) and thalamic (THA) tissues, or 0.2% trypsin and 30 mg DNase for subventricular zone (SVZ) tissue. A Percoll (Amersham, Merck, Germany) gradient was generated to separate viable cells from myelin, cellular debris, and erythrocytes. The middle layer was collected and washed twice, followed by positive selection of myeloid cells with CD11b-conjugated magnetic beads (Miltenyi Biotec, Germany) according to the manufacturer's protocol. MACS-isolated CD11b$^+$ cells were fixed with fixation/stabilization buffer (SmartTube) and frozen at −80 °C until analysis by mass cytometry[39].

Intracellular barcoding for mass cytometry

MACS-isolated CD11b$^+$ cells were thawed and subsequently stained with premade combinations of six different palladium isotopes: ^{102}Pd, ^{104}Pd, ^{105}Pd, ^{106}Pd, ^{108}Pd, and ^{110}Pd (Cell-ID 20-plex Pd Barcoding Kit, Fluidigm). This multiplexing kit applies a 6-choose-3 barcoding scheme that results in 20 different combinations of three Pd isotopes. After 30 min staining at room temperature, individual samples were washed twice with cell staining buffer (0.5% bovine serum albumin in PBS containing 2 mM EDTA). All samples were pooled together, washed, and stained with antibodies.

Antibodies

Anti-human antibodies (Supplementary Tables 4 and 5) were purchased either pre-conjugated to metal isotopes (Fluidigm), or from commercial suppliers in purified form and then conjugated by us using the MaxPar X8 kit (Fluidigm) according to the manufacturer's protocol. Each antibody was titrated and validated using different cell types from different body compartments, as described previously[39].

Cell surface and intracellular staining

After cell barcoding, washing and pelleting, the combined samples were stained and processed as described previously[39]. Briefly, cells were resuspended in 100 μl of antibody cocktail directed against cell surface markers (Supplementary Tables 4 and 5) and incubated at 4 °C for 30 min. Then, the cells were washed twice with cell staining buffer (PBS containing 0.5% bovine serum albumin and 2mM EDTA). For intracellular staining, the stained (non-stimulated) cells were incubated in fixation/permeabilization buffer (Fix/Perm Buffer, eBioscience) at 4 °C for 60 min. After two washes with permeabilization buffer (eBioscience), the samples were stained with antibody cocktails directed against intracellular molecules (Supplementary Tables 4 and 5) in permeabilization buffer at 4 °C for 1 h. Cells were subsequently washed twice with permeabilization buffer and incubated overnight in 4% methanol-free formaldehyde solution. The fixed cells were washed and resuspended in 1 ml iridium intercalator solution (Fluidigm) at room temperature for 1 h, followed by two washes with cell staining buffer and two washes with ddH$_2$O (Fluidigm). Finally, cells were pelleted and kept at 4 °C until CyTOF measurement.

Bead staining

For the bead-based compensation of the signal spillover, AbC total antibody compensation beads (Thermo Fisher Scientific) were stained with each of the antibodies used in all three antibody panels according to the manufacturer's instructions. Stained beads were then measured with CyTOF and the compensation matrix was generated as described previously[40].

CyTOF measurements

Cells were analyzed using a CyTOF2 upgraded to Helios specifications, with software version 6.7.1014[39]. The instrument was tuned according to the manufacturer's instructions with tuning solution (Fluidigm), and measurement of EQ four element calibration beads (Fluidigm) containing $^{140/142}$Ce, $^{151/153}$Eu, ^{165}Ho, and $^{175/176}$Lu served as a quality control for sensitivity and recovery. Immediately prior to analysis, cells were resuspended in ddH$_2$O, filtered through a 20 μm cell strainer (Celltrix, Sysmex), counted and adjusted to 3–5 × 10^5 cells/ml. EQ four element calibration beads were added at a final concentration of 1:10 v/v in order to normalize the data to compensate for signal drift and day-to-day changes in instrument sensitivity. Samples were acquired with a flow rate of 300–400 events/s. The lower convolution threshold was set to 400, with noise reduction mode turned on and cell definition parameters set at event duration of 10–150 pushes (push = 13 μs). The resulting flow cytometry standard (FCS) files were normalized and randomized using the CyTOF software's internal FCS-Processing module on the non-randomized ("original") data. The default settings in the software were used with time interval normalization (100 s/minimum of 50 beads) and passport version 2. Intervals with less than 50 beads per 100 s were excluded from the resulting FCS file.

Mass cytometry data processing and analysis

Following the workflow from our previous study[40], Cytobank (www.cytobank.org) was used for initial manual gating on live single cells and Boolean gating for de-barcoding. Nucleated single intact cells were manually gated according to the signals of DNA intercalators ^{191}Ir/^{193}Ir and event length. For de-barcoding, Boolean gating was used to deconvolute individual samples according to the barcode combination. Prior to data analysis, each FCS file was compensated for signal spillover using R package *CATALYST*[41]. For dimensionality reduction, visualization and further exploration, (2D)-tSNE maps were generated based on the expression levels of all markers in each panel. For embedding, we set hyperparameters to perplexity of 30, theta of 0.5, and iterations of 1000 per 100,000 analyzed cells. To visualize marker expression, arcsinh transformation was applied to the data. All FCS files were then loaded into R and further data analysis was performed with a custom written script based on the workflow proposed by Nowicka and colleages[42]. Briefly, for unsupervised cell population identification, we performed cell clustering with the *FlowSOM*[43] and *ConsensusClusterPlus*[44] packages using all markers in each panel. We then performed visual inspection of cluster-colored tSNE plots and phenotypic heat maps for a more detailed profile of each cluster, and we determined the number of meta-clusters with consistent phenotypes

for statistical testing. Based on visual inspection of t-SNE plots and heat maps generated at the merging step, a final number of meta-clusters was chosen that merged clusters into populations with consistent phenotypes (with a minimal mean frequency of 0.1% of parent)[40].

Statistical analysis

No randomization and blinding strategies were applied in this study. However, data processing and analysis, as well as statistical testing were carried out in an unsupervised manner. Dichotomous variables of the sample cohort were analyzed with Fisher's exact test (GraphPad Prism). Quantitative data are shown as independent data points with Box-Whisker. Exploratory analyses of statistical significance were performed using multiple *t*-test available through GraphPad Prism 8 with a false discovery rate (FDR) adjustment at 10% using the Benjamini–Krieger–Yekutieli procedure for multiple hypothesis testing, unless otherwise stated. A *P* value < 0.05 was considered statistically significant.

Results

Samples

MDD and controls did not differ in age, gender or post-mortem characteristics (Supplementary Table 1). The average post-mortem delay was 8 h (range 4½–12¾ h). Both groups were medicated, and donors differed with regard to medication used and psychiatric history (Supplementary Tables 2 and 3).

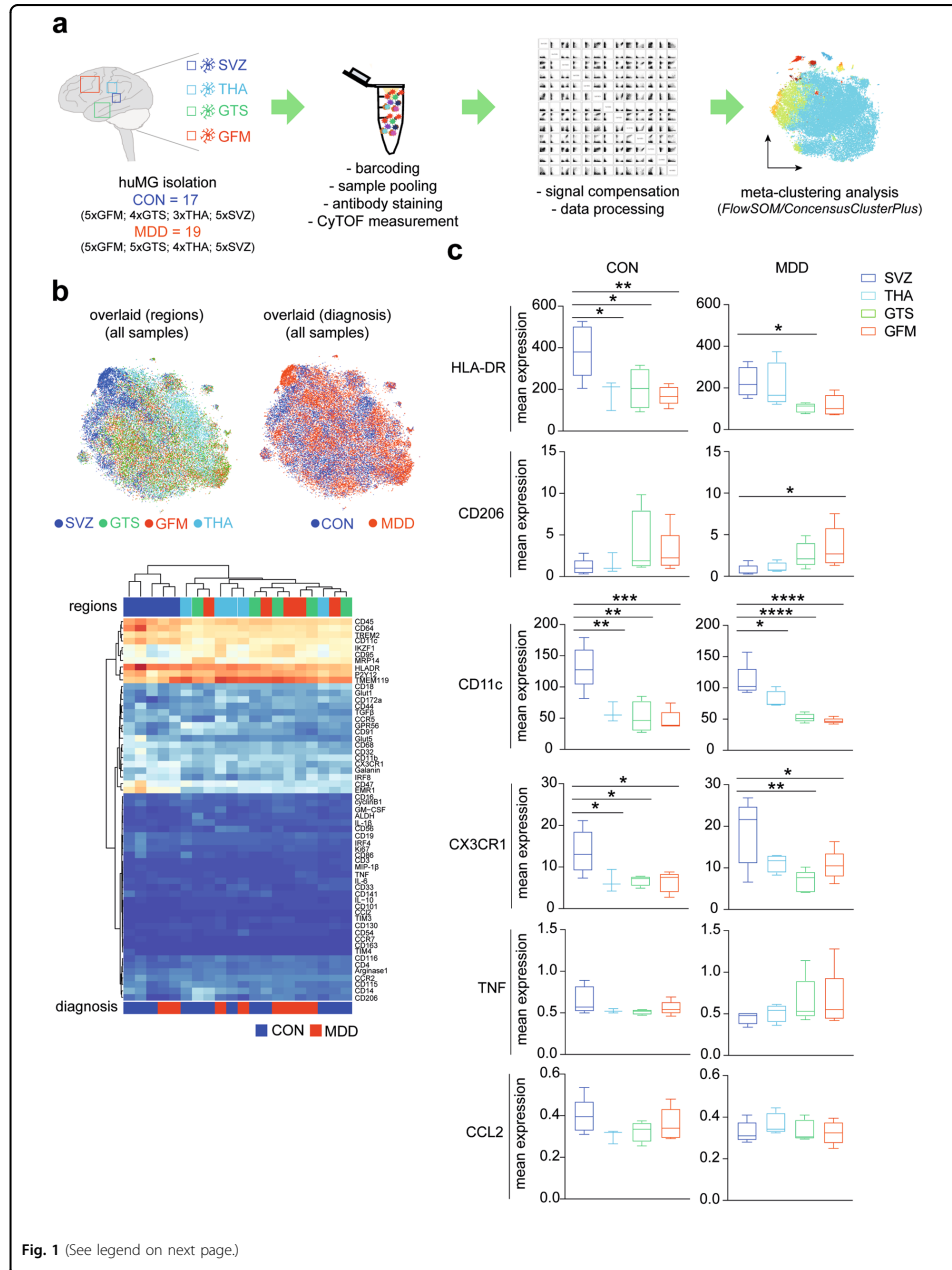### Regional diversity of human microglia is preserved in MDD

Human microglia (huMG) were isolated from postmortem brain tissue of subventricular zone (SVZ), thalamus (THA), temporal lobe (GTS) and frontal lobe (GFM) (Fig. 1a). In order to minimize the run-to-run variation and to facilitate the comparison of cellular profiles from different brain regions and individuals, we simultaneously profiled huMG samples from different brain regions of donors with MDD and controls in the same run. To do so, huMG were intracellularly barcoded using different combinations of palladium isotopes as described previously[39]. Up to twenty samples were pooled, split equally and stained with two different antibody panels (Supplementary Tables 4 and 5). The antibody *Panel A* (36 antibodies) was designed to distinguish the major circulating immune cell subsets, including T & B lymphocytes, monocytes, natural killer (NK) cells, from CNS immune cells, including microglia and border-associated macrophages. The panel also focused on cytokines, chemokines and other inflammatory mediators, and comprised antibodies against $P2Y_{12}$ receptor, TREM2, CD45, CD3, CD14, CD16, CD11c, CD64, CD11b, CD56, EMR1, CD115, CD47, CD19, HLA-DR, CD56, CD68, CD33 (Siglec-3), CD192 (CCR2), CD195 (CCR5), CX3CR1,

CD141, CD32, CD206, CD163, MIP-1β, IL-10, CCL2, IRF8, TGFβ, and TNF (Supplementary Table 4). The antibody *Panel B* was designed to investigate functional and activity changes in huMG subsets using 35 antibodies, including HLA-DR, IKZF1, ALDH, IL-1β, IL-6, MRP14 (S100A9), CD11b, CD116, CD44, Galanin, CD54 (ICAM1), CCR7, GPR56, CD141, CD86, CD91 (LRP1), CD95, CD172a, Glut1, Glut5, TIM3, TIM4, Arginase-1 (Supplementary Table 5). Multiplexed and stained samples were simultaneously acquired on a CyTOF instrument. To validate the robustness of the results, we performed three independent measurements with a total of 36 huMG samples (summarized in Supplementary Table 1).

We used the commercially available analysis platform Cytobank (www.cytobank.org) to capture and visualize all huMG cells in a single two-dimensional (2D) map using unsupervised high-dimensional data analysis, the t-distributed stochastic linear embedding (t-SNE) algorithm (Fig. 1b). In line with our previous evidence for regional heterogeneity of human microglia[39], we observed a unique phenotype of SVZ microglia compared to microglia isolated from other brain regions (Fig. 1b, c). The huMG from control SVZ showed significantly higher expression of HLA-DR, CD11c, and CX3CR1 (Fig. 1c). Most importantly, we did not observe separation of huMG from donors with MDD and controls (Fig. 1b), which is in strong contrast to what we had previously observed for glioma-associated huMG[45]. No differences in the expression of HLA-DR, CD206, CD11c, CX3CR1, TNF, and CCL2 were observed for huMG from different brain regions between control and MDD cases (Fig. 1c). However, huMG from MDD cases expressed attenuated levels of HLA-DR in SVZ (Fig. 1c).

Increased $P2Y_{12}$ and TMEM119 expression in microglia from MDD brains

Next, to fully harness the high-dimensionality of the mass cytometry data and to study huMG in more detail, we performed a comprehensive analysis on R/Bioconductor using the over-clustering approach[40]. Of note, the number of defined clusters may not solely represent biological functional subsets of huMG, but should be considered as an exploratory tool for the discovery of differential abundance of small/rare huMG populations between the two analyzed groups. All markers of antibody *Panels A and B* were included in the meta-clustering analysis, revealing eight distinct phenotype clusters of huMG (Fig. 2a–d). The defined clusters displayed a differential distribution across the different brain regions (Fig. 2c, d). The main cluster 2 (C2) was significantly less abundant in SVZ, whereas cluster 3 (C3) was more abundant in SVZ (Fig. 2d). No significant differences in cluster distribution were observed between huMG from MDD and control cases (Fig. 2d).

Fig. 1 (See legend on next page.)

Comparison of microglia phenotypes within defined clusters revealed significant differences between MDD and control cases (Fig. 2e–g). Notably, the main cluster C2 contained huMG with significantly higher expression of the homeostatic markers P2Y$_{12}$ and transmembrane protein (TMEM)119[46] in MDD compared to controls (Fig. 2e). At the same time, huMG from cluster C2 expressed lower levels of the activation markers HLA-DR and CD68[47] in MDD (Fig. 2e). HuMG from the SVZ-enriched cluster C3 also expressed more TMEM119 and less HLA-DR and CD68 in MDD cases (Fig. 2f). In contrast, CD206^{hi} (P2Y$_{12}$^{lo}TMEM119^{lo}) macrophages from cluster C8 expressed more HLA-DR, TMEM119 and CD91 (LRP1) in MDD than control cases (Fig. 2g). Importantly, huMG/macrophages from clusters C2, C3, and C8 expressed higher levels of the chemokine CD195 (CLL5), but comparable levels of IL-1β, IL-6, TNF, MIP-1β (CCL4), IL-10, and MCP-1 (CCL2) between MDD and control cases (Fig. 2e–g). None of the other examined markers from *Panels A and B*, including among others CX3CR1, IRF8, IRF7, CD11b, CD11c, CD86, CD45, TREM2, APOE, AXL, CD33 (Siglec-3), CD54 (ICAM1), CD56 (NCAM), GPR56, CD74, TGFβ, IFN-α, Galanin, CD95 (Fas), PD-L1, and Glut5, were differentially expressed between huMG/macrophages from MDD and control cases (data not shown).

Discussion

This is the first study to examine human microglia in MDD at the single-cell level. We found a non-inflammatory phenotype of microglia with enhanced homeostatic functions in medicated MDD cases.

Our results are in line with recent microarray-based transcriptomic profiling of cerebral cortex in 87 cases of MDD, revealing no significant changes (FDR-corrected P value > 0.05) in the gene expression of *HLA-DR*, *TNF*, *IL6*, *IL1B*, *IL1A*, *IL3*, *IL5*, *IL8*, *IL10*, *ITGAM* (*CD11b*), *FKBP5*, *TLR2*, *CCL2*, and *CD14* compared with matched controls[48]. Notably, the study detected increased transcript levels of *IL17* and *CCL5*, the latter binding to the chemokine receptor CCR5, which we found increased by CyTOF in human microglia from MDD brains. Interestingly, systemic inflammation can trigger CCR5-dependent migration of microglia to the cerebral vasculature[49]. Gene expression profiling of post-mortem frontal lobe tissue from 14 MDD cases showed increased expression of *IL1A*, *IL3*, *IL5*, *IL8*, *IL10*, but not *IL6* or *TNF*[33]. Gene expression of *TNF*, *IL1B* and *IL10* was also unchanged in the prefrontal cortex of depressed suicides[28]. We have performed PCR analysis of myeloid cells from post-mortem brain tissue of 20 MDD cases compared with 27 controls and found no differential expression of *IL6*, *IL1B*, and *TNF* mRNAs, even after in vitro challenge with lipopolysaccharide and dexamethasone (Snijders et al., submitted for publication). However, we detected increased expression of *CX3CR1* and *TMEM119* mRNAs, and decreased expression of *CD163* and CD14 protein (Snijders et al., submitted for publication), underscoring the results of this single-cell CyTOF analysis of human microglia in the MDD brain.

The power of high-dimensional single-cell analysis lies in the precise identification of cell populations and the detection of rare disease-associated microglia states that would go undetected with bulk analysis and the use of single markers[45,50–52]. Even though the sample size is very small and medication effects cannot be excluded, our study suggests that homeostatic functions may be enhanced in MDD microglia. It is tempting to speculate that the increased expression of TMEM119 and P2Y$_{12}$ in microglia clusters from MDD cases may reflect enhanced neuron-microglia communication via transforming growth factor (TGF)β1, which shows significant gene-environment interactions predicting adult depression in the context of early life trauma[53], as well as purines, in an attempt to protect neuronal function[54,55]. Along these lines, monocyte-derived microglia-like cells from individuals with schizophrenia exhibit increased synapse engulfment[56]. Expression of P2Y$_{12}$ in microglia is
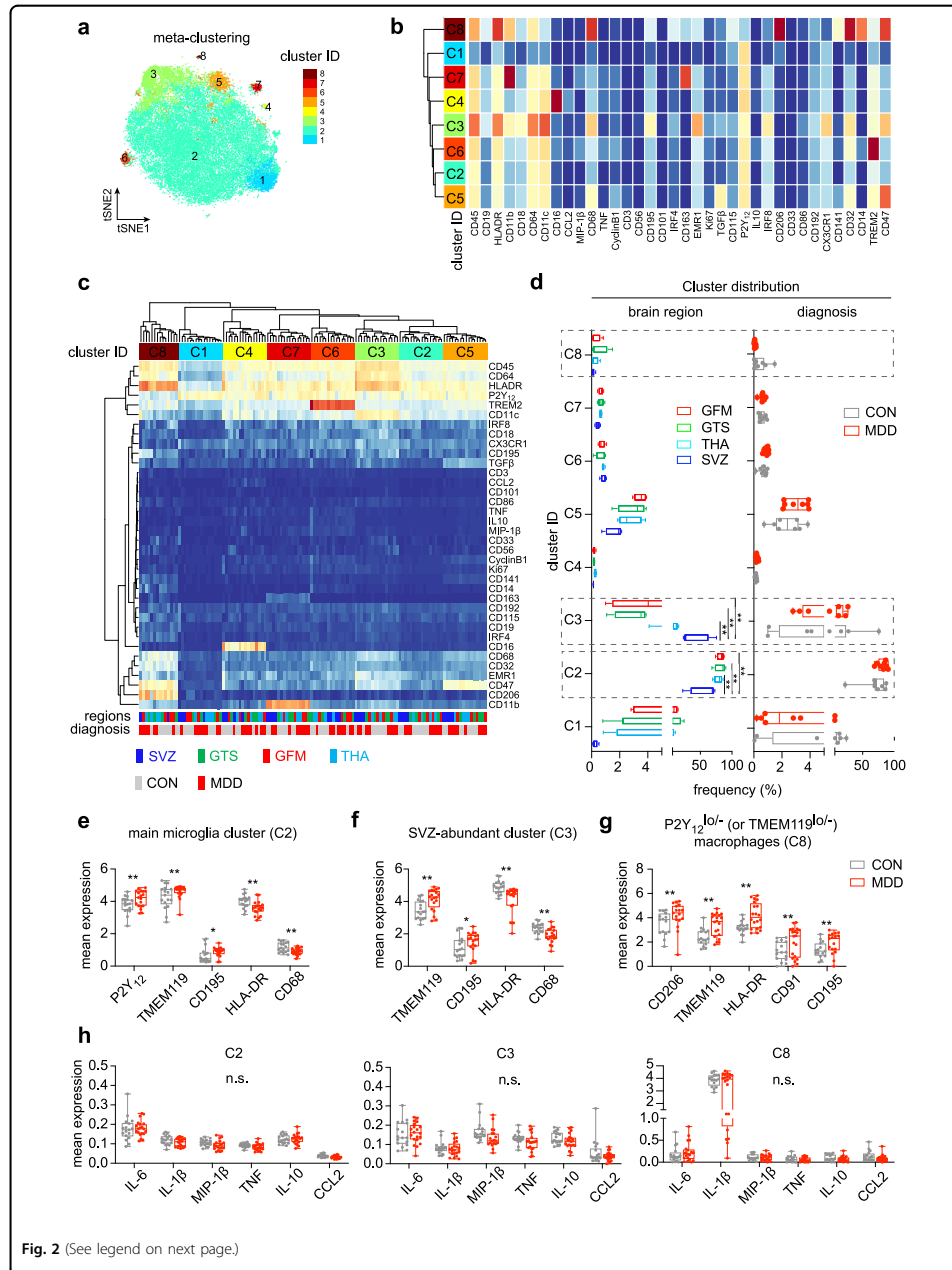
Fig. 2 (See legend on next page.)

(see figure on previous page)

Fig. 2 Phenotypic diversity of myeloid cells in the MDD brain. a The overlaid t-SNE plot of 16 huMG samples (SVZ = 4; THA = 4; GTS = 4; GFM = 4) isolated from four biologically independent donors (CON = 2; MDD = 2) is shown. The 2D t-SNE maps were generated based on expression levels of all markers of *Panel A* (Supplementary Table 4). The coloring indicates eight defined clusters representing diverse myeloid cell phenotypes. **b** Heat map and cluster analysis of all samples demonstrates the phenotypes of all eight defined clusters on the basis of the mean expression levels of 36 markers used for the cluster analysis. Identified clusters are indicated by dendrograms. Heat colors show overall marker expression levels (red: high expression; dark blue: no expression). **c** Heat map cluster demonstrates the expression levels of 36 analyzed markers for all eight clusters of each sample. Samples are indicated by dendrograms. Heat colors show overall expression levels (dark blue: no expression; red: high expression). **d** Boxplots on the left show the cluster distribution across four different brain regions (SVZ, blue; THA, light blue; GTS, green; GFM, red) and on the right the cluster distribution for the two groups (CON and MDD). Whisker plots show the min (smallest) and max (largest) values. A dot indicates the frequency (%) of an individual sample. The line in the box denotes the median. $**P < 0.01$, multiple t-test with FDR adjustment (at 10% using the Benjamini–Krieger–Yekutieli procedure). (**e–g**) Boxplots showing markers with differential expression (arcsinh) between CON and MDD for (**e**) the main microglia cluster C2, (**f**) the SVZ-enriched huMG cluster C3, and (**g**) the $P2Y_{12}^{lo/-}$ (or $TMEM119^{lo/-}$) macrophage cluster C8. A dot indicates the mean expression of an individual sample from all three measurements. $*P < 0.05$, $**P < 0.01$, multiple t-test with FDR adjustment (at 10% using the Benjamini-Krieger-Yekutieli procedure). **h** Boxplots showing selected cytokines and chemokines (IL-6, IL-1β, MIP-1β, TNF, IL-10, CCL2) that are not differentially expressed (arcsinh) between CON and MDD for the clusters C2, C3, and C8. A dot indicates the mean expression of an individual sample from all three measurements. A P value < 0.05 was considered statistically significant (multiple t-test with FDR adjustment at 10% using the Benjamini–Krieger–Yekutieli procedure).

important for synaptic plasticity[57] and for adult hippocampal neurogenesis[58], which has been associated with the response to antidepressant treatment[59]. Neuronal activity regulates the surveilling function of microglia processes in the cortex via the monoamine neurotransmitter norepinephrine[60,61], which is reduced in the brains of patients with depression[62,63]. A reduction in norepinephrine tone results in microglial extension and territory surveillance[60]. Interestingly, microglia were found to be hyper-ramified in a chronic despair mouse model of depression, and this morphological change was mediated by neuron-microglia signaling via CX3CR1, and restored by antidepressant treatment[64].

Neuroinflammation is associated with the marked downregulation of homeostatic markers like $P2Y_{12}$ and TMEM119 in microglia[52,65,66]. In contrast, we found that both markers were increased in microglia from MDD brains and none of the proinflammatory mediators were altered, calling into question the presence of an active inflammatory process. In fact, we even detected a downregulation of the immune molecules, HLA-DR and CD68, in the main cluster of microglia from MDD brains compared with controls. HLA-DR is a major histocompatibility complex (MHC) class II molecule involved in antigen presentation, which is constitutively expressed by human microglia with higher expression levels in white than gray matter[45,67]. Expression of HLA-DR is strongly induced in activated microglia across a variety of neuroinflammatory and neurodegenerative diseases[52,68], and axonal damage in multiple sclerosis has been associated with HLA-DR[+] microglia[69]. CD68 is a glycoprotein that primarily localizes to the endosomal/lysosomal compartment, but also acts as a class D scavenger receptor on the plasma membrane of monocytes/macrophages[70]. Human microglia constitutively express CD68 with higher expression levels in white than gray matter[39,45]. Microglial

expression of CD68 is strongly induced by neuroinflammation[52,71], which may also represent a tipping point in the pathogenesis of Alzheimer's disease[72]. Interestingly, the brains of individuals resilient to dementia despite robust Alzheimer's neuropathology (amyloid plaques and neurofibrillary tangles) displayed lower numbers of CD68^{+} microglia in the temporal lobe and higher levels of the cytokines IL-6, IL-1β, IL-10[73]. Recent evidence from genome-wide association studies suggests shared genetic architecture between MDD and late-onset Alzheimer's disease[74,75], and some of the identified genes were highly expressed in monocytes/macrophages and involved in immune response and endocytosis. However, the findings of our high-dimensional single-cell analysis of microglia in MDD do not lend support to neuroinflammatory changes in any of the examined cortical and subcortical brain regions. The results are in line with earlier studies of candidate markers like HLA-DR and CD68 in postmortem brain tissue from MDD cases with and without suicidality[28–32].

Our study has several limitations. The sample size is very small due to the difficulties in obtaining sufficient quality post-mortem brain tissue for CyTOF analysis. We were particularly interested in comparatively assessing different brain regions as human microglia are diverse, and we were able to replicate our earlier findings of regional heterogeneity of human microglia[39] in this independent cohort. Although microglia from different post-mortem brain regions did not differ between MDD and controls, the attenuated expression of HLA-DR in microglia from the microenvironment of the subventricular zone may warrant further exploration. An important study has recently found that the brain transcriptional profile of MDD differs greatly by gender; men with MDD exhibited increases in oligodendrocyte- and microglia-related genes, while women with MDD had

decreases in these markers[76]. Notably, *P2RY12* expression in the anterior cingulate cortex was increased in men with MDD and decreased in women with MDD compared to controls[76]. Our sample size was too small to correct for gender effects, but we did not observe different response patterns of microglia (including expression of $P2Y_{12}$) between the three women and three men with MDD versus controls in our sample. Another confounder of our study may be the effects of medication, in particular antidepressants, on immune responses in the brain. It is well known that tricyclic antidepressants, selective serotonin reuptake inhibitors (SSRI), and serotonin and noradrenaline reuptake inhibitors (SNRI) can reduce the expression of proinflammatory cytokines like IL-6, IL-1β, and TNF-α, and increase the expression of IL-10, but the opposite effects have also been described[77]. Moreover, many of these studies examined peripheral blood and the cytokine changes may actually reflect treatment response. We cannot control for the effects of the diverse range of medication in our small sample, but it is important to note that the majority of MDD cases (at least 4/6) were clinically depressed at the time of death based on retrospective chart analysis and one case did not receive antidepressant medication during the last 3 months before death. Furthermore, 24 h before death, both control and MDD donors received morphine, opioids, sedatives and/or anesthetic agents (Supplementary Table 2). It has been demonstrated that these drugs may exert suppressive effects on the immune system and impair monocyte/macrophage function[78–80]. However, as a common limitation of studies performed in humans, the effects reported in the literature were variable and potentially confounded by different methods used to assess immune responses, large spectrum of drugs with different dosages, and low numbers of study participants[80]. In the future, it will be important to comparatively assess the effects of medication on peripheral immune cells and microglia in MDD by controlled trials. Finally, we were also unable to control for agony, comorbid conditions, and bias introduced by diagnosis based on retrospective medical chart review by two independent psychiatrists.

The results of this first high-dimensional single-cell analysis of microglia in MDD provide a missing piece in the concept of neuroinflammation in mood disorders. Further validation in larger cohorts and the use of additional techniques like single-cell RNA sequencing are required to ascertain the findings. Our results may be of particular value for PET studies which have relied on TSPO ligand binding to determine microglial responses in the CNS. Our findings also raise the intriguing possibility that supporting the functions of microglia in the brain may be more beneficial in MDD than the use of anti-inflammatory agents.

Author details
[1]Department of Neuropsychiatry and Laboratory of Molecular Psychiatry, Charité – Universitätsmedizin Berlin, Berlin, Germany. [2]Department of Psychiatry, Brain Center Rudolf Magnus, University Medical Center Utrecht, Utrecht, The Netherlands. [3]BIH Center for Regenerative Therapies (BCRT), Charité – Universitätsmedizin Berlin, Berlin, Germany. [4]Department of Psychiatry, Icahn School of Medicine at Mount Sinai, New York, NY, USA. [5]Flow & Mass Cytometry Core Facility, Charité – Universitätsmedizin Berlin and Berlin Institute of Health (BIH), 10178 Berlin, Germany. [6]Mental Illness Research, Education and Clinical Center (MIRECC), James J Peters VA Medical Center, Bronx, NY, USA. [7]DZNE and BIH, Berlin, Germany. [8]University of Edinburgh and UK Dementia Research Institute (DRI), Edinburgh, UK

Conflict of interest
The authors declare that they have no conflict of interest.

Publisher's note
Springer Nature remains neutral with regard to jurisdictional claims in published maps and institutional affiliations.

References
1. GBD 2017 Disease and Injury Incidence and Prevalence Collaborators. Global, regional, and national incidence, prevalence, and years lived with disability for 354 diseases and injuries for 195 countries and territories, 1990–2017: a systematic analysis for the Global Burden of Disease Study 2017. *Lancet* **392**, 1789–1858 (2018).
2. Kupfer, D. J., Frank, E. & Phillips, M. L. Major depressive disorder: new clinical, neurobiological, and treatment perspectives. *Lancet* **379**, 1045–1055 (2012).
3. Wray, N. R. et al. Genome-wide association analyses identify 44 risk variants and refine the genetic architecture of major depression. *Nat. Genet.* **50**, 668–681 (2018).
4. Chan, R. F. et al. Cell type-specific methylome-wide association studies implicate neurotrophin and innate immune signaling in major depressive disorder. *Biol. Psychiatry* **87**, 431–442 (2020).
5. Peyrot, W. J. et al. Does childhood trauma moderate polygenic risk for depression? A meta-analysis of 5765 subjects from the Psychiatric Genomics Consortium. *Biol. Psychiatry* **84**, 138–147 (2018).
6. Normann, C. & Buttenschøn, H. N. Gene-environment interactions between HPA-axis genes and stressful life events in depression: a systematic review. *Acta Neuropsychiatr.* **31**, 186–192 (2019).
7. Zannas, A. S. et al. Epigenetic upregulation of FKBP5 by aging and stress contributes to NF-κB-driven inflammation and cardiovascular risk. *Proc. Natl Acad. Sci. USA* **116**, 11370–11379 (2019).
8. Wohleb, E. S., Franklin, T., Iwata, M. & Duman, R. S. Integrating neuroimmune systems in the neurobiology of depression. *Nat. Rev. Neurosci.* **17**, 497–511 (2016).
9. Leonard, B. E. Inflammation and depression: a causal or coincidental link to the pathophysiology? *Acta Neuropsychiatr.* **30**, 1–16 (2018).
10. Enache, D., Pariante, C. M. & Mondelli, V. Markers of central inflammation in major depressive disorder: A systematic review and meta-analysis of studies examining cerebrospinal fluid, positron emission tomography and post-mortem brain tissue. *Brain Behav. Immun.* **81**, 24–40 (2019).
11. Miller, A. H., Maletic, V. & Raison, C. L. Inflammation and its discontents: the role of cytokines in the pathophysiology of major depression. *Biol. Psychiatry* **65**, 732–741 (2009).

12. Culmsee, C. et al. Mitochondria, microglia, and the immune system-how are they linked in affective disorders? *Front. Psychiatry* **9**, 739 (2019).
13. Himmerich, H., Patsalos, O., Lichtblau, N., Ibrahim, M. A. A. & Dalton, B. Cytokine research in depression: principles, challenges, and open questions. *Front. Psychiatry* **10**, 30 (2019).
14. Clark, S. L. et al. A methylation study of long-term depression risk. *Mol. Psychiatry* https://doi.org/10.1038/s41380-019-0516-z (2019).
15. Euteneuer, F. et al. Peripheral immune alterations in major depression: the role of subtypes and pathogenetic characteristics. *Front. Psychiatry* **8**, 250 (2017).
16. Köhler, C. A. et al. Peripheral alterations in cytokine and chemokine levels after antidepressant drug treatment for major depressive disorder: systematic review and meta-analysis. *Mol. Neurobiol.* **55**, 4195–4206 (2018).
17. Arteaga-Henríquez, G. et al. Low-grade inflammation as a predictor of anti-depressant and anti-inflammatory therapy response in MDD patients: a systematic review of the literature in combination with an analysis of experimental data collected in the EU-MOODINFLAME Consortium. *Front. Psychiatry* **10**, 458 (2019).
18. Syed, S. A. et al. Defective inflammatory pathways in never-treated depressed patients are associated with poor treatment response. *Neuron* **99**, 914–924.e3 (2018).
19. Drexhage, R. C. et al. Inflammatory gene expression in monocytes of patients with schizophrenia: overlap and difference with bipolar disorder. A study in naturalistically treated patients. *Int. J. Neuropsychopharmacol.* **13**, 1369–1381 (2010).
20. Carvalho, L. A. et al. Inflammatory activation is associated with a reduced glucocorticoid receptor alpha/beta expression ratio in monocytes of inpatients with melancholic major depressive disorder. *Transl. Psychiatry* **4**, e344 (2014).
21. Grosse, L. et al. Clinical characteristics of inflammation-associated depression: Monocyte gene expression is age-related in major depressive disorder. *Brain Behav. Immun.* **44**, 48–56 (2015).
22. Leday, G. G. R. et al. Replicable and coupled changes in innate and adaptive immune gene expression in two case-control studies of blood microarrays in major depressive disorder. *Biol. Psychiatry* **83**, 70–80 (2018).
23. Zhang, H. X. et al. Difference in proinflammatory cytokines produced by monocytes between patients with major depressive disorder and healthy controls. *J. Affect. Disord.* **234**, 305–310 (2018).
24. Alvarez-Mon, M. A. et al. Abnormal distribution and function of circulating monocytes and enhanced bacterial translocation in major depressive disorder. *Front. Psychiatry* **10**, 812 (2019).
25. Prinz, M., Jung, S. & Priller, J. Microglia Biology: one century of evolving concepts. *Cell* **179**, 292–311 (2019).
26. Clark, S. M. et al. Dissociation between sickness behavior and emotionality during lipopolysaccharide challenge in lymphocyte deficient Rag2(−/−) mice. *Behav. Brain Res.* **278**, 74–82 (2015).
27. Steiner, J. et al. Severe depression is associated with increased microglial quinolinic acid in sub regions of the anterior cingulate gyrus: evidence for an immune-modulated glutamatergic neurotransmission? *J. Neuroinflamm.* **8**, 94 (2011).
28. Torres-Platas, S. G., Cruceanu, C., Chen, G. G., Turecki, G. & Mechawar, N. Evidence for increased microglial priming and macrophage recruitment in the dorsal anterior cingulate white matter of depressed suicides. *Brain Behav. Immun.* **42**, 50–59 (2014).
29. Bayer, T. A., Buslei, R., Havas, L. & Falkai, P. Evidence for activation of microglia in patients with psychiatric illnesses. *Neurosci. Lett.* **271**, 126–128 (1999).
30. Hamidi, M., Drevets, W. C. & Price, J. L. Glial reduction in amygdala in major depressive disorder is due to oligodendrocytes. *Biol. Psychiatry* **55**, 563–569 (2004).
31. Steiner, J. et al. Immunological aspects in the neurobiology of suicide: elevated microglial density in schizophrenia and depression is associated with suicide. *J. Psychiatr. Res.* **42**, 151–157 (2008).
32. Brisch, R. et al. Microglia in the dorsal raphe nucleus plays a potential role in both suicide facilitation and prevention in affective disorders. *Eur. Arch. Psychiatry Clin. Neurosci.* **267**, 403–415 (2017).
33. Shelton, R. C. et al. Altered expression of genes involved in inflammation and apoptosis in frontal cortex in major depression. *Mol. Psychiatry* **16**, 751–762 (2011).
34. Setiawan, E. et al. Role of translocator protein density, a marker of neuroinflammation, in the brain during major depressive episodes. *JAMA Psychiatry* **72**, 268–275 (2015).
35. Li, H., Sagar, A. P. & Kéri, S. Microglial markers in the frontal cortex are related to cognitive dysfunctions in major depressive disorder. *J. Affect. Disord.* **241**, 305–310 (2018).
36. Setiawan, E. et al. Association of translocator protein total distribution volume with duration of untreated major depressive disorder: a cross-sectional study. *Lancet Psychiatry* **5**, 339–347 (2018).
37. Owen, D. R. et al. Pro-inflammatory activation of primary microglia and macrophages increases 18 kDa translocator protein expression in rodents but not humans. *J. Cereb. Blood Flow. Metab.* **37**, 2679–2690 (2017).
38. Perry, V. H. Microglia and major depression: not yet a clear picture. *Lancet Psychiatry* **5**, 292–294 (2018).
39. Böttcher, C. et al. Human microglia regional heterogeneity and phenotypes determined by multiplexed single-cell mass cytometry. *Nat. Neurosci.* **22**, 78–90 (2019).
40. Böttcher, C. et al. Multi-parameter immune profiling of peripheral blood mononuclear cells by multiplexed single-cell mass cytometry in patients with early multiple sclerosis. *Sci. Rep.* **9**, 19471 (2019).
41. Chevrier, S. et al. Compensation of signal spillover in suspension and imaging mass cytometry. *Cell Syst.* **6**, 612 (2018).
42. Nowicka, M. et al. CyTOF workflow: differential discovery in high-throughput high-dimensional cytometry datasets. *Version 2. F1000Res.* **6**, 748 (2017).
43. Van Gassen, S. et al. FlowSOM: Using self-organizing maps for visualization and interpretation of cytometry data. *Cytom. A* **87**, 636 (2015).
44. Wilkerson, M. D. & Hayes, D. N. *ConsensusClusterPlus*: a class discovery tool with confidence assessments and item tracking. *Bioinformatics* **26**, 1572–1573 (2010).
45. Sankowski, R. et al. Mapping microglia states in the human brain through the integration of high-dimensional techniques. *Nat. Neurosci.* **22**, 2098–2110 (2019).
46. Butovsky, O. et al. Identification of a unique TGF-β-dependent molecular and functional signature in microglia. *Nat. Neurosci.* **17**, 131–143 (2014).
47. Hendrickx, D. A. E., van Eden, C. G., Schuurman, K. G., Hamann, J. & Huitinga, I. Staining of HLA-DR, Iba1 and CD68 in human microglia reveals partially overlapping expression depending on cellular morphology and pathology. *J. Neuroimmunol.* **309**, 12–22 (2017).
48. Gandal, M. J. et al. Transcriptome-wide isoform-level dysregulation in ASD, schizophrenia, and bipolar disorder. *Science* **362**, eaat8127 (2018).
49. Haruwaka, K. et al. Dual microglia effects on blood brain barrier permeability induced by systemic inflammation. *Nat. Commun.* **10**, 5816 (2019).
50. Keren-Shaul, H. et al. A unique microglia type associated with restricting development of alzheimer's disease. *Cell* **169**, 1276–1290 (2017).
51. Krasemann, S. et al. The TREM2-APOE pathway drives the transcriptional phenotype of dysfunctional microglia in neurodegenerative diseases. *Immunity* **47**, 566–581 (2017).
52. Masuda, T. et al. Spatial and temporal heterogeneity of mouse and human microglia at single-cell resolution. *Nature* **566**, 388–392 (2019).
53. Cattaneo, A. et al. FoxO1, A2M, and TGF-β1: three novel genes predicting depression in gene X environment interactions are identified using cross-species and cross-tissues transcriptomic and miRNomic analyses. *Mol. Psychiatry* **23**, 2192–2208 (2018).
54. Attaai, A. et al. Postnatal maturation of microglia is associated with alternative activation and activated TGFβ signaling. *Glia* **66**, 1695–1708 (2018).
55. Cserép, C. et al. Microglia monitor and protect neuronal function through specialized somatic purinergic junctions. *Science* **367**, 528–537 (2020).
56. Sellgren, C. M. et al. Increased synapse elimination by microglia in schizophrenia patient-derived models of synaptic pruning. *Nat. Neurosci.* **22**, 374–385 (2019).
57. Sipe, G. O. et al. Microglial P2Y12 is necessary for synaptic plasticity in mouse visual cortex. *Nat. Commun.* **7**, 10905 (2016).
58. Diaz-Aparicio, I. et al. Microglia actively remodel adult hippocampal neurogenesis through the phagocytosis secretome. *J. Neurosci.* **40**, 1453–1482 (2020).
59. Park, S. C. Neurogenesis and antidepressant action. *Cell Tissue Res.* **377**, 95–106 (2019).
60. Liu, Y. U. et al. Neuronal network activity controls microglial process surveillance in awake mice via norepinephrine signaling. *Nat. Neurosci.* **22**, 1771–1781 (2019).
61. Stowell, R. D. et al. Noradrenergic signaling in the wakeful state inhibits microglial surveillance and synaptic plasticity in the mouse visual cortex. *Nat. Neurosci.* **22**, 1782–1792 (2019).

62. Post, R. M., Gordon, E. K., Goodwin, F. K. & Bunney, W. E. Jr. Central norepinephrine metabolism in affective illness: MHPG in the cerebrospinal fluid. *Science* **179**, 1002–1003 (1973).

63. Lambert, G., Johansson, M., Agren, H. & Friberg, P. Reduced brain norepinephrine and dopamine release in treatment-refractory depressive illness: evidence in support of the catecholamine hypothesis of mood disorders. *Arch. Gen. Psychiatry* **57**, 787–793 (2000).

64. Hellwig, S. et al. Altered microglia morphology and higher resilience to stress-induced depression-like behavior in CX3CR1-deficient mice. *Brain Behav. Immun.* **55**, 126–137 (2016).

65. Mildner, A., Huang, H., Radke, J., Stenzel, W. & Priller, J. P2Y12 receptor is expressed on human microglia under physiological conditions throughout development and is sensitive to neuroinflammatory diseases. *Glia* **65**, 375–387 (2017).

66. Zrzavy, T. et al. Loss of 'homeostatic' microglia and patterns of their activation in active multiple sclerosis. *Brain* **140**, 1900–1913 (2017).

67. Gehrmann, J., Banati, R. B. & Kreutzberg, G. W. Microglia in the immune surveillance of the brain: human microglia constitutively express HLA-DR molecules. *J. Neuroimmunol.* **48**, 189–198 (1993).

68. McGeer, P. L., Itagaki, S. & McGeer, E. G. Expression of the histocompatibility glycoprotein HLA-DR in neurological disease. *Acta Neuropathol.* **76**, 550–557 (1988).

69. Huizinga, R. et al. Phagocytosis of neuronal debris by microglia is associated with neuronal damage in multiple sclerosis. *Glia* **60**, 422–431 (2012).

70. Chistiakov, D. A., Killingsworth, M. C., Myasoedova, V. A., Orekhov, A. N. & Bobryshev, Y. V. CD68/macrosialin: not just a histochemical marker. *Lab Invest* **97**, 4–13 (2017).

71. Wierzba-Bobrowicz, T. et al. Morphological analysis of active microglia–rod and ramified microglia in human brains affected by some neurological diseases (SSPE, Alzheimer's disease and Wilson's disease). *Folia Neuropathol.* **40**, 125–131 (2002).

72. Streit, W. J. et al. Microglial activation occurs late during preclinical Alzheimer's disease. *Glia* **66**, 2550–2562 (2018).

73. Barroeta-Espar, I. et al. Distinct cytokine profiles in human brains resilient to Alzheimer's pathology. *Neurobiol. Dis.* **121**, 327–337 (2019).

74. Ni, H. et al. The GWAS risk genes for depression may be actively involved in Alzheimer's Disease. *J. Alzheimers Dis.* **64**, 1149–1161 (2018).

75. Lutz, M. W., Sprague, D., Barrera, J. & Chiba-Falek, O. Shared genetic etiology underlying Alzheimer's disease and major depressive disorder. *Transl. Psychiatry* **10**, 88 (2020).

76. Seney, M. L. et al. Opposite molecular signatures of depression in men and women. *Biol. Psychiatry* **84**, 18–27 (2018).

77. Kopschina Feltes, P. et al. Anti-inflammatory treatment for major depressive disorder: implications for patients with an elevated immune profile and non-responders to standard antidepressant therapy. *J. Psychopharmacol.* **31**, 1149–1165 (2017).

78. Prud'homme, G. J., Glinka, Y. & Wang, Q. Immunological GABAergic interactions and therapeutic applications in autoimmune diseases. *Autoimmun. Rev.* **14**, 1048–1056 (2015).

79. Sedghi, S., Kutscher, H. L., Davidson, B. A. & Knight, P. R. Volatile anesthetics and immunity. *Immunol. Invest.* **46**, 793–804 (2017).

80. Franchi, S., Moschetti, G., Amodeo, G. & Sacerdote, P. Do all opioid drugs share the same immunomodulatory properties? A review from animal and human studies. *Front. Immunol.* **10**, 2914 (2019).

Complete list of own publications

1. Friedrich, M., Sankowski, R., Bunse, L., Kilian, M., Green, E., Ramallo Guevara, C., Pusch, S., Poschet, G., Sanghvi, K., Hahn, M., Bunse, T., Münch, P., Gegner, H. M., Sonner, J. K., von Landenberg, A., Cichon, F., Aslan, K., Trobisch, T., Schirmer, L., Abu-Sammour, D., Kessler, T., Ratliff, M., Schrimpf, D., Sahm, F., Hopf, C., Heiland, D. H., Schnell, O., Beck, J., Böttcher, C., **Fernandez-Zapata, C**., Priller, J., Heiland, S., Gutcher, I., Quintana, F. J., von Deimling, A., Wick, W., Prinz, M. & Platten, M. Tryptophan metabolism drives dynamic immunosuppressive myeloid states in IDH-mutant gliomas. *Nat. Cancer* (2021) doi:10.1038/s43018-021-00201-z.

2. **Fernández-Zapata C,** Leman JKH, Priller J, Böttcher C. The use and limitations of single-cell mass cytometry for studying human microglia function. Brain Pathol. 2020 Nov;30(6):1178-1191.

3. Fernandez-Klett F, Brandt L, **Fernández-Zapata C**, Abuelnor B, Middeldorp J, Sluijs JA, Curtis M, Faull R, Harris LW, Bahn S, Hol EM, Priller J. Denser brain capillary network with preserved pericytes in Alzheimer's disease. Brain Pathol. 2020 Nov;30(6):1071-1086.

4. Ormel PR, Böttcher C, Gigase FAJ, Missall RD, van Zuiden W, **Fernández Zapata MC**, Ilhan D, de Goeij M, Udine E, Sommer IEC, Priller J, Raj T, Kahn RS, Hol EM, de Witte LD. A characterization of the molecular phenotype and inflammatory response of schizophrenia patient-derived microglia-like cells. *Brain Behav Immun.* 2020 Nov;90:196-207.

5. Böttcher C*, **Fernández-Zapata C***, Snijders GJL, Schlickeiser S, Sneeboer MAM, Kunkel D, De Witte LD, Priller J. Single-cell mass cytometry of microglia in major depressive disorder reveals a non-inflammatory phenotype with increased homeostatic marker expression. Transl Psychiatry. 2020 Sep 11;10(1):310.

6. Böttcher C*, van der Poel M*, **Fernández-Zapata C***, Schlickeiser S, Leman JKH, Hsiao CC, Mizee MR, Adelia, Vincenten MCJ, Kunkel D, Huitinga I, Hamann J, Priller J. Single-cell mass cytometry reveals complex myeloid cell composition in active lesions of progressive multiple sclerosis. Acta Neuropathol Commun. 2020 Aug 18;8(1):136.

7. Böttcher C*, **Fernández-Zapata C***, Schlickeiser S*, Kunkel D, Schulz AR, Mei HE, Weidinger C, Gieß RM, Asseyer S, Siegmund B, Paul F, Ruprecht K, Priller J. Multi-parameter immune profiling of peripheral blood mononuclear cells by multiplexed single-cell mass cytometry in patients with early multiple sclerosis. Sci Rep. 2019 Dec 19;9(1):19471.

Acknowledgements

I would like to thank all my supervisors who had guided me and helped me get to the end of this thesis,

Prof. Dr. Josef Priller for continuously giving me the opportunity to work in your group.

PD. Dr. rer. nat Chotima Böttcher, for guiding me, teaching me, being so patient and believing in my habilities.

Thank you Dr. rer. nat. Stephan Schlickeiser, for being so patient and such a great teacher.

Thank you to all the AG Priller for all your support, I would hardly had made anything without you, Christian, Jasmin, Tanja, Koliane, Adeline an all the students who have been around.

Thank you Dr. Francisco Fernández-Klett, for helping me join this path, for the laughs and all the advice.

Me gustaría especialmente agradecer a mis padres, por todo lo que han hecho para que yo esté aquí, por enseñarme tanto y por siempre siempre apoyarme.

Gracias a mi familia, a Pablo y a Tomás, por la ayuda incondicional, por darme la mejor llegada a Berlín, por llevarme siempre de la mano.

Gracias Valen por toda tu ayuda.

Thank you to all my Berlin friends, who have made this PhD journey much more fun, Laura, Sebastiano, Adrian, Angharad, Isa GT, Anniki, Daniel, Luis, Larissa, Jas, Julia, and Stephan (thank you for giving me the best stories).

Gracias Ana, Carmen, Jordi, Adrià, Eulalia, Joan, Andreu y Juli, por estar ahí siempre, en las buenas y en las malas.

Thank you, Julian, for being by my side, for all your support, for listening more than you had to about microglia and for being always ready to make me smile.